PATH GENERATION FOR FILAMENT WINDING OF ASYMMETRIC FIBRE COMPOSITE COMPONENTS

Thesis submitted
to the School of Graduate Studies
in partial fulfilment of the requirements for the
degree of Master of Applied Science in
Mechanical Engineering

by

Etienne Bernard

Ottawa-Carleton Institute for
Mechanical and Aeronautical Engineering
University of Ottawa
Ottawa, Ontario
Canada, K1N 6N5

ISBN 0-315-75043-X

UNIVERSITÉ D'OTTAWA
UNIVERSITY OF OTTAWA

ABSTRACT

This thesis describes several fibre path prediction techniques used for filament winding of continuous fibre composite components. A literature review dealing with different aspects of CAD/CAM related to filament winding is provided. The insight gained through the review is used in the selection of specific path prediction techniques for two types of components. The mathematical technique is selected for surfaces of revolution while a geometric approach based on flat triangular patches is chosen for general asymmetric shapes. Since it can be used for a wider variety of components, this latter technique, along with the critical parameters affecting its performance, is described in greater detail. Three factors are shown to directly affect the accuracy of the predicted path. They are the starting condition, the separation distance between the actual surface and the triangle approximation and finally, the local curvature of the surface in the direction of the fibre path. A general discussion on the structure of the filament winding CAD environment in terms of hardware and software is also given.

RÉSUMÉ

Cette thèse présente différentes techniques pour la prédiction de trajet de fibre utilisée lors de la fabrication de composantes en matériaux composites par le procédé d'enroulement filamentaire. Elle inclue une revue de la littérature traitant de divers aspects reliés à la conception et à la fabrication assistées par ordinateur (CAO/FAO) pour l'enroulement filamentaire. La connaissance acquise par cette revue est ensuite utilisée lors de la sélection des techniques de prédiction de trajet pour deux types de surfaces. L'approche mathématique est choisie pour des surfaces de révolution (ayant une axe de symétrie) et une approche géométrique - à partir d'unités triangulaires plates - est sélectionnée pour des formes assymétriques générales. Cette dernière technique, avec les paramètres critiques influençant sa performance, est décrite en détail puisqu'elle peut être utilisée pour une très grande variété de structures. Trois facteurs exercent une influence directe sur la précision du trajet prédit: les conditions au point de départ, la distance qui sépare la surface réelle de la surface de l'unité triangulaire et finalement, la courbure locale de la surface dans la direction du trajet décrit par la fibre. Une discussion générale sur la structure d'un environnement informatique "CAO" pour l'enroulement filamentaire, en terme d'équipements et de logiciels, est inclue dans cet ouvrage.

ACKNOWLEDGEMENTS

I would first like to express my appreciation to my supervisors, Drs. Mike Munro and Atef Fahim, for providing me with their guidance and assistance while allowing me to pursue other interest (RALOS solar vehicle) during the course my studies.

I am grateful to the National Science and Engineering Research Council for the financial support provided over the years.

These studies would not have been as rewarding without the contribution of numerous people. To name everybody is to run the chance of forgetting someone. My appreciation goes out to the entire administration staff of the Mechanical Engineering Department. I would especially like to thank the following people with which the discussions were always enjoyable: Luc Ménard, Rudy Tolkamp, Chris Aleong and, for the heated debates, my close friends: Mike Tenace, Hans Öhman, François Costisella and Tom Dickson.

TABLE OF CONTENTS

LIST OF FIGURES

LIST OF TABLES

NOMENCLATURE

α fibre orientation angle (wind angle).

Θ rotation angle about mandrel axis.

γ fibre path direction vector pivot angle about triangle boundary.

ω intersection angle of fibre path direction vector with triangle boundary.

β rotation angle of fibre path direction vector to obtain stable non-geodesic fibre path.

K fibre path curvature.

K_n normal component of fibre path curvature.

K_g geodesic (or tangential) component of fibre path curvature.

μ coefficient of surface friction.

δ multiplier for coefficient of surface friction.

S function for surface representation.

u units of measure for length, u can be substituted by any length units i.e. inches, meters, feet, etc.

CHAPTER 1

INTRODUCTION

1.1 Composite Materials

In engineering disciplines, the term composite materials refers to the structure obtained when two or more materials are combined in order to benefit from the advantages of each. Reinforced concrete is a composite whereby the high compressive strength of the concrete is combined with the tensile strength of the steel reinforcement rods to produce a structure which exhibits good compressive and tensile properties. There are two categories of materials in any composite structure. The external load is applied to the "matrix" which transfers a certain portion of the load to the "reinforcement". In the case of reinforced concrete the cement is the matrix and the steel rods are the reinforcement. The load is transferred from the concrete to the steel rods by shear at the interface through mechanical keying. In any composite the constituent materials must be joined together by either mechanical keying or chemical bonding.

High performance fibre composites have a polymer matrix which is a thermosetting or a thermoplastic material while the reinforcement originates from small diameter fibres such as carbon, aramid (Kevlar) or glass. These composites are characterized by high specific (per unit weight) properties including specific modulus, specific strength, etc. when compared to conventional materials such as steel, aluminum or titanium. Figure 1.1 shows the specific strength and specific modulus of a variety of materials. In this thesis, the term composite will always refer to high performance fibre composites.

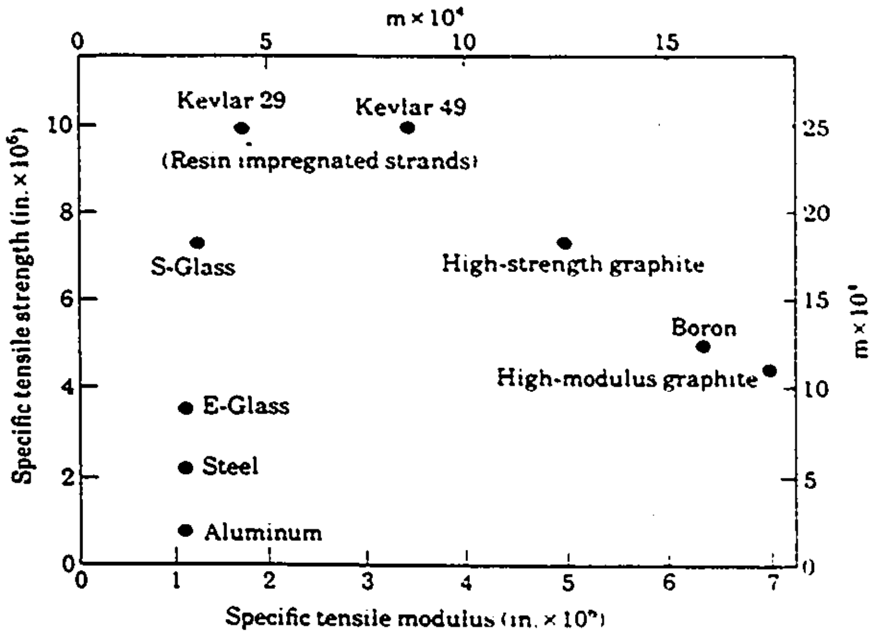

Figure 1.1 Specific tensile strength (tensile strength to density ratio) and specific tensile modulus (modulus of elasticity to density ratio) for various engineering materials [1].

An attractive feature of composites is the possibility of engineering desired mechanical properties into the final product. Some of the advantages of using composites include low thermal expansion, resistance to harsh environment, low density, high specific stiffness and the possibility to produce predetermined mechanical properties along chosen directions. An example of this is the Canadarm used for manipulating equipment aboard the space shuttle. The properties were engineered in the long booms so that it would not deflect more than two inches at its tool end when subjected to the large temperature gradient encountered in space.

High performance fibre composites can be grouped in two classes depending on the length of the fibres. Composites with short fibres have been used extensively in commercial applications. These products include fibreglass canoes, chairs, bathtubs, car panels and more. The fibre orientation is usually not controlled resulting in a simple manufacturing process. Although the fibre length can vary anywhere from a few millimetres to hundreds of meters, the term continuous fibre will apply to fibres whose orientation can be controlled directly. Composites having continuous fibre reinforcement where used initially in the aerospace industry but have now propagated to various other industries. Products include solid rocket booster casings for the shuttle, tennis rackets, canoes, pressure vessels, pipes for transporting harsh products, airplane wing and fuselage sections. In the aerospace industry, the cost factor associated with design and manufacturing was less important than the high quality demand. Although the design methods developed for continuous fibre composites can also be used in commercial applications, the challenges lie in reducing the manufacturing cost.

1.2 Manufacturing Processes

There are four well known manufacturing methods which use a dedicated machine to place continuous fibres along specific directions to fabricate fibre composite components: filament winding, braiding, tape laying and pultrusion. A brief description of each is given below:

Filament winding: Continuous fibre strands in the form of a band are place on a mandrel (usually rotating) in an attempt to cover the entire surface. Composite pressure vessels are usually produced by filament winding.

Braiding: Technology taken from the textile industry where several fibre strands are interwoven to produce a variety of shapes. The process has been used to produce flat and circular fibre mats having specific fibre orientation.

Tape laying: Used in the aerospace industry and similar to filament winding in that bands of fibres are placed on a female mould. The fibre strands are not continuous, as was the case for filament winding, but are cut at exterior boundaries. Typical components include wing and fuselage sections.

Pultrusion: This recently developed process is used in commercial applications. Fibres in different formats (unidirectional roving, woven mats, etc.) are pulled continuously through a heated formation die where they are impregnated with resin. Curing occurs as the product continues through the die with subsequent cooling. It exits the die in a cured state where the pulling is performed and then is cut to length while the process continues. Products include pipes, square tubes and various other cross sections (I-beam sections, triangular sections, etc.).

To take advantage of certain features of individual methods, hybrid processes have also been developed [2, 3, 4]. Filament winding is the focus of this study.

1.3 Filament Winding

Filament winding is a process in which continuous fibres are wrapped on a rotating mandrel along a predetermined path, under controlled tension. The conventional machine configuration, needed to place the fibres, resembles a lathe with the cutting tool replaced by a fibre delivery eye, and the work piece by a mandrel as depicted in Figure 1.2 [5, 6].

The process has many features which fulfil present manufacturing demands. By nature it is an economical, high volume process compared to other alternatives (tape laying or braiding), it can accommodate components of widely varying size and can easily be automated [3, 7]. It also offers high repeatability of components thereby giving better control over quality assurance. Its major disadvantage is the difficulty associated with programming the filament winding machine to produce pay out eye trajectories necessary for placing the fibre strand on the desired path.

Older machines use mechanical gearing to synchronize the mandrel rotation with the delivery eye motion. This limits the complexity of components which can be produced. The type of products fabricated included, among others, pressure vessels, cylindrical tubes, rocket motor casings and drive shafts.

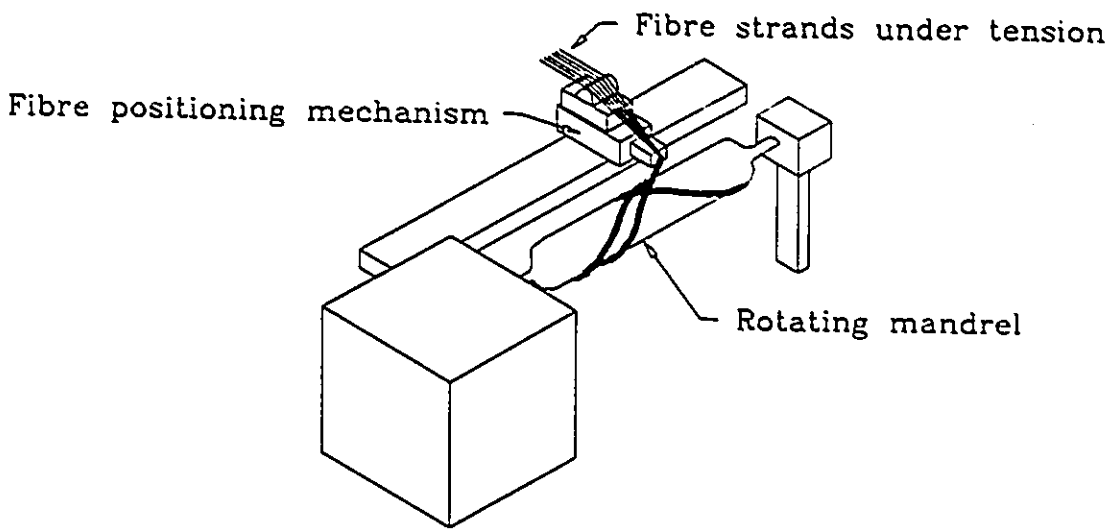

Figure 1.2 Basic elements of a filament winding machine.

With the advent of computers came cost effective controllers powerful enough to manage not only pay out eye position but also process parameters such as resin temperature, impregnation, fibre strand tension and others. It is now possible to have up to seven independent axes of motion (three for delivery eye orientation, three for delivery eye position and one for mandrel rotation, Figure 1.3) [8, 9]. Also, a robotic manipulator can replace the conventional lathe configuration for filament winding. The pay-out eye position and orientation is provided by the robot's end effector, while an external drive is used for mandrel rotation. The robot can also be used to load and unload the mandrel as well as performing various other tasks. This configuration provides a whole new dimension in manufacturing flexibility [3, 7, 10, 11, 12].

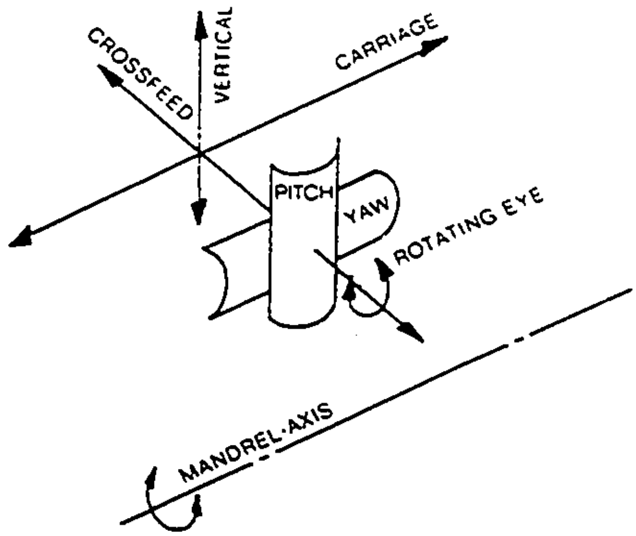

Figure 1.3 Typical axes of control for a computer-controlled helical filament winder [3].

The modernization of filament winding machines allows the fabrication of components having complex geometries and the optimization of process parameters (tension, machine dynamics, resin impregnation) [13]. The new variety of products which can be filament wound include, among others, airfoils (tapered wind turbine blades), pipe tees, and elbows, robot arms and automotive parts. Simple methods developed to obtain the delivery eye trajectory for filament winding of rotationally symmetric mandrels are no longer valid for these asymmetric shapes.

The delivery eye trajectory can be defined using a "teach-in" method where the filament winding machine is guided through its motions by an operator. This labour intensive process is classified as a trial and error method since an acceptable trajectory will not be obtained on the first try. There is a high cost associated with using trial and error methods resulting from expensive machinery being occupied in unproductive time.

This high cost has created a need to further develop path prediction capabilities [8, 14, 15, 16]. Although the prediction of the fibre path is the primary objective, the optimization of the manufacturing process is also of great interest [17]. Designers are concerned about predicting fibre slippage in unstable locations, collision avoidance between the delivery eye and its surroundings, compensation for fibre build-up in localized areas and whether or not the complex delivery eye path can be reproduced by the filament winding machine.

1.4 Thesis Overview

Choosing a particular method for determining the fibre path is not a simple task. The decision is based on many interrelated concepts. It is unacceptable to choose a particular alternative blindly, therefore a literature review dealing with the trends in CAD/CAM filament winding is presented in Chapter 2. The choice of a technique used to predict fibre path depends on whether the component is rotationally symmetric or asymmetric. The selection of specific techniques for each case along with their description is given in Chapter 3. The technique used to obtain fibre strand (fibre path, orientation, distribution) and machine data (tool path) for asymmetric mandrels is described in greater detail in Chapter 4. The next chapter deals with the accuracy of this method and how it can be improved. Practical aspects for the hardware and software implementation of the algorithms developed in Chapter 4, is the topic of Chapter 6. The general structure of the filament winding design environment is also discussed. Recommendations and conclusions are given in Chapter 7.

CHAPTER 2

LITERATURE REVIEW

The literature review is divided into several topics, each dealing with the different aspects of computer aided filament winding. The concepts are described in detail in an effort to define their role within the CAD/CAM environment. Additional information, not found in the literature, is given to insure continuity in the text.

2.1 Path Prediction

The objective in filament winding is to lay a continuous fibre on a rotating mandrel along predetermined paths. An attempt is made to place the fibres in the principal stress direction of the component [6, 17, 18, 19, 20]. This is not always feasible because, in these chosen directions, it may be impossible to position the fibre along stable paths. The term stable path needs further clarification since it is the most important factor in filament winding.

A stable path, in filament winding, is any path along which a tensed fibre strand will remain in position once it is placed. There are several ways to prevent the fibre from moving out of position. Mechanical fastening in the form of anchors on the mandrel surface or even thermoplastic welding can be used to permanently position the strand. A less obvious approach, and one of greater interest, is the use of surface geometry along with the surface friction to place the strand along stable paths. This latter method is at the heart of this study and the term stable path, unless specified otherwise, will refer to this type of path only. A stable path can also be referred to as a non-slip path.

The stable paths can be of two types, one where the coefficient of surface friction is assumed to be zero and one where this parameter is different from zero. When the friction is assumed to be zero the stable paths, called geodesics, are a function of surface geometry only. A characteristic of the geodesic path is that it traces the shortest distance between two sufficiently close points on a surface. A tensed fibre strand placed between two points on a frictionless surface will always slip to position itself along the geodesic path. This is the physical interpretation of the geodesic path. The mathematical explanation is discussed later in Section 2.1.2.

If surface friction is taken into account, then a stable path, different from a geodesic, can be determined and is called a stable non-geodesic path. Using a geodesic path as a reference, the amount of deviation allowed is a function of the local curvature of the surface and the magnitude of the coefficient of surface friction i.e. larger deviation for larger coefficient of friction. This type of path gives more flexibility in placing the fibre strand along principal stress directions.

There are two categories of methods used for predicting stable fibre paths. The geometric approach is based on simple vector algebra while the mathematical approach uses a differential equation along with special numerical methods to predict stable fibre paths. The techniques belonging to each category are discussed in the coming sections. They are listed in Table 1 along with their important characteristics.

2.1.1 Geometric techniques for geodesic path prediction

The fibre path computation for rotationally symmetric components is relatively straightforward. Many methods exist to obtain geodesic paths on surfaces of revolution. The simplest case arises when the component is made up of a series of basic shapes i.e. conical, cylindrical or spherical sections (Figure 2.1). The geodesic paths for these basic geometric shapes are well known. Both the cylindrical and the conical shapes are developable surfaces since they can be formed by folding a flat surface.

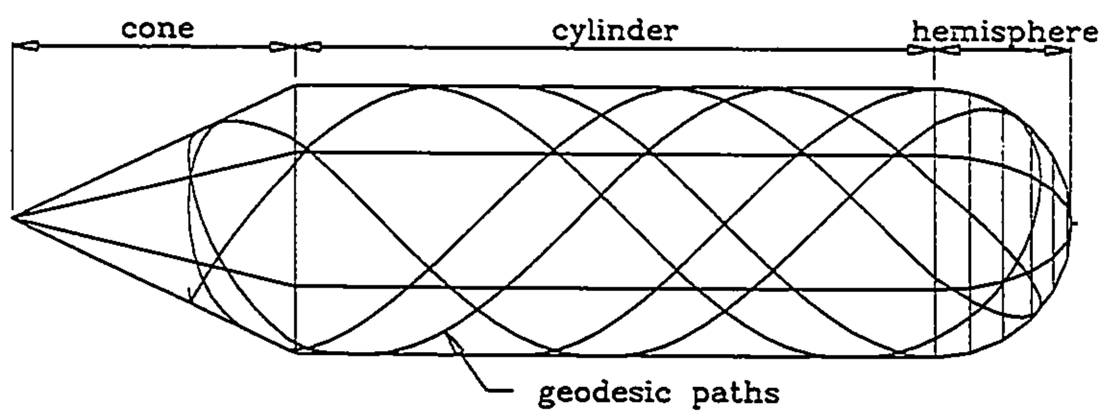

Figure 2.1 Component is an assembly of basic shapes.

Table 2.1 Compilation of path prediction techniques.

CHARACTERISTIC	SOLUTION METHOD FOR GEODESIC PATH				
	DIFFERENTIAL EQUATION			GEOMETRIC	
Surface representation	Function for profile of rotationally symmetric mandrel	Bivariate function of entire mandrel surface	Bivariate function of several distinct surface patches	Cone and cylinder sections for rotationally symmetric mandrels	Flat triangular patches to represent entire surface
Solution for stable non-geodesic path	Yes	Yes	Yes	No	Yes
Component shape characteristic	Rotationally symmetric	Asymmetric, unbranched components	Asymmetric including branched components	Rotationally symmetric	Asymmetric including branched components
Accuracy	High	High	High	Medium to High	Low to Medium
Difficulties	None to report	Stiff differential equation	Stiff differential equation	Optimum sampling of surface profile data points	Large surface topology data files, requires fast access storage media
References	[17, 28, 33, 34]	[28]	[12, 17, 18, 19, 31, 32, 34]	Internal publications	[6, 16, 20, 21, 22, 23, 24, 25, 26]

For surfaces which are developable, the geodesics are straight lines on the developed surface. On the spherical shape, the geodesic paths are the great circles[1].

When the component is not made up of these basic geometric shapes, a different approach must be used. The surface of revolution of Figure 2.2 can be **approximated** by a series of truncated cones and cylinders while the asymmetric elbow of Figure 2.3 is **approximated** by flat triangular patches. For such approximations, the geodesic path can easily be generated with low computational effort [21].

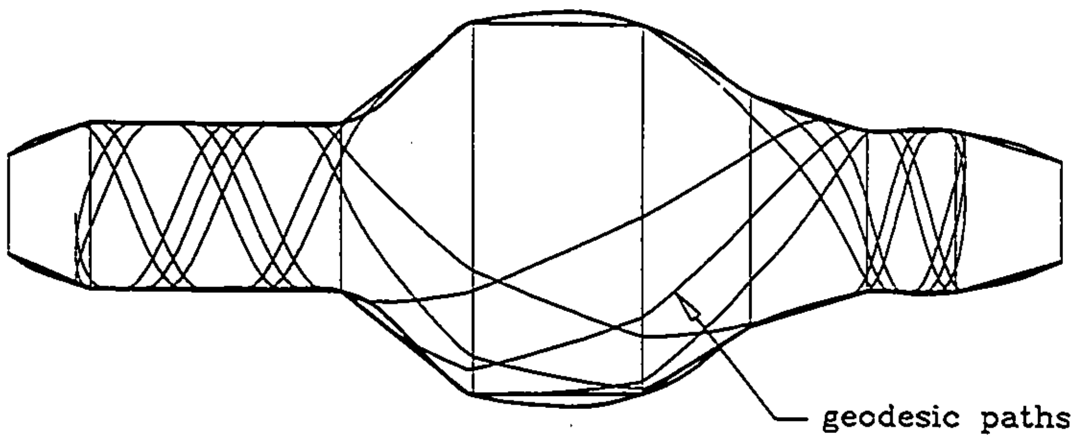

Figure 2.2 Rotationally symmetric mandrel is approximated by a series of cones and cylinders.

The geodesic paths on cones, cylinders and flat triangular patches are defined geometrically and, at the element boundary, the angle of intersection of the path and the common boundary of two adjacent element is kept constant as shown in Figure 2.4. The rotationally symmetric limitation imposed by a cones and cylinders approximation does

[1] Great circle: The circle of intersection of a sphere and a plane passing through its centre, e.g. the equator is a great circle.

not exist when triangular elements are used to model the surface. Any complex surface such as elbows, tees or S shapes can be approximated using flat triangular patches.

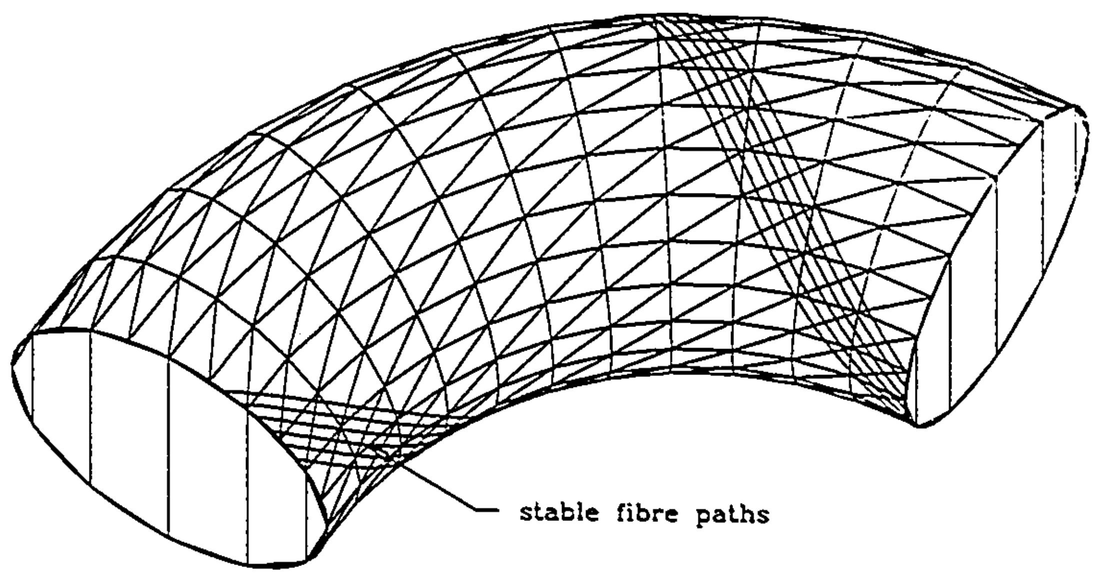

Figure 2.3 Tubular elbow mandrel is approximated by a series of flat triangular patches.

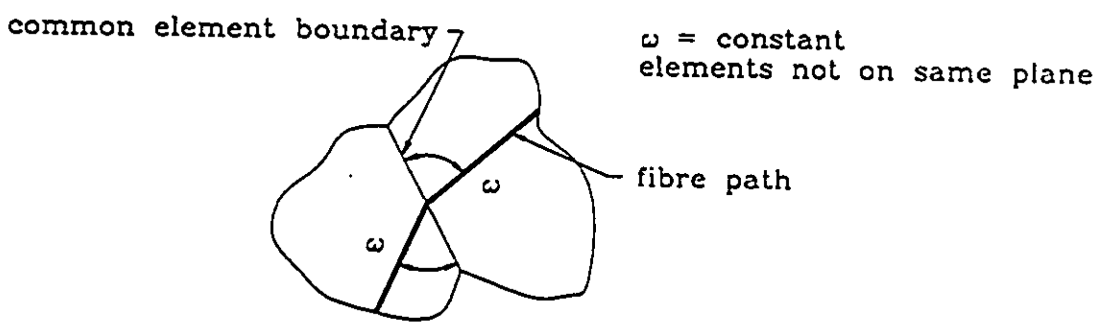

Figure 2.4 Intersection of fibre path at common element boundary.

Flat triangular patches are the base element in the method described in [6, 16, 20, 22, 23, 24, 25] by the Composite Group at the University of Nottingham. Their commercially available software package "CADFIL" predicts the geodesic path along a surface represented by flat triangles. Although it is less accurate, this approach is simpler than solving the differential equation for stable paths detailed in Chapter 3. Furthermore, this method can easily accommodate the prediction of stable non-geodesic paths. Since any surface can be approximated by triangles, the method is very flexible. This flexibility has inherent disadvantages with respect to surfaces of revolution. It is less accurate than a cones and cylinders approximation, less efficient from a computational point of view and requires more storage space for the model which contains redundant information [22].

The method described in [21, 26], by the composite group at the IKV[2] in Germany, is also based on flat triangular patches as a means to represent the mandrel surface. The software developed for this purpose is "CADFIBER". Again the same software can be used for both rotationally symmetric and asymmetric components.

2.1.2 Mathematical techniques for geodesic path prediction

Methods for fibre path computation presented above are all based on a geometric approach. The mandrel surface is approximated by elements for which the geodesic path is known. A mathematical approach can also be used to predict the fibre path. The constraints for the paths are expressed in terms of an initial value second order differential equation. This equation is a function of the mandrel surface tangent and curvature and cannot be solved analytically except for simple surfaces such as cones and cylinders [27]. The starting point and direction are the only necessary parameters required to define a

[2] Institut für Kunststoffverarbeitung, University of Aachen, Germany

path. The method based on this mathematical approach involves the numerical solution of the initial value second order differential equation and, as such can be classified as an approximate method.

The simplest implementation of this method results when the mandrel is a surface of revolution and the generatrix (or profile) is represented by a function. The simplicity originates from the differential equation where the circumferential derivative, cross derivative and surface friction coefficient terms are zero. By eliminating these null terms the equation can be rearranged in a compact form. The function representing the profile can either be the exact analytical equation or, if such an equation does not exist, an efficient interpolation equation such as a spline or Bézier curve[3]. The acute angle between the fibre path and the surface of revolution meridian can be calculated by means of Clairaut's theorem. With reference to the symbols in Figure 2.5, this theorem is defined by the following expression:

$$R_{mandrel}\sin(\alpha)=R_{TA}=Constant \qquad (2.1)$$

The R_{TA} constant, called the turn around radius, is equal to the radius of the mandrel at the point where the fibre path changes direction with respect to the axis of revolution. This equation can be used to calculate the wind angle, α, anywhere along the mandrel axis as long as the path is geodesic.

[3] Interactive curve fitting technique available on most CAD software packages. Developed by Pierre Bézier at Renault Corporation in France in the 1970's [29].

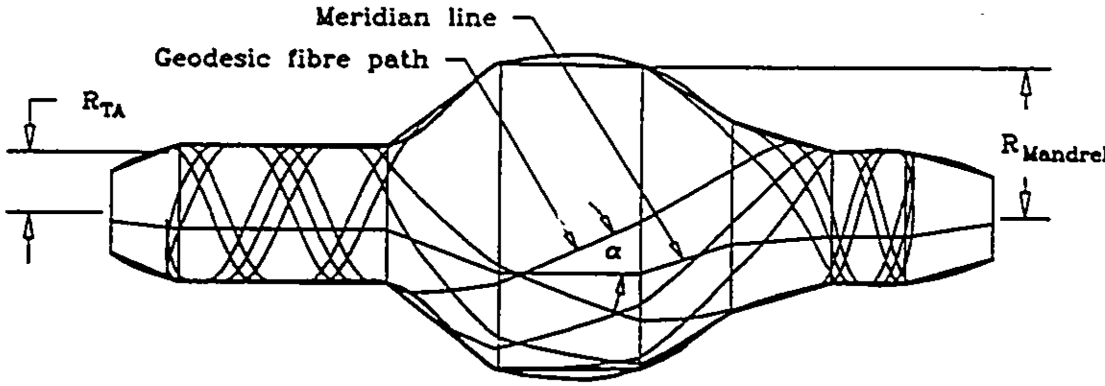

Figure 2.5 Symbols for Clairaut's theorem.

When the mandrel is not a surface of revolution the differential equation cannot be simplified since none of the terms can be eliminated except for the coefficient of surface friction term. The asymmetric surface is described by a bivariate function which can either be the exact analytical equation for the surface or one obtained from surface fitting.

The differential equation method was employed by Lawless [28] where the surface of revolution profile was approximated by a cubic spline. The differential equation was solved using an Adams predictor-corrector method with a Runge-Kutta algorithm to start the solution (predictor-corrector methods are not self starting). Asymmetric mandrels were represented by a bicubic spline which approximated the entire surface. It provided accurate results in the case of smooth profiles but the examples given in [28] do not include components having sharp transitions. Such components create difficulties since splines cannot negotiate sharp turns without excessive undulations and must be used with care [29].

The independent variables of the bicubic spline used for asymmetric shapes are the axial position and circumferential angle. The bicubic spline function represents the radius for different values of axial and angular position as shown in Figure 2.6. This limits the variety of surfaces which can be modelled since the rotation axes is not permitted to extrude the mandrel except at the extremities. When the rotation axis extrudes the asymmetric surface there are two possible values for the radius for the axial-angular coordinates as shown in Figure 2.7. Lawless also noted in [28] that the differential equation for asymmetric components is stiff[4].

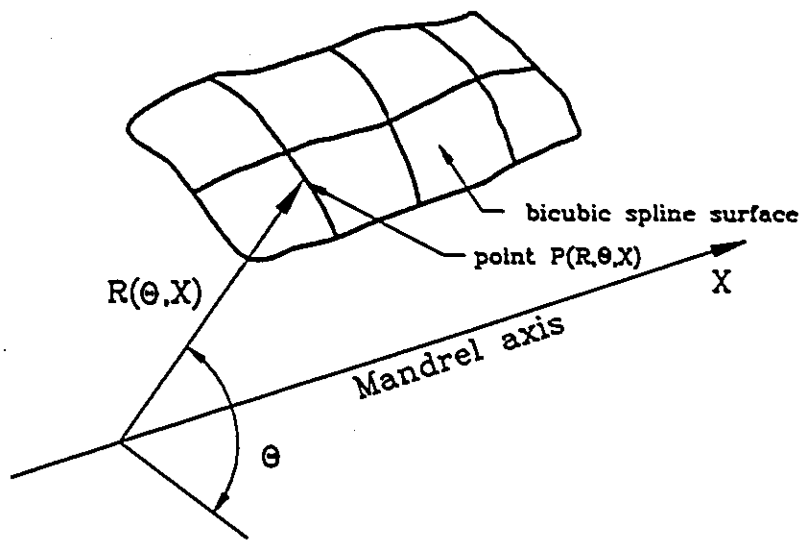

Figure 2.6 Coordinate system used to define asymmetric surface with a bicubic spline.

[4] "Stiffness occurs in a problem where there are two or more very different scales of the independent variable on which the dependent variables are changing" [30] page 592

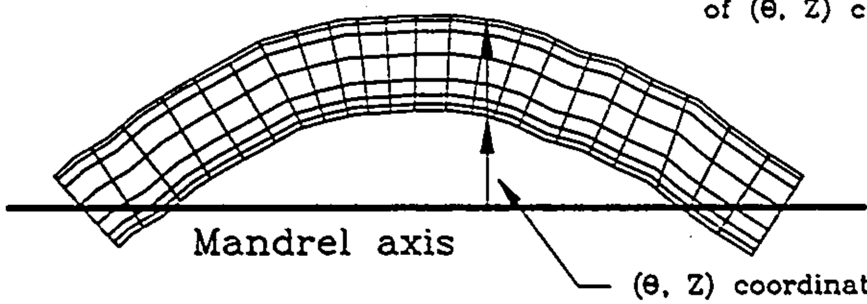

Figure 2.7 Axis of revolution extruding asymmetric shape, undefined bicubic spline using variables defined.

The stiff nature of the differential equation becomes apparent when solving the equation using regular numerical methods. If regular numerical methods are used, the step size will need to be exceptionally small to prevent divergence of numerical solution from the actual solution [29, 30]. Special algorithms are required to deal with this difficulty; Gears method [30] was used by Lawless [28]. The cause of this problem may be due to the choice of surface modelling technique (bicubic spline) employed since this difficulty is not reported anywhere else in literature where the differential equation approach has been used [17, 19, 31, 32, 33].

A mathematical approach has also been used by the composite group at the Harwell Laboratory in the U.K. [19, 31, 32] to obtain the fibre path. The component surface was modelled by a series of Bézier patches[5]. A commercially available software package "SYSTRID" was purchased to perform this task. It was modified to allow an in-

[5] Interactive surface fitting technique available on most CAD software packages. Developed by Pierre Bézier in the 1970's [29].

house developed software, "CADMAC", to access its database and extract the necessary information required to solve the second order differential equation. The references do not report the method of solving the differential equation. Again, this method is excessively complex for surfaces of revolution but it has the flexibility of being powerful enough for asymmetric components. The reported approach offers definitive advantages over the bicubic spline. The nature of Bézier patches allows easy interactive editing of surfaces [29]. They can also be controlled in sharp transitions by adjusting the degree of continuity. Because it is a local scheme (each patch is a separate entity with its own representation and boundary constraints), there are no limitations to the complexity of the component.

The exact equations for the profiles of surfaces of revolutions were used at the Research Centre for Composite Materials in China [33]. The derivation of the differential equation was presented for several basic geometric profiles (cylinder, cone, sphere, ellipsoidal and paraboloid). A Runge-Kutta algorithm was used to solve the differential equation. The reference suggested using these elementary profiles as building blocks for more complex surfaces of revolution.

A similar approach to the one described above was discussed by the composite group at the Centro Italiano Ricerche Aerospaziali in Rome, Italy [17, 34]. The equations used to obtain the fibre path on a general rotationally symmetric mandrel were presented. The nature of the equation used to represent the mandrel profile was not discussed, but examples were given for simple shapes (cones, cylinders, isotensoid domes) where the analytical equation for the profile was used. The method was extended to include tapered asymmetric components. Sections of cones and cylinders were used to represent the surface of a wing shape. The references do not report the numerical method used to solve the differential equation.

The method described by a composite group in Belgium consists of modelling the mandrel surface by series of analytical surface patches such as cylindrical, spherical, planar or toroidal sections [12]. The differential equation is used to predict the fibre path on the individual sections. The terms in the differential equation are calculated using the analytical equation of the surface. This equation is not defined at the patch boundary. The path was transferred from one patch to the next by maintaining the intersection angle between the fibre path and the common boundary constant similar to the approach shown in Figure 2.4.

2.1.3 Prediction of stable non-geodesic fibre paths

Filament winding on geodesic paths imposes limitations on the position and orientation of the fibre strands. The consequence of these limitations is reflected through the resulting fibre pattern on the mandrel surface in terms of surface coverage and fibre build-up. Another negative effect is the difficulty in aligning the fibre strands along the principal stress directions [20]. A solution to this problem is to place the fibre strand on a path which is not geodesic but is nonetheless stable. This can be accomplished if the surface friction is taken into account. The magnitude of the deviation is a function of the coefficient of friction, the local curvature of the surface and the direction of the fibre.

With reference to Figure 2.8, the curvature of the fibre path can be represented by two components, one component pointing in the same direction as the surface normal and called the normal curvature, K_n, the other component perpendicular to the fibre path and lying in a plane tangent to the surface called the geodesic curvature, K_g. For a geodesic path, the magnitude of the geodesic curvature component is equal to zero. If the path is non-geodesic but stable, then the ratio of the geodesic component to the normal component for the path curvature must be smaller than the coefficient of friction at that point [17, 21, 26, 33, 34, 35]. This is commonly known as a stable non-geodesic path and can be obtained by one of two methods or a combination of thereof.

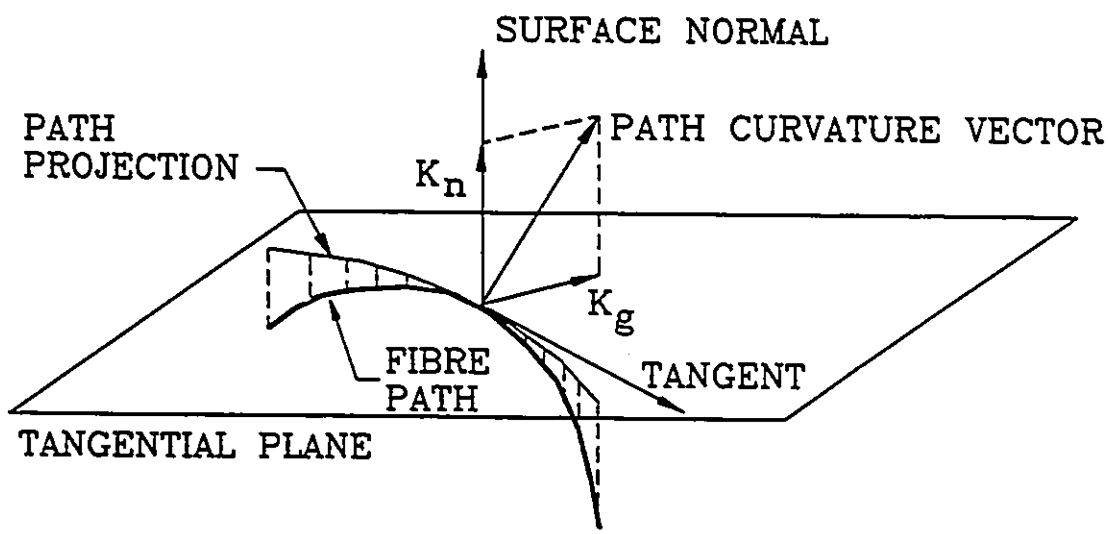

Figure 2.8 Normal curvature K_n and geodesic curvature K_g of the fibre path.

The simplest but least accurate approach is to use triangular patches to model the mandrel surface and proceed with a geometric technique to predict the fibre path. The path remains straight across the triangle patch but is allowed to deviate at the boundary to account for the coefficient of friction [6, 16, 20, 24, 25]. Unlike the geodesic path obtained with the geometric technique, the angle between the fibre path direction and the common boundary between two consecutive triangles does not remain constant for a stable non-geodesic path.

The other alternative is based on the second order differential equation [17, 18, 19, 32, 33, 34, 35]. The term for the coefficient of surface friction is no longer zero and, as a result, is not eliminated from the differential equation.

In both approaches, the amount of deviation from the geodesic path is controlled by varying the magnitude of a friction multiplier. The friction multiplier is used to scale the coefficient of friction from zero to its maximum value. Control of deviation along the path is an important factor in obtaining acceptable fibre orientation and good surface coverage [17, 35]. Clairaut's theorem, Equation 2.1, implies that the turn around radius of geodesic paths on surfaces of revolution are equal for each mandrel extremity. With stable non-geodesic paths it is a simple task to obtain fibre paths for which the turn around radius is not equal at both mandrel extremities [35].

2.2 Surface Coverage

The prediction of fibre paths is important but more details are required to assess surface coverage, bridging[6] and fibre build-up[7] at different locations along the mandrel axis. The prediction of these parameters is a simple task for surfaces of revolution since the path appearance does not change. The same path can therefore be mirrored over and over again. Adjustments in wind angle, friction multiplier and part geometry are made

[6] Occurs when the fibre crosses a valley and is separated from the mandrel surface.

[7] The final thickness obtained when the fibre strands are placed on the surface is not constant over the entire mandrel. A cylinder with fibre strands placed on geodesic paths is the only shape on which the thickness remains constant.

until the repeatable pattern obtained produces the desired fibre strand orientation and thickness distribution. For asymmetric components, each path is distinct and there are no repeatable patterns. Consequently, more effort is required to predict the final appearance of the fibre strands on the mandrel surface [6, 12, 18]. The fibre distribution and orientation is recorded at different positions along the stable path. This information is used in later analysis to locate areas of difficulty. Fibre build-up alters the mandrel shape and, if multiple fibre layers are wound, compensation of the original model geometry will be necessary to reflect new surface conditions [6].

It is very difficult to define an acceptable surface coverage philosophy for asymmetric mandrels. A method dealing with this problem is discussed vaguely in [6, 16, 24, 25]. The method is based on constant angle path and can only be used for a limited variety of shapes, it is not appropriate for branched components (e.g. pipe tee).[8] More research is required to develop optimization methods to obtain good surface coverage properties (fibre bridging, distribution, and orientation).

2.3 Computer Aided Design (CAD) in Filament Winding

The designer needs to have a general idea about surface coverage properties for both rotationally symmetric and asymmetric components. The mandrel shape can be design in the CAD environment [12] and this data sent to the specialized software for path calculations. The results can then be shown on the screen. For asymmetric shapes,

[8] "The definition of a constant angle path is the direction taken by a fibre across a patch that is at a fixed angle to a reference plane. This reference plane is a flat plane containing the starting position, the patch surface normal and the mandrel axis." [6] page 6

each fibre path is generated as part of a small group of paths or, in the worst case, individually [12]. A method is required to represent the appearance of the mandrel once several fibre paths have been traced. The interpretation of the winding data can be simplified by the use of a high resolution colour graphic monitor [8, 17, 20, 36]. The winding pattern, surface coverage and fibre build-up characteristics can easily be displayed using a combination of geometry and colour.

The CAD environment can be further extended to included a stress analysis of the resulting fibre patterns [6, 12, 17, 18, 19, 24, 25, 32, 37]. This task can be perform by specialized algorithms or a finite element software. For rotationally symmetric parts, the elements will have similar properties along any particular cross section but may vary along the axis of the mandrel. On asymmetric components this task is much more difficult since the material properties vary from location to location. The results of the stress analysis will be a factor in the design of the winding pattern.

The different tasks, required to obtain the representation of the filament wound component, can be combined into one integrated CAD package. Many CAD software packages are readily available for a whole range of computer hardware. Also, third party software can be added to perform specific filament winding tasks.

2.4 Computer Aided Manufacturing (CAM) in Filament Winding

The stress analysis completes the pure design phase of the filament wound component. The control data for the winding machine must then be extracted from the results. This data is used in creating the part program which will control the winding machine [12]. It is not guaranteed however, that the winding machine will be able to execute all the commands. Several factors may prevent the filament winder from achieving its prescribed function. Collision between the fibre delivery eye and its surroundings is a primary concern [18, 19]. Velocities and accelerations of individual axis may prevent the smooth motion of the fibre delivery eye. One way to avoid these problems, is to perform a multilevel simulation of the process [8]. The motion of the fibre delivery eye relative to its surroundings can be animated on the screen [6, 16]. Since this animation cannot be carried out in real time due to the extensive computation required, it becomes necessary to display position/time relationships in an effort to smooth out motor operation and fibre delivery eye motion [7, 21]. These efforts are useful since the results collected can be transformed directly into a part program using a machine command translation table. The part program can then be transferred to the filament winder controller via a communication link [7, 8, 16, 17, 18, 19, 20, 38].

2.5 CAD/CAM and Filament Winding Cell

The full power of a CAD/CAM environment can be used for the design and manufacturing of filament wound rotationally symmetric and asymmetric components. This environment can be further enhanced by adding automatic loading and unloading of components [7]. Curing, cutting and finishing processes can also be automated. The final environment obtained is a flexible filament winding cell with analysis capabilities for both design and manufacturing stages [6, 15, 16, 29, 40].

2.6 Problem Definition

One of the main problems associated with filament winding is programming the new multi-axis computerized filament winding machines. Although the fibre delivery eye can generally accomplish any complex motion, it is the designer's responsibility to determine what should be the resulting fibre arrangement. The cost associated with trial and error methods are no longer acceptable. There is a need for efficient software tools that will enable the designer to program the filament winder off-line. These tools should also include design analysis and optimization facilities for the filament wound component.

The motion of the fibre delivery eye depends on the nature of the fibre arrangement on the mandrel. A prelude to obtaining the delivery eye position is to predict stable fibre paths. These paths can be obtained using a variety of methods which were discussed in Section 2.1. It is important to consider all aspects of computerized filament winding when making the selection of the path prediction technique since it will serve as a foundation for later developments in design analysis and optimization.

The purpose of this thesis is first to summarize the state of the art in computerized filament winding. This has been dealt with in the literature review. The next step involves selecting a particular path prediction technique for two classes of components, rotationally symmetric and asymmetric respectively. The method selected for asymmetric components will then be implemented and its performance evaluated.

2.7 Scope of Work

The evaluation of the different path prediction techniques requires a thorough understanding of the intricacies involved. Computer algorithms along with the associated programs were developed for the following techniques:

- Cones and cylinders technique for rotationally symmetric components.
- Mathematical technique for rotationally symmetric components.
- Triangulation technique for rotationally symmetric components.
- Triangulation technique for tubular asymmetric components.

Only general information pertaining to path prediction techniques can be found in the literature, for example, graduate theses at the University of Nottingham on the triangulation method are restricted, they are not even available from the university library. The methods listed above were consequently developed from basic concepts. The important characteristics of the techniques listed in this section are given in Chapter 3. Specifics of the triangulation technique are further discussed in Chapter 4.

There are no published conventions for evaluating the merits of a specific fibre path prediction technique. Hence, the author has defined a set of error measurement parameters. The algorithms and computer programs required to calculate these parameters were developed from basic vector algebra concepts (Chapter 5).

In an effort to show the usefulness of the work undertaken in this thesis, a chapter on the implementation of triangulation was included. Several practical aspects, related to user friendly interfaces and efficient data storage, were investigated by the author. The result of this work is given in Chapter 6.

CHAPTER 3

SELECTION OF FIBRE PATH PREDICTION TECHNIQUES

Different methods exist to predict the fibre path on a variety of mandrels. The literature survey revealed that authors have selected specific techniques without documenting the factors affecting the decision of using a particular method over another. The objective of this chapter is to describe different solution techniques and then proceed with the selection of the best alternative for predicting both geodesic and stable non-geodesic fibre paths on different types of surfaces.

The first part of the chapter describes three path prediction techniques in detail. With reference to Table 2.1, a mathematical method and two geometric methods are discussed. The second part of the chapter is dedicated to the evaluation of the techniques. The most important characteristic of a mandrel is symmetry. Another important characteristic is whether the fibre strand is placed along geodesic paths or stable non-geodesic paths. The evaluation of the path prediction techniques will therefore be based on their performance in dealing with rotationally symmetric and asymmetric components and their ability to predict stable paths. The concepts presented can be used as guidelines for the development of CAD based filament winding.

3.1 Mathematical Path Prediction Technique

The techniques grouped under the mathematical class all originate from the same differential equation. The differences between the methods result from the type of surface modelling used. Although the technique described in this section pertains to surfaces of revolution, the same derivation would be used for asymmetric surfaces.

For rotationally symmetric shapes, the mandrel profile is represented by a certain function such as a spline, Bézier curve or the exact analytical equation. The function used must be of order two or higher. This requirement is necessary because the differential equation uses the second order derivative of the profile which must be continuous. Care must be taken if a spline is used since it tends to excessively undulate when it encounters abrupt transitions. It must therefore be adjusted when such transitions occur or, alternatively, appropriate end conditions can be used to smooth out excessive undulations [29]. The function representing the surface of revolution profile is used to obtain the mandrel properties (tangents and curvatures) anywhere along the rotation axis (Figure 3.1).

The relationship used to derive the differential equation is based on the stable path which was discussed in the literature review and is expressed in Equation 3.1.

$$\left|\frac{K_g}{K_n}\right| \leq \mu \tag{3.1}$$

K_g=geodesic curvature component
K_n=normal curvature component
μ =*coefficient of surface friction*

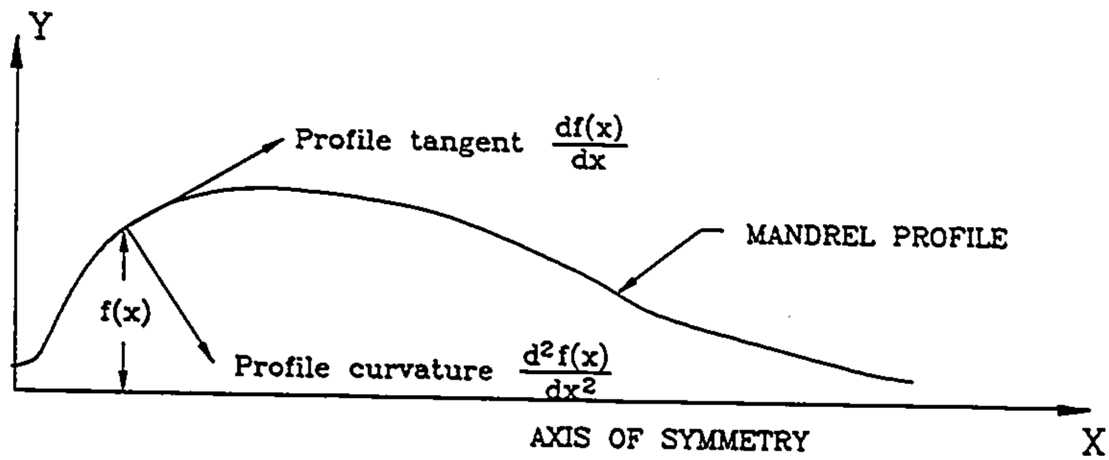

Figure 3.1 Mandrel profile represented by a function of order two or higher with surface properties shown.

A multiplier is used with the coefficient of friction term to eliminate the absolute value operation and replace the "less than or equal sign" with an equality relationship:

$$\frac{K_g}{K_n}=\delta\mu, \quad -1.0 \leq \delta \leq 1.0 \tag{3.2}$$

δ =*friction multiplier*

Equation 3.2 relates the two components of the path curvature, K_g and K_n, to the surface friction. The relationship is expressed in terms of the local surface geometry, the direction of the fibre and the magnitude of the coefficient of friction. The surface friction μ and its multiplier δ (between -1.0 and 1.0) are used to modify the deviation of the fibre path from the geodesic path.

To obtain expressions for K_g and K_n the surface must first be expressed in terms of two independent variables. A surface S in three dimensional space can be represented by a parametric equation S(u,v) where u and v are called the parameters and S(u,v) is a three dimensional vector and is called the parametric representation of the surface. The reference coordinate frame for the rotationally symmetric mandrel is shown in Figure 3.2 along with parametric curves.

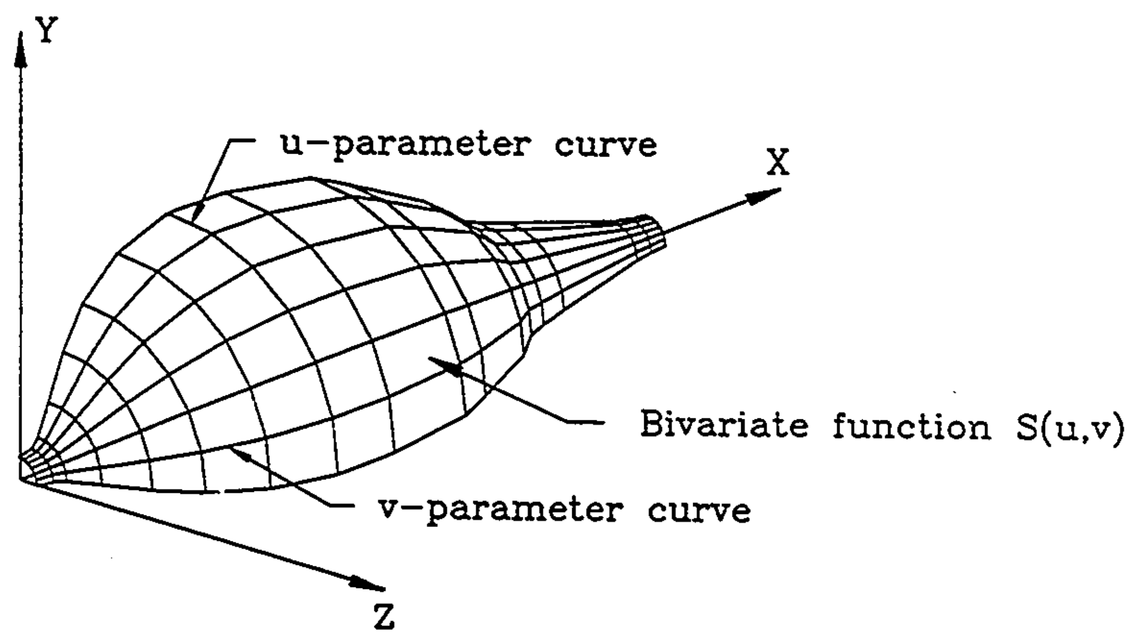

Figure 3.2 Reference frame for rotationally symmetric mandrel.

These latter curves are obtained by keeping one of the variables (u or v) constant and varying the other. This reference frame is used to represent the mandrel surface in the coordinate system in terms of u and v as shown by Equation 3.3.

$$S(u,v)=\{\Phi(v),\Omega(v)\cos(u),\Omega(v)\sin(u)\} \tag{3.3}$$

The function Φ represents the position along the mandrel axis while the function Ω represents the radius. U is therefore equivalent to the rotation angle while v represents displacement along the mandrel profile. These parameters will later be replaced by the variables used in the coordinate system (i.e. axial position, rotation angle and radius). U and v are used here to generalize the derivation of the equations.

The equations for K_n and K_g are given in [27] and are shown below. These equations can be used for any type of surface.

$$K_n=\frac{e\,du^2+2f\,du\,dv+g\,dv^2}{E\,du^2+2F\,du\,dv+G\,dv^2} \tag{3.4}$$

$$\begin{aligned}K_g=\Big[&\Gamma_{11}^2\left(\frac{du}{ds}\right)^3+\left(2\Gamma_{12}^2-\Gamma_{11}^1\right)\left(\frac{du}{ds}\right)^2\frac{dv}{ds}+\left(\Gamma_{22}^2-2\Gamma_{12}^1\right)\frac{du}{ds}\left(\frac{dv}{ds}\right)^2-\\&\Gamma_{22}^1\left(\frac{dv}{ds}\right)^3+\frac{du}{ds}\frac{d^2u}{ds^2}-\frac{d^2u}{ds^2}\frac{dv}{ds}\Big]\sqrt{EG-F^2}\end{aligned} \tag{3.5}$$

The definition for the different symbols are given by the following expressions. The equation modelling surfaces of revolution is used in this derivation and, therefore, the resulting differential equation is valid for rotationally symmetric shapes only. The partial

$$S_u=(0,\ -\Omega\sin(u),\ \Omega\cos(u)\ )$$

$$S_v=(\Phi_v,\ \Omega_v\cos(u),\ \Omega_v\sin(u)\ )$$

$$S_{uu}=(0,\ -\Omega\cos(u),\ -\Omega\sin(u)\ ) \tag{3.6}$$

$$S_{uv}=S_{vu}=(0,\ -\Omega_v\sin(u),\ \Omega_v\cos(u)\ )$$

$$S_{vv}=(\Phi_{vv},\ \Omega_{vv}\cos(u),\ \Omega_{vv}\sin(u)\ )$$

$$\begin{aligned} E &= S_u\cdot S_u=\Omega^2 \\ E_u &= 2S_u\cdot S_{uu}=0 \\ E_v &= 2S_{uv}\cdot S_u=2\Omega\Omega_v \end{aligned} \tag{3.7}$$

$$\begin{aligned} F &= S_u\cdot S_v=0 \\ F_u &= S_u\cdot S_{vu}+S_{uu}\cdot S_v=0 \\ F_v &= S_{uv}\cdot S_v+S_u\cdot S_{vv}=0 \end{aligned} \tag{3.8}$$

$$\begin{aligned} G &= S_v\cdot S_v=\Phi_v^2+\Omega_v^2 \\ G_u &= 2S_{vu}\cdot S_v=0 \\ G_v &= 2S_{vv}\cdot S_v=2(\Phi_v\Phi_{vv}+\Omega_v\Omega_{vv}) \end{aligned} \tag{3.9}$$

$$e=\frac{S_{uu}S_uS_v}{\sqrt{EG+F^2}}=-\frac{\Omega\Phi_v}{\sqrt{\Phi^2+\Omega^2}}$$

$$f=\frac{S_{uv}S_uS_v}{\sqrt{EG+F^2}}=0 \tag{3.10}$$

$$g=\frac{S_{vv}S_uS_v}{\sqrt{EG+F^2}}=\frac{\Phi_v\Omega_{vv}-\Phi_{vv}\Omega_v}{\sqrt{\Phi_v^2+\Omega_v^2}}$$

$$\Gamma_{11}^1=\frac{GE_u-2FF_u+FE_v}{2(EG-F^2)}=0 \qquad \Gamma_{11}^2=\frac{2EF_u-EE_v+FE_u}{2(EG-F^2)}=-\frac{\Omega\Omega_v}{\Phi_v^2+\Omega_v^2}$$

$$\Gamma_{12}^1=\frac{GE_v-FG_u}{2(EG-F^2)}=\frac{\Omega_v}{\Omega} \qquad \Gamma_{12}^2=\frac{EG_u-FE_v}{2(EG-F^2)}=0 \tag{3.11}$$

$$\Gamma_{22}^1=\frac{2GF_v-GG_u-FG_v}{2(EG-F^2)}=0 \qquad \Gamma_{22}^2=\frac{EG_v-2FF_v+FG_u}{2(EG-F^2)}=\frac{\Phi_v\Phi_{vv}+\Omega_v\Omega_{vv}}{\Phi_v^2+\Omega_v^2}$$

With reference to Figure 3.3 and Equations 3.4 to 3.11, the curvature components can now be expressed as:

$$K_n=\left[-r+\frac{d^2r}{dx^2}\left(\frac{dx}{d\theta}\right)^2\right]\left(\frac{d\theta}{ds}\right)^2\frac{dx}{dv} \tag{3.12}$$

$$K_g=-\frac{r}{\sin(\alpha)}\left[\frac{dr}{dv}+\frac{d\alpha}{d\theta}\right]\left(\frac{d\theta}{ds}\right)^2 \tag{3.13}$$

Substituting for K_n and K_g with Equations 3.12 and 3.13 into Equation 3.2 gives:

$$\frac{d^2x}{d\theta^2}=\frac{dr}{dx}\left(\frac{dx}{d\theta}\right)^2\left[\frac{1}{r}-\frac{d^2r}{dx^2}\left(\frac{dx}{dv}\right)^2\right]+ \frac{1}{\sin(\alpha)}\left(\frac{dx}{dv}\right)^2\left[\delta\,\mu\left(-r+\frac{d^2r}{dx^2}\left(\frac{dx}{d\theta}\right)^2\right)+\frac{r}{\sin(\alpha)}\frac{dr}{dx}\right] \tag{3.14}$$

In the above equation the rotation angle Θ is chosen as the independent variable since its differential variation $d\Theta$ never goes to zero for a filament winding path and, therefore, the differential equation is always defined.

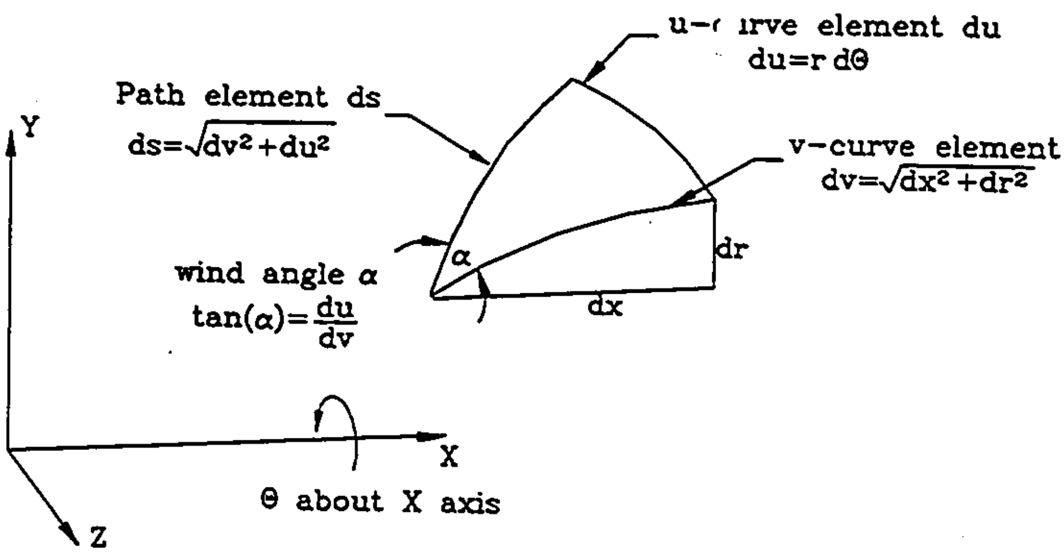

Figure 3.3 Relationship of different variables on differential path element ds.

The Adams-Bashford predictor-corrector method [29, 30] is used to solve the differential equation. This implicit type of numerical method is not self-starting and, consequently, a 4th order Runge-Kutta method is used to start the solution. The predicted path obtained is highly accurate as is explained in Chapter 5. The degree of accuracy can be adjusted with the integration step size. In order to verify if the predicted path converges to the exact solution, the integration step size is reduced until the deviation between two consecutive predicted fibre path becomes insignificant. The high accuracy is required to verify the existence of a truly repeatable pattern (many cycles are required) on the surface of revolution mandrel.

The computational effort is low when using efficient multi-step methods since it minimizes the number of times the differential equation is evaluated. A computer is required to implement the method and also to graphically represent the fibre path. Clairaut's theorem can only be used for geodesic path to get fibre orientation. For stable non-geodesic paths, the properties of the fibre path must therefore be recorded as it is being generated and stored for later use. This information will be required to obtain structural and surface coverage properties.

3.2 Geometric Path Prediction Techniques

Geometric techniques rely on basic geometric elements such as cones, cylinders, spheres and flat triangles to model the component surface (Table 2.1). The stable fibre paths are well defined for these elements and can be transferred from one element to the next in a sequential fashion until the entire path is obtained.

3.2.1 Cones and cylinders method

The cones and cylinders technique can explicitly predict geodesic paths on rotationally symmetric mandrels. The mandrel is divided into a series of truncated cones and cylinders (both right angled). These shapes are developable and the geodesic on their developments is a straight line. Any surface of revolution can be modelled using this method. An approximation is used to represent most mandrels since they seldom consist of an assembly of cones and cylinders. Even pressure vessels usually have end domes which are not hemispherical but rather parabolic or isotensoid[9].

The mandrel profile may be represented by a continuous function such as a spline, Bézier curve or the exact analytical equation which is then used to divide the profile into a series of line segments. The predicted fibre path accuracy is dependent on the ability of the line segments to represent the true nature of the profile slopes and curvatures. Three different approach can be used to obtain these line segments; equal steps on the axis of revolution Figure 3.4a, equal segment length along the profile Figure 3.4b or an optimized version where the maximum separation distance between the segment and the actual profile is controlled Figure 3.4c.

Using equal segments (Figure 3.4a) on the axis of revolution method yields the worst accuracy for path prediction. As the slope (profile tangent) of the profile increases, the line segments get longer and the profile approximation becomes coarse. This situation can be remedied by taking smaller steps along the axis of revolution. It is obvious that

[9] "In filament wound reinforced plastic pressure vessels, a dome contour in which the filaments are placed on geodesic paths so that the filaments will exhibit uniform tensions throughout their length under pressure loading." Glossary in [41]

this is a "brute force" approach where the number of steps along the axis of revolution is increased until the desired accuracy is obtained.

The second alternative consist of using line segments of equal length to represent the profile. This technique is not affected by the slope of the profile and yields better results than the first alternative in terms of path accuracy. The mandrel profile representation can however become coarse when negotiating sharp curvatures. The deviation of the line segment from the profile may be large for these large curvatures. Again the remedy is to increase the number of equal length line segments. This method is more refined than the "brute force" approach of taking equal step size along the mandrel axis.

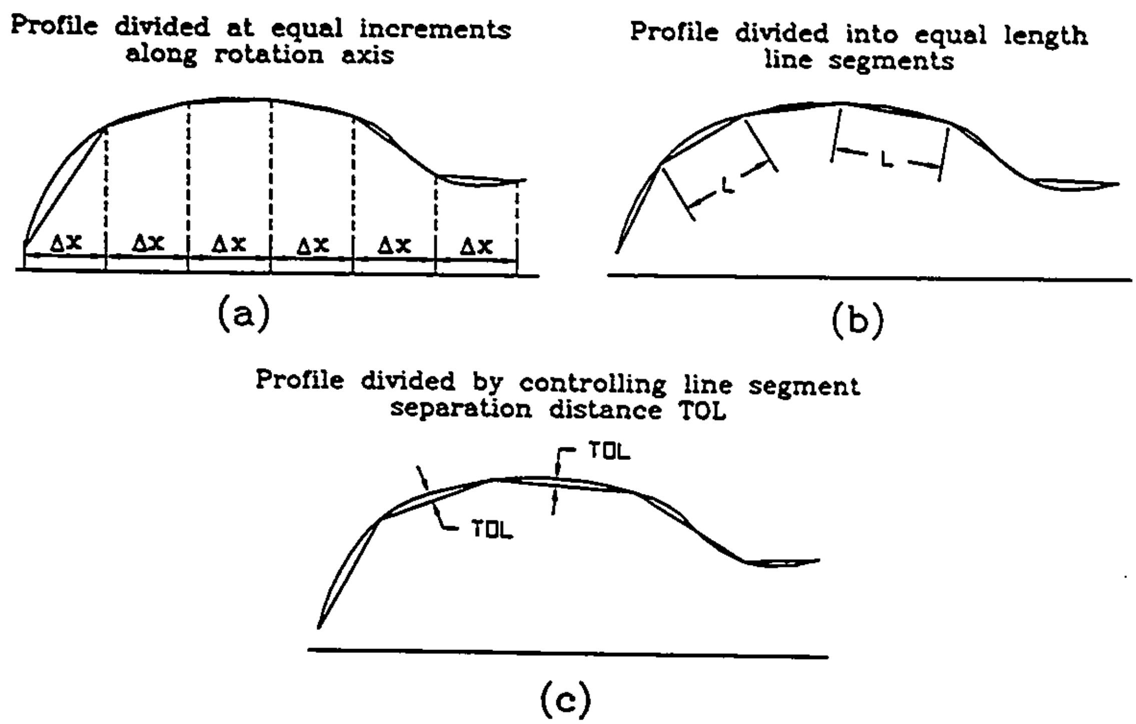

Figure 3.4 Alternatives in approximating mandrel profile by line segments; (a) equal steps along axis of revolution, (b) equal line segment length along profile, (c) specified maximum distance between line segment and actual profile.

The last alternative takes care of large profile slopes and large curvatures by controlling the maximum separation distance that the segment may have with respect to the original profile. Limiting this deviation would assure a certain degree of accuracy. To increase the resulting path accuracy the maximum deviation allowed simply needs to be decreased. The technique also minimizes the number of line segments used to represent the profile. The discussion on the accuracy of the triangulation technique in Chapter 5 shows how accuracy is affected by the maximum deviation of the triangles from the original surface. The same arguments apply for the cones and cylinders method since both are geometric types of solutions.

The line segments obtained by one of the three methods described above are used to define a series of cones and cylinders on which geodesic fibre paths can easily be generated. The geometric relationships used to extend the fibre path from its starting point are shown in Figures 3.5 and 3.6 for a cylinder and a cone respectively. Two equations, relating the circumferential position to the axial position, are derived for the cylinder and the cone. Clairaut's theorem is also used to calculate the wind angle at specific locations along the rotation axis. The equations are given below:

$$\Delta\theta_{cylinder} = \frac{L\tan(\alpha)}{R} \tag{3.15}$$

L=displacement along rotation axis
R=radius of cylinder
α=wind angle on cylinder

$$\Delta\theta_{cone}=\frac{\sqrt{(1+k^2)}}{k}\left(\sin^{-1}\left(\frac{R_{TA}}{R_1}\right)-\sin^{-1}\left(\frac{R_{TA}}{R_2}\right)\right) \tag{3.16}$$

R_{TA} = *turn around radius*
R_1 = *radius of cone at position* 1
R_2 = *radius of cone at position* 2
k = *slope of cone*

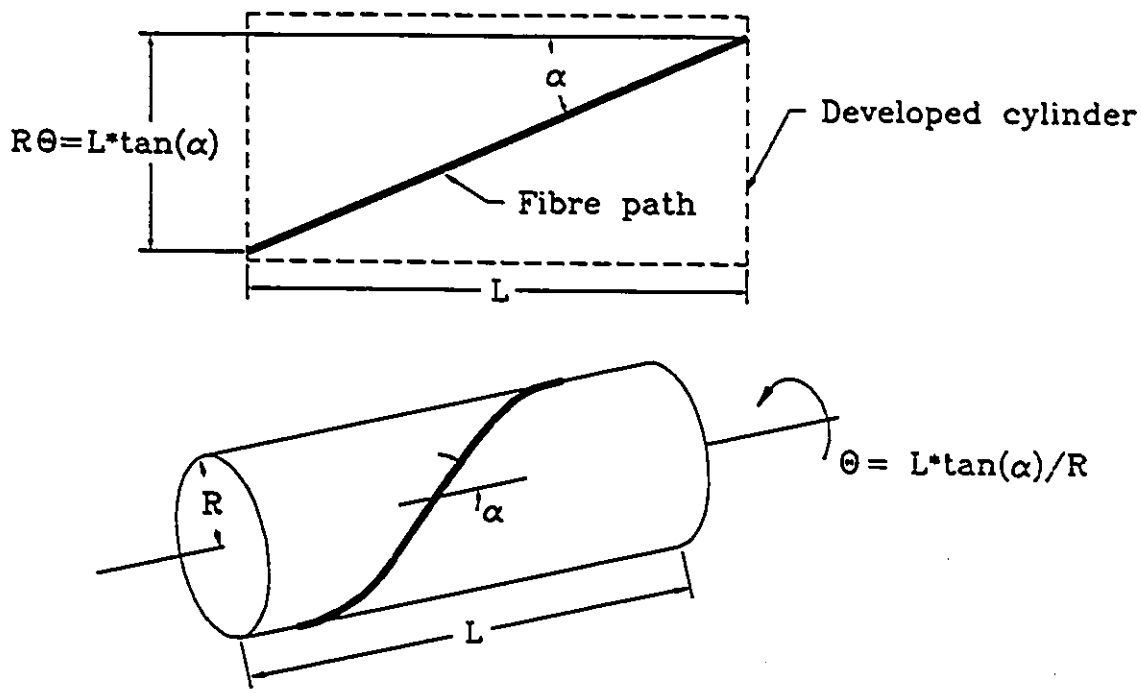

Figure 3.5 Geodesic fibre path on cylinder.

There is no need to use special numerical methods to obtain results. The basic technique is easy to implement even in the absence of a computer. The cones and cylinders technique is appropriate in situations where the designer elects not to use a computer based algorithm but requires some insight into the appearance of the fibre path. In this case, a computer is not required and the necessary information can be obtained using the above relations and/or classical graphical techniques. Aside from obtaining the fibre path, simple relationships can be used to get surface coverage properties. Clairaut's theorem is used to calculate fibre angles at different axial locations. A second relationship is used to describe the thickness distribution and is given by:

$$t_2=\frac{t_1 R_1 \cos(\alpha_1)}{R_2 \cos(\alpha_2)} \tag{3.17}$$

R_1=*radius at position* 1
α_1=*wind angle at position* 1
t_1=*thickness at position* 1 (*known*)
R_2=*radius at position* 2
α_2=*wind angle at position* 2
t_2=*thichness at position* 2 (*unknown*)

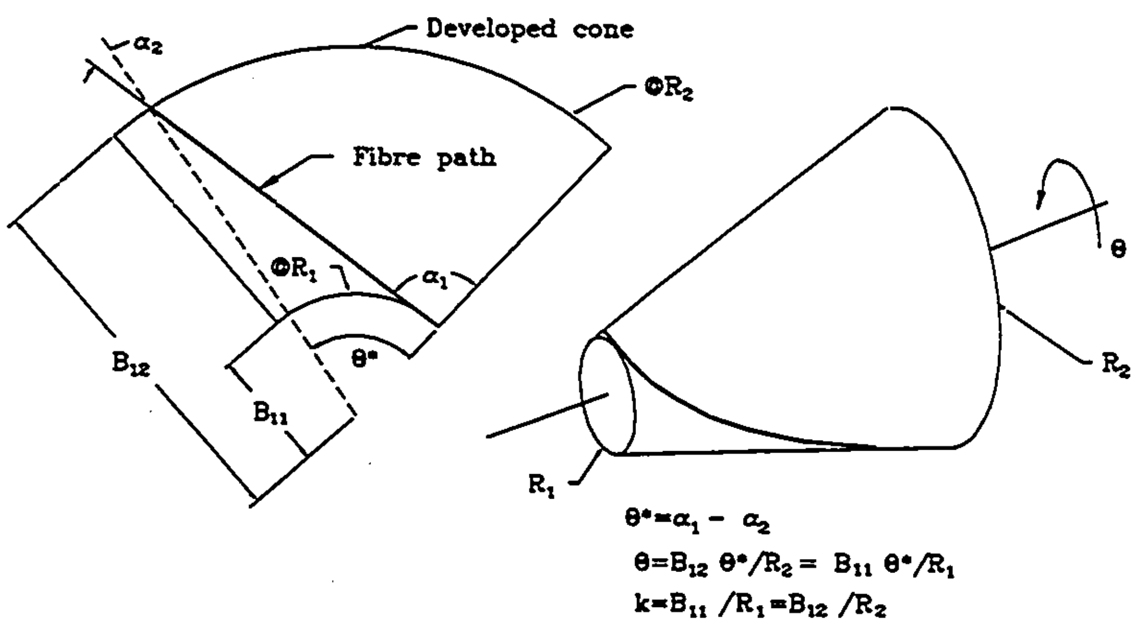

Figure 3.6 Geodesic fibre path on cone.

It should be noted that even though the basic concept of using a cones and cylinders approximation is simple, it nonetheless required innovative algorithms in order to extract useful information from the predictions. The difficulties encountered in extracting necessary data (fibre orientation in 3-D space, delivery eye position) from the cones and cylinders method are the result of having to work in two dimensional space for predicting the fibre path on the developed surface and then mapping the data to three dimensional space.

3.2.2 Triangulation method

The general aspects of this method were outlined in the literature review and will now be examined in greater detail. Any rotationally symmetric or asymmetric surface can be represented using flat triangular patches of various size. With knowledge of the initial position and orientation, the fibre path can be extended from one triangle to the next in a sequential fashion. With reference to Figure 3.7, across the triangle, the path is a straight line and, at the boundary, it pivots onto the adjacent triangle while maintaining a constant angle between itself and the common boundary. This results in a theoretical geodesic path whereby the surface friction has no active role. The accuracy of this path is discussed in Chapter 5.

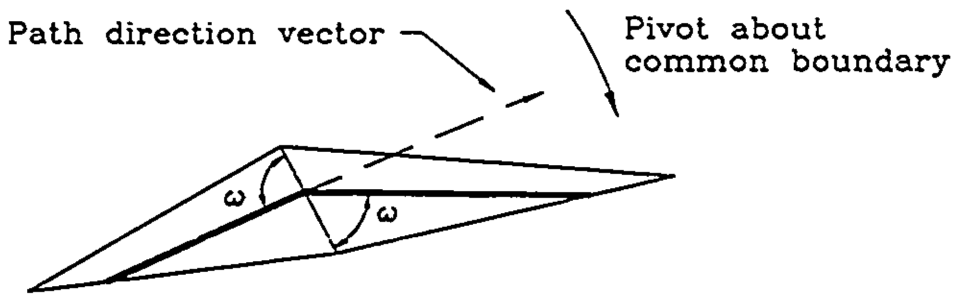

Figure 3.7 Triangulation; extending the geodesic path from one triangle to another.

When surface friction is taken into account, in the control of the fibre orientation, a special relationship must be derived for directing the path across the triangle boundary. The path across the triangle still remains straight. Again Equation 3.2 relating the components of the path curvatures to the surface friction serves as a starting point for the derivation of the relationships. The surface friction coefficient μ and its multiplier δ are known. Expressions for K_g and K_n in terms of path direction and triangle properties are therefore required. These expressions are much simpler than those obtained in the differential equation approach. The final equation relates the pivot angle of the fibre across the boundary (γ) to the rotation of the new fibre direction about the triangle normal (β). To understand the derivation of this expression, consider the following.

Because the path is composed of a series of straight line segments there is no true curvature but an artificial curvature can be defined at the segment intersection. The geodesic path is found on two consecutive triangles. The normal curvature is obtained by defining a plane containing the two path segments as shown on Figure 3.8. An arbitrary distance L from the intersection marks a point on the two individual path segments. An arc, tangent to these segments at the locations marked by L, can be drawn.

The radius of the arc can easily be found knowing the values of L and the pivot angle γ. The artificial curvature is equal to the inverse of this radius:

$$K_n = \frac{\tan(\frac{\gamma}{2})}{L} \tag{3.18}$$

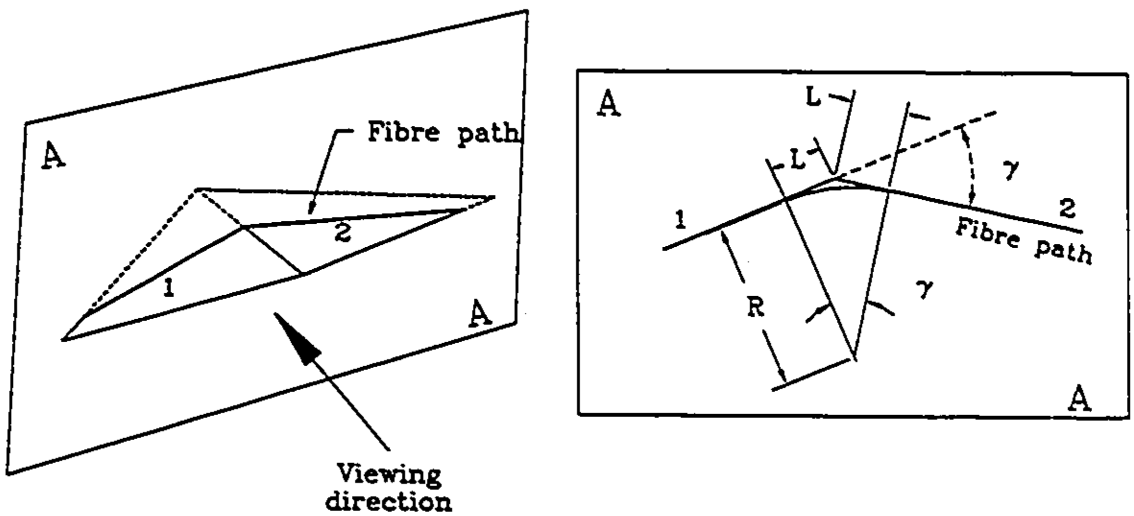

Figure 3.8 Artificial normal curvature of the fibre path at the triangle boundary.

Another plane is defined which contains segment 2 and intersects the first plane at right angle as shown in Figure 3.9. The projection of the segment 1 on this plane makes a straight line with segment 2. This is always the case for a geodesic path.

For a stable non-geodesic path, segment 2 is rotated at the boundary about the surface normal by an angle β. The straight line obtained earlier is now broken (Figure 3.9). The artificial curvature in this case is not equal to zero and can be defined just as the normal curvature. Again the same arbitrary distance L is used to trace a tangent arc between the two segments. The angle β and length L are used to obtain the radius of the arc. The inverse of this radius is the artificial geodesic (or tangential) curvature of the path at the intersection of these two segments:

$$K_g = \frac{\tan(\frac{\beta}{2})}{L} \tag{3.19}$$

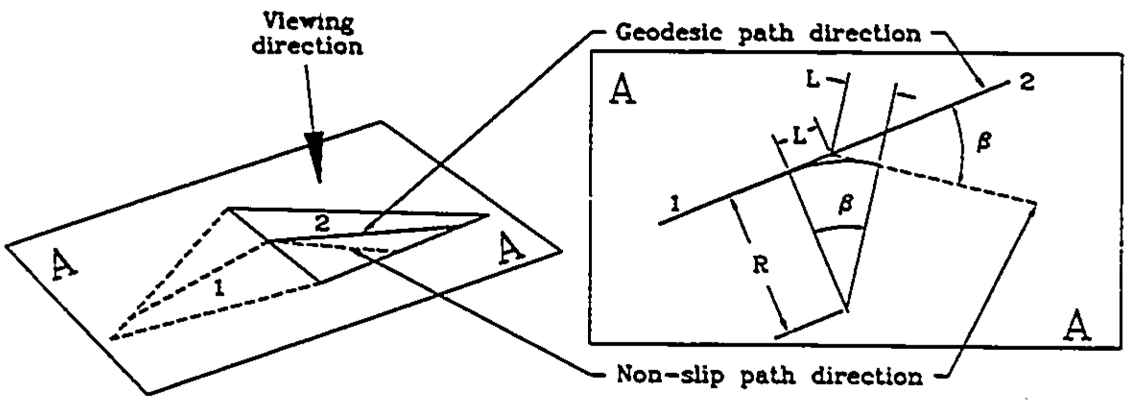

Figure 3.9 Artificial geodesic (tangential) curvature of the fibre path at triangle boundary.

For small angles, the tangent can be approximated by the angle itself. Using this fact and Equation 3.2 the expression for stable non-geodesic paths is obtained:

$$\beta = \delta \mu \gamma \tag{3.20}$$

In order to predict a stable non-geodesic path from one triangle to the next, the geodesic path is found first. With this, the value of γ is calculated and substituted in the expression above to get the rotation angle β. The geodesic path direction on the second triangle is then rotated about surface normal by the amount β to obtain a stable non-geodesic path. The cycle then starts over by obtaining a geodesic path segment on the next triangle. Due to the approximation of the tangent function by the angle itself, the relative inclination of adjacent triangles must be kept small for predicting stable non-geodesic paths. The accuracy associated with generating this type of path is discussed in Chapter 5.

The computational efficiency of the triangulation technique is the same for both rotationally symmetric and asymmetric shapes. The major factor affecting the efficiency is the data access speed. Large amount of storage space are required for the triangulation topology file. The efficiency of path computation will therefore be limited by the data access speed instead of the computing speed.

Surface coverage optimization techniques should easily adapt to the triangulation algorithm. The fibre build-up on the mandrel surface requires an alteration of the surface geometry. This is a simple task for the triangulation technique where the triangle vertices are simply translated to reflect changes in geometry.

Stress analysis software package should be able to retrieve specific information. The topology file for the triangular mesh could possibly be used directly for stress analysis along with the data it has on the fibre strand orientation.

It would also be possible to trace the path in real time instead of storing the huge amounts information for later retrieval. This is possible using triangulation because of the low computational effort. All that would be required in this case are the starting condition and the variation on the friction multiplier.

3.3 Evaluation of Path Prediction Techniques

3.3.1 Path prediction on surfaces of revolution

The fibre path for rotationally symmetric components is repeatable: after a certain number of circuits the fibre will be laid next to the initial path resulting in a characteristic pattern. Consequently, there is a need for high accuracy in order to determine the required parameters for this repeatable pattern.

(i) Cones and cylinders method

The cones and cylinders method produces highly accurate results but difficulties arise during data sampling. Because of its simplicity, it can be implemented using classical graphical techniques. Its main disadvantage is that it cannot be used to predict stable non-geodesic paths.

(ii) Triangulation method

Although the triangulation technique can be used to deal with rotationally symmetric mandrels, it is not appropriate. The amount of storage space required for the triangulation topology file is several orders of magnitude greater than that required by the other methods discussed in this chapter. Instead of storing information on the surface of revolution profile, the entire surface geometry is recorded in the form of triangle vertex coordinates. Furthermore, the information stored is redundant since the triangles at a particular section of the mandrel are similar and only their position in space changes. Although triangulation can be used to predict stable non-geodesic paths, it is less accurate than the mathematical technique.

(iii) Mathematical method

The mathematical technique generates highly accurate results and can predict both geodesic and stable non-geodesic paths. The demands on storage space for the profile model is similar to the cones and cylinders method and much less than that of triangulation. The technique is quite efficient when multi-step numerical methods are used.

(iv) Summary

All three methods presented exhibit similar efficiencies in terms of computational effort. The cones and cylinders method is appropriate for classical graphical techniques but is not recommended for a filament winding CAD environment. The triangulation approach is not highly accurate and has large demands on storage space.

It is therefore recommended that the highly accurate mathematical technique, with modest storage requirements, be used within the CAD environment to predict stable fibre path on rotationally symmetric shapes.

3.3.2 Path prediction on asymmetric surfaces

Because of the nature of the stable fibre path on asymmetric mandrels, high accuracy is not required. As stated earlier, the paths usually do not turn around on the mandrel surface and instead, mechanical anchors are used to locate the fibre at the mandrel extremities while the pay out eye is realigned to place the fibre strand on a completely new path.

Laying the fibre on a stable path and obtaining acceptable surface coverage properties are the main concerns for filament winding of asymmetric mandrels. Unfortunately, no equation exists to predict the fibre distribution on this type of mandrel. As new fibre paths are calculated, changing surface coverage properties, at specific locations on the mandrel, must also be recorded.

(i) Cones and cylinders method

The cones and cylinders technique cannot be used since it is suitable for rotationally symmetric shapes only.

(ii) Mathematical method

The computing efficiency of the mathematical technique decreases for asymmetric mandrels. The circumferential and cross derivative terms in the differential equation are no longer equal to zero for asymmetric shapes and, consequently, cannot be eliminated. These terms must be computed and substituted into the differential equation at every step of the numerical solution. The efficiency is also affected by an increase in data sampling required for recording surface coverage properties such as fibre orientation and thickness distribution. Moreover, it was reported in [28] that the differential equation is stiff by nature and that special numerical methods are required to obtain a solution.

The mathematical technique remains highly accurate when compared to any geometric approach. However, high accuracy is not required since finding a repeatable pattern is not the objective.

The geometry of the mandrel surface also changes as more fibre strands are placed. For rotationally symmetric shapes, the profile could easily be modified to reflect these changes. The task is not as simple for asymmetric shapes since a three-dimensional surface representation, instead of a two-dimensional profile, must be altered.

(iii) Triangulation method

This method is less accurate than the mathematical technique but again high accuracy is not as important for asymmetric surfaces. The efficiency of the triangulation method does not change when going from rotationally symmetric to asymmetric shapes since the algorithms are identical.

A definitive advantage of this technique is the ease with which the mandrel surface geometry can be modified to reflect fibre build-up. It is therefore adaptable to surface coverage optimization algorithm. Another advantage is the similarity between the triangulation surface model and the models used by finite element stress analysis techniques. Finally, the possibility of predicting the stable fibre path in real time is a very attractive feature for a filament winding CAD environment.

(iv) Summary

Although the mathematical approach generates more accurate results, the triangulation method has several advantages which compensate for this. There is strong evidence that the triangulation computational efficiency is higher. It is also more readily adaptable for recording surface coverage properties (topology file already exists) and for modifying the surface geometry to reflect fibre build-up. In short, triangulation is more appropriate for the filament winding CAD environment.

The triangulation method is recommended over a differential equation approach for predicting stable fibre paths on asymmetric components. The scheme used to implement the triangulation method is discussed in greater detail in Chapter 4. To use the method effectively, factors affecting accuracy, computational efficiency and storage difficulties must be well understood. Accuracy evaluation is discussed in Chapter 5.

CHAPTER 4

DEVELOPMENT OF ALGORITHMS

There are several steps involved in obtaining a stable fibre path on a mandrel using the triangulation method. The initial step is to construct a triangulated model of the mandrel surface. The approach will vary depending on whether or not the triangle distribution is to be optimized. The triangle information is then stored in a topology file. The specified starting conditions are used to find the starting triangle and path direction vector. The path is then extended from one triangle to the next until it satisfies a certain termination criterion. The following sections describe the methods developed in this work to accomplish the different tasks presented above.

4.1 Surface Description

The surface representation using triangle patches can be carried out under designer control or with an algorithm which optimizes the triangle distribution. The former approach is simpler and less demanding in terms of surface definition. The coordinates of points on the surface, needed to construct the topology file, are required for a finite number of discrete locations only. When optimization of the triangular patches is required, the coordinates of any point on the surface must be available and therefore, the surface must be defined everywhere. If the component is composed of geometric shapes for which the analytical equation is known then these equations can be used to get the triangle vertices. This approach does not result in a general procedure since the mandrel will rarely be an assembly of such geometric shapes. A better alternative is to use a surface representation which can easily be manipulated by the designer. Most CAD software packages come equipped with a facility for describing free form surfaces. The nature of the surface definition technique must be interactive in allowing the operator to shape the mandrel surface to fulfil design specifications. After completing the surface definition, its parametric curves can be used to generate the triangle vertices with respect to the optimization procedure. The details of the approach used by the author are given below. Three cases are covered, two for rotationally symmetric components and one for asymmetric components.

4.1.1 Non-optimized triangles for rotationally symmetric shapes

The non-optimized triangulation for surfaces of revolution is performed as follows. The operator specifies the meridian angle (increment angle along circumference), the height to base ratio of the triangles and the triangle apex offset as shown in Figure 4.1. The result is a series of similar triangles of different size. The meridian angle, measured from the mandrel axis, controls the length of the base at a specific radius by generating two points on the circumference. The base length is then multiplied by the height to base ratio to get the height of the triangle. Finally, the apex position is defined in the axial direction by the triangle height and in the circumferential direction by means of the apex offset angle. This angle is measured from the mandrel axis using as a zero reference the same angular position as "B1" in Figure 4.1. An apex offset angle of zero degrees means the apex is at the same longitude position as the origin of the base "B1".

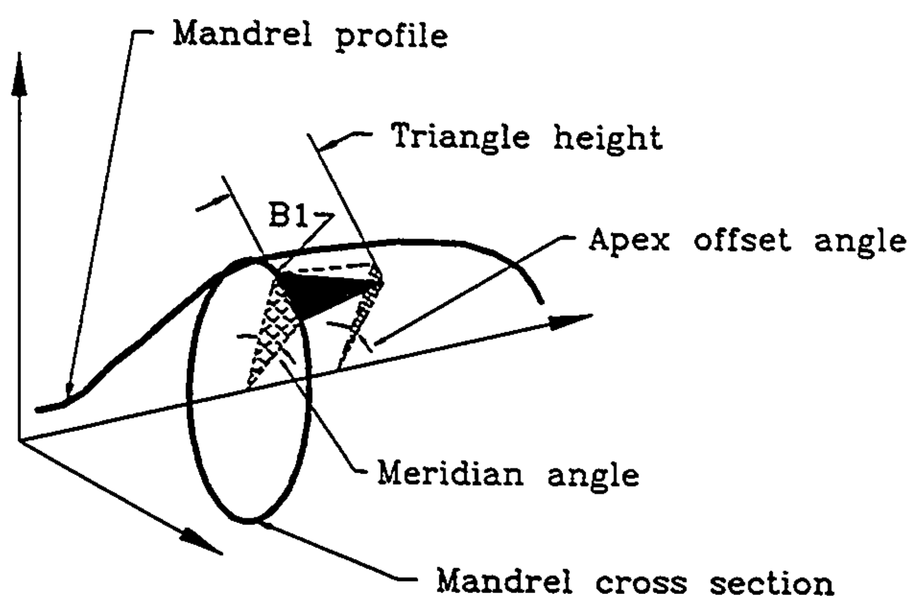

Figure 4.1 Non-optimized triangle parameters for rotationally symmetric shapes.

4.1.2 Optimized triangles for rotationally symmetric shapes

The optimized triangulation of surfaces of revolution is somewhat different from the non-optimized version. Here the operator specifies the maximum deviation, calculated at the triangle boundary, of the mandrel surface from the surface of the triangle patch. Figure 4.2 shows two cross sectional views of a surface of revolution. The circumferential and profile surface deviation limit is used to modify the density of triangles. Again here, an offset angle is used to position the apex in the circumferential direction. This method has the advantage of generating models using fewer triangles for the same accuracy on the path since the triangle height is not limited by the length of the base. Also, the surface deviation criterion gives a much better results in terms of accuracy on the fibre path. Both of these points will be discussed later in Chapter 5.

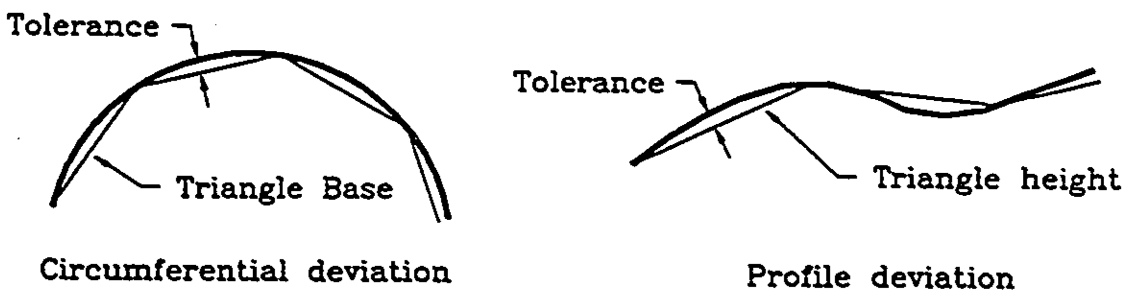

Figure 4.2 Optimized triangle parameters for rotationally symmetric shapes.

4.1.3 Non-optimized triangles for asymmetric shapes

The last triangulation method to be discussed is that for a certain class of asymmetric shapes. In the first step, a backbone for the asymmetric surface is defined in three dimensional space as shown in Figure 4.3. The designer specifies the radius of a circle which will then be driven perpendicular to the backbone in order to define the surface. The circle's centre corresponds to the piercing point of the backbone. The operator also specifies a minimum separation distance between the cross sections used to define the triangles. As the circle is driven along the backbone, and the minimum distance is obtained, the triangles are defined along the circumference using the meridian angle. Again here, the information obtained from the triangulation procedure is stored in the topology file.

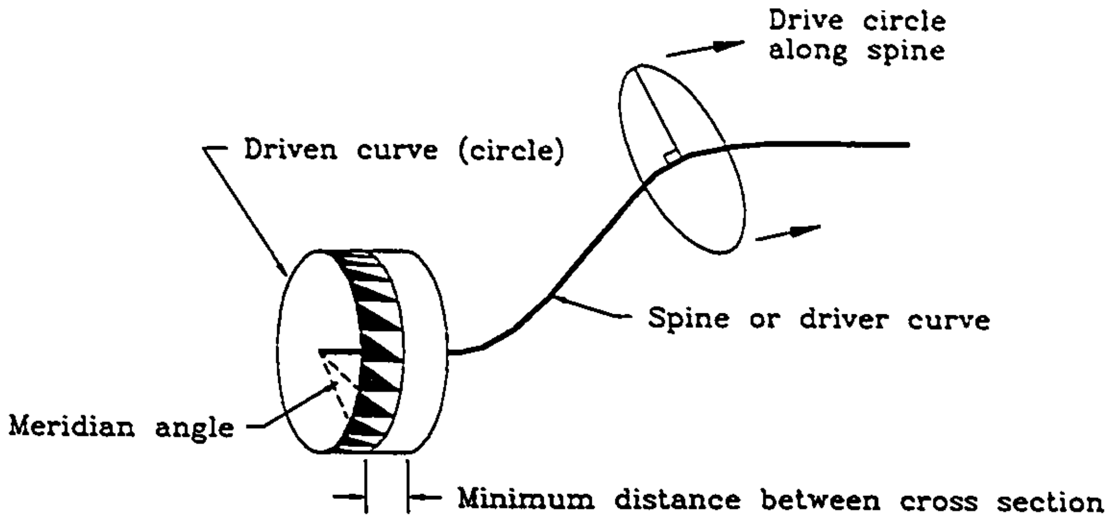

Figure 4.3 Non-optimized triangle parameters for tubular asymmetric shapes.

At present, the algorithm is limited to shapes having constant circular cross sections along the entire length of the backbone. This can easily be expanded to include any unbranched component by using varying cross sections along the backbone. Branched components are more difficult to triangulate using this procedure because of the step change encountered in the cross-section at the beginning of the branch.

4.2 Topology File Contents

Each record in the topology file contains information corresponding to a specific triangle on the mandrel surface. The information is stored in binary format as opposed to text format to speed up information access. The structure of the record is discussed in Chapter 6 and consist of: coordinates in 3-D space of the vertices, vector for surface normal (used often and saves repetitive calculation) and for each boundary, the identification number of the adjacent triangles. This identification number corresponds to the location of the triangle record in the topology file. The record information can be expanded to include other details deemed important. The laminate thickness could also, for example, be recorded for each triangle affected as the fibre path is being generated.

4.3 Fibre Path Prediction

The information required to start a fibre path are the starting position on the surface and the direction to follow. The starting point can be specified anywhere along the axis for rotationally symmetric surfaces and only at the exterior boundary for asymmetric surfaces. The circumferential position is defined by a user entered angle measured from the axis revolution or from the backbone curve depending on the type of surface. Vector algebra is then used to find the corresponding starting triangle in the topology file. The initial path direction is obtained by rotating the orientation of the triangle base by a specified angle about the triangle surface normal as depicted in Figure 4.4.

Prediction of the stable fibre path can now begin and proceeds as was explained in Chapter 3.

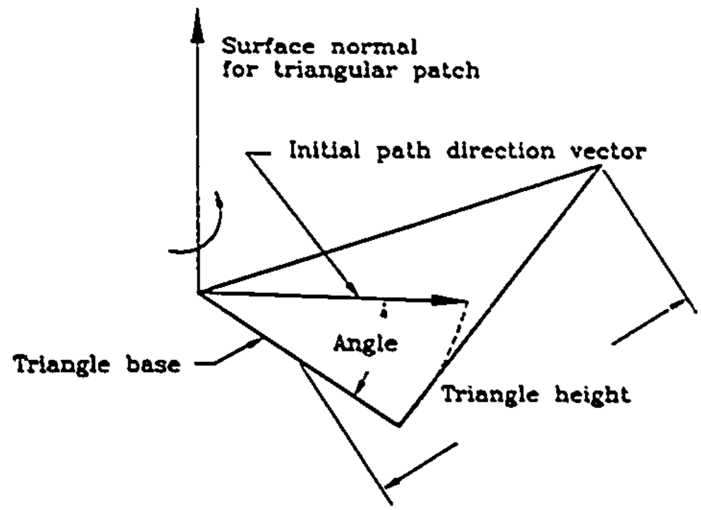

Figure 4.4 Initial orientation of fibre path obtained by rotating triangle base about surface normal.

4.4 Termination Criteria

4.4.1 Rotationally symmetric shapes

The nature of the termination criteria depends on whether the mandrel is rotationally symmetric or asymmetric. For rotationally symmetric components, the displacement along the rotation axis is monitored. The designer specifies the maximum number of turn arounds which becomes the termination criterion. The occurrence of a turn around is identified when the direction of axial displacement changes. The path generation can also be halted if it extends outside the boundaries of the surface. This latter situation can easily occur when computing stable non-geodesic paths.

4.4.2 Tubular asymmetric shapes

The termination criteria are different for asymmetric mandrels since turn arounds are not likely to occur and, as a rule, are not desired. Again here, there is a normal termination process and a secondary one used to prevent endless loops. Normal termination occurs when the predicted path reaches an external surface boundary. This situation is monitored, and when it occurs the designer is notified and given the option to generate a new path. In some cases it is possible for the path to turn around before it reaches a boundary. If this occurs over and over the program is caught in an endless loop. To prevent this situation from occurring, the designer prescribes an upper bound on the number of triangles that a particular path can intersect.

4.5 Surface Coverage

Fibre coverage for rotationally symmetric mandrels is predictable and easily controllable however, as mentioned in Chapter 3, this is not the case for asymmetric shapes. The approach used by the author is to lay several neighbouring paths parallel to each other until the stability criterion is violated. When this occurs, a new template path is generated from which a series of parallel fibre paths will again be defined. The two most important factors to obtaining many parallel fibre path adjacent to each other are: minimization of the friction multiplier magnitude and verification of parallelism at specified path segment intervals rather than for each individual path segment.

The first task in starting a parallel path consist of finding the initial starting point and path orientation. Poor results are obtained if the position and orientation are simply translated by the offset distance. A better alternative is to use the following procedure in defining the starting parameters for parallel paths. With reference to Figure 4.5, a path segment close to the starting point of the template "a" is chosen as a reference. A new direction "b" perpendicular to "a" is defined and a path is extended in this direction until the total distance travelled is equal to the bandwidth of the fibre. The path direction is then again rotated ninety degrees so that it points towards the starting external boundary. This path direction "c" is extended until it intersects the external boundary. The point of intersection "d" and the last direction vector "e" are then used as the starting parameters.

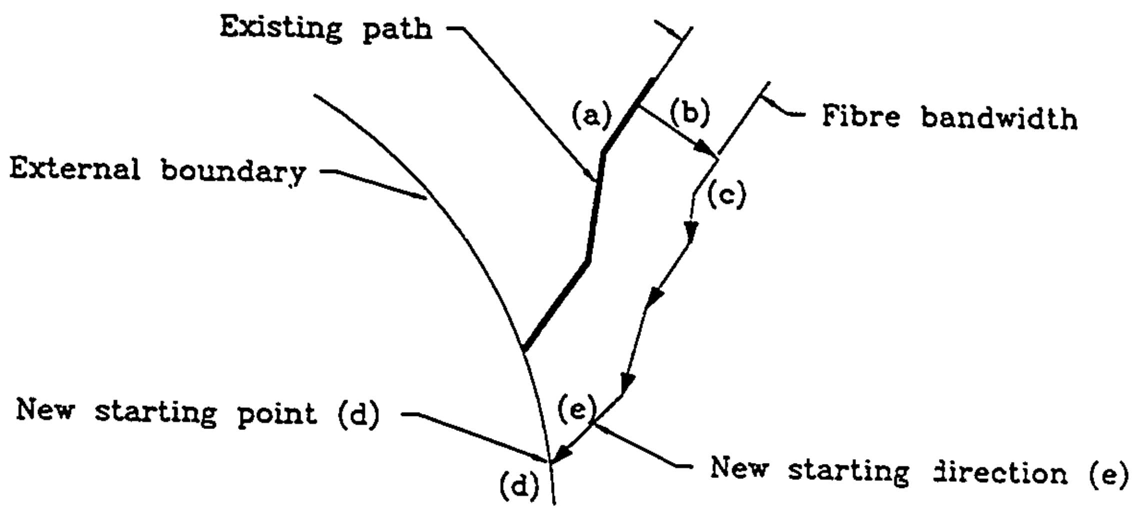

Figure 4.5 Defining the starting parameters for a path parallel to a reference path on tubular asymmetric shapes.

The paths begins with these parameters and extends through several triangles whose number is specified by the designer. The distance between the current path and the previous parallel path is calculated to determine if it violates the parallelism criterion. The criterion is based on the following: the calculated distance between the adjacent paths is subtracted from the required offset distance, the absolute value of this result must be smaller than a fibre bandwidth tolerance value specified by the designer. If the criterion is violated, the surface friction multiplier, defined in Chapter 3, is increased and the path is recalculated from the last acceptable point. This continues until this portion of the path is deemed acceptable. The separation distance, between the points where parallelism is evaluated, may exceed the bandwidth tolerance. This, however, is acceptable since it is extremely difficult to control each data point along the way due to the fact that the generated path is an assembly of line segments drawn on a triangulated surface approximation and not an analytical function. The process continues until the external boundary is reached at the other extremity. The newly generated path is now used as the reference template for evaluation of parallelism, and the entire cycle is repeated.

Parallel fibre paths will be generated sequentially on both sides of the first template path used. The final result, shown on the tubular S-bend shape of Figure 4.6, is a group of fibre paths forming a wide band. The designer controls the placement of these bands in an effort to cover the entire mandrel surface. The resulting bands are shown on the computer screen to facilitate this process.

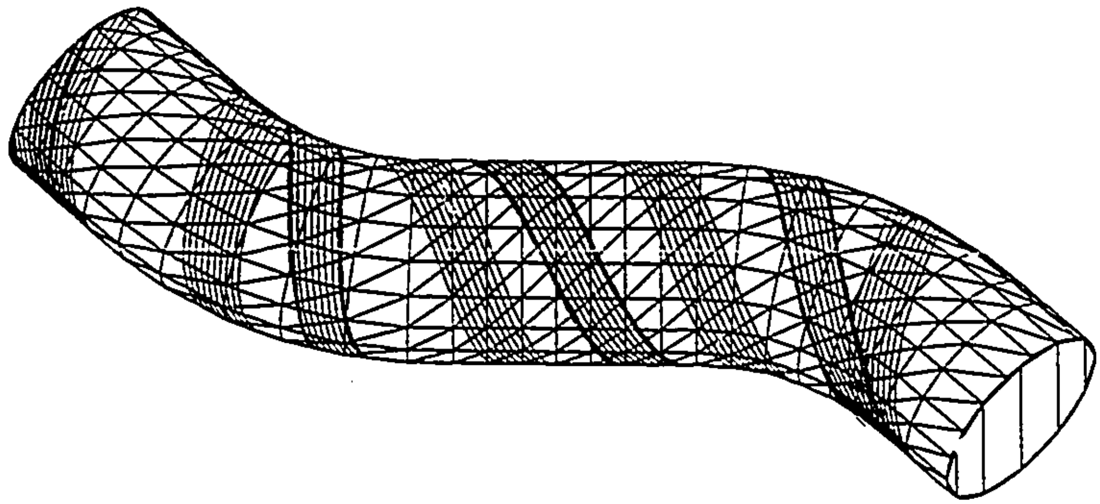

Figure 4.6 Tubular S-bend showing two wide bands of parallel fibre paths.

CHAPTER 5

ACCURACY EVALUATION OF THE TRIANGULATION TECHNIQUE

A thorough understanding of the factors affecting the accuracy of the predicted fibre path is essential for the development of effective path prediction algorithms. This knowledge will also guide the designer during the construction of the triangulation topology file.

In the opening section of this chapter, the terms used to describe the accuracy of the predicted fibre paths are defined. Two methods developed to evaluate the accuracy of fibre paths obtained from triangulated surface models are then presented. The first technique is capable of evaluating path prediction errors on a spherical shape while the second is appropriate for any rotationally symmetric surface. These topics are followed by a series of error calculation tests through which some of the critical parameters affecting accuracy are identified.

5.1 Definition of Important Terms

5.1.1 Error calculation

There are two terms used to describe error calculations. The term deviation error signifies the distance between a fibre path obtained by the triangulation method and a reference path. The separation distance is always calculated perpendicular to the path being evaluated. The deviation error has a dimension of length with the same units as those used to describe the mandrel geometry. To show this fact, all dimensions with the same length units are attributed the symbol u: eg. sphere radius = 50u, triangle tolerance = 0.001u.

The nondimensional error is an artificial representation of the rate at which the deviation error increases along the path. The artificial nature results from the assumption that the deviation error term is equal to zero at the beginning of the path and steadily increases as the path progresses. The nondimensional error is obtained as follows: each calculated deviation error is multiplied by the incremental distance travelled since the last error calculation. The cumulative result of this operation is divided by the square of the total distance travelled to complete the path. Multiplication of the nondimensional error by the distance travelled along the path represents the total surface area between the reference path and the path being evaluated.

5.1.2 Graphical representation of error terms

The deviation error is a qualitative representation which shows the relative oscillations between the path being evaluated and the reference path. It is plotted as a function of the normalized displacement along the path. The normalization is performed by dividing the actual distance travelled by the total displacement required to complete one path cycle. The horizontal scale ranges from 0.0 to 1.0 since the deviation error is evaluated for one path cycle only. The nondimensional error is used as a quantitative accuracy representation to compare the accuracy of fibre paths subjected to different conditions. It is plotted as a function of the parameter being evaluated.

5.1.3 Triangulation surface tolerance

In Chapter 4, the term tolerance was used to characterize the deviation of the original mandrel surface from the surface of the triangle used in the approximation. The same definition of tolerance is used here, with dimension of length having the same units as those used for mandrel sizing.

5.2 Description of Error Calculation Techniques

Two methods are needed to evaluate the error terms on different types of mandrels. The sphere is used for initial testing but due to certain limitations, more tests are performed on general surfaces of revolution. The description of the individual methods is given in the following sections.

5.2.1 Spherical shapes

The accuracy of path prediction methods is evaluated by calculating the deviation error between the predicted fibre path and the exact path. Geometric shapes for which the exact fibre path is known are limited. These shapes were discussed in the literature review while describing geometric techniques for fibre path prediction. For a sphere, the geodesic paths are described by great circles. The stable non-geodesic paths, on the other hand, are defined by the circles of intersection of a plane passing at a specified distance from the sphere centre. This distance is a function of the coefficient of surface friction and the friction multiplier (Equation 3.2). Knowledge of the exact solution for both geodesic and stable non-geodesic paths makes the sphere a excellent candidate for accuracy evaluation.

Due to the nature of stable paths on spherical mandrels, only two parameters are needed to describe the exact path. These two parameters are the plane orientation and its distance from the sphere centre. The distance from the sphere centre is calculated using the surface friction and the friction multiplier. In Figure 5.1, the exact fibre path appears as a straight line in the side view and as a circle in the front view. Both the path curvature K and its component directed along the surface normal K_n are known. K equals the inverse of the radius for the circle of intersection while K_n equals the inverse of the sphere radius. The geodesic component K_g of the curvature can therefore easily be found:

$$K = \frac{1}{\sqrt{R_{sphere}^2 - d^2}}$$

$$K_n = \frac{1}{R_{sphere}} \tag{5.1}$$

$$K_g = \sqrt{K^2 - K_g^2} = \frac{d}{R_{sphere}\sqrt{R_{sphere}^2 - d^2}}$$

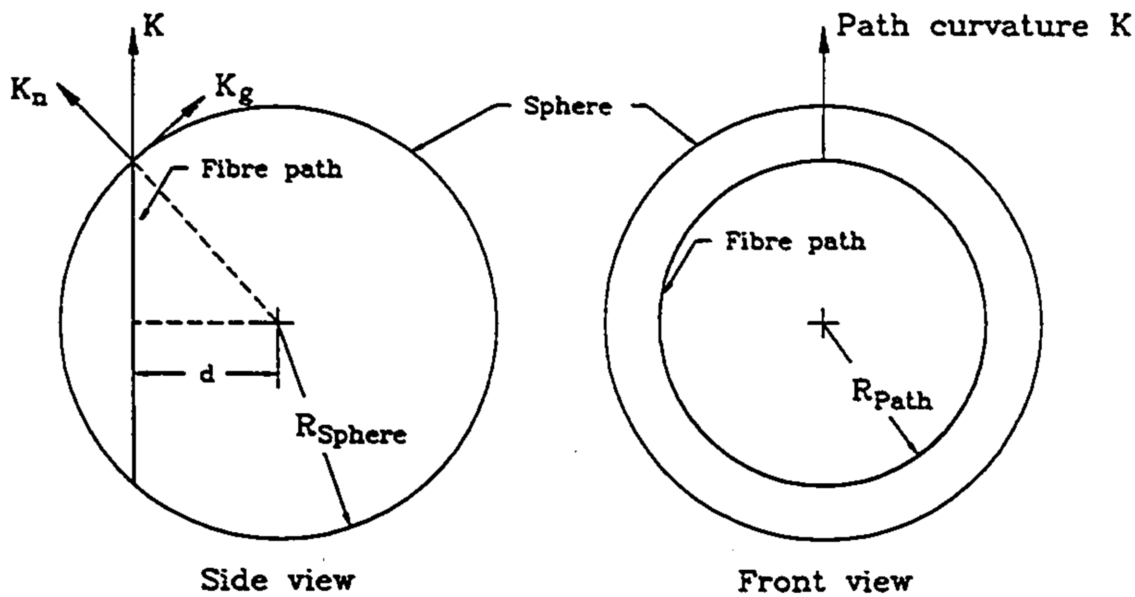

Figure 5.1 Exact fibre path on the sphere.

The distance of the cutting plane from the sphere centre is calculated using the path stability criterion and the definitions obtained for the curvature component K_n and K_g:

$$d = \frac{\delta \mu R_{sphere}}{\sqrt{1 + (\delta \mu)^2}} \tag{5.2}$$

The orientation of the plane defined by the fibre path is calculated from the path data points. The starting position is taken as a reference point. Vectors are defined using the reference point as the origin and points along the path as the end. A cross product vector is obtained using two non-consecutive vectors separated by eight data points as shown in Figure 5.2. More cross product vectors are calculated by indexing this procedure along the entire path. These newly obtained vectors are added together vectorially and normalized. The normalized vector obtained represents the normal vector of the fitted plane used for error calculation on the sphere.

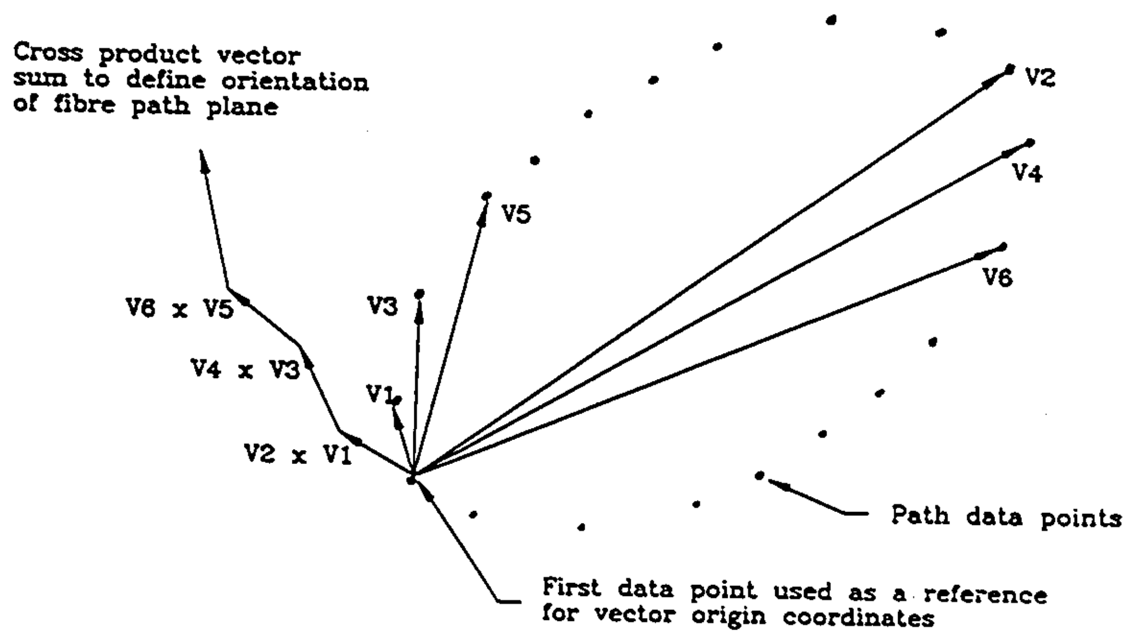

Figure 5.2 Technique used to define orientation of cutting plane.

With the plane representing the exact solution positioned it is possible to calculate the distance which separates the data points from the plane surface. This is done using vector algebra, the details of which can be found in the computer program given in Appendix C.

5.2.2 General rotationally symmetric shapes

The exact solution for the stable fibre path is not known for general surfaces of revolution. The alternative is to use the best approximation for the exact fibre path as a reference. The mathematical approach described in Section 3.1 is used to calculate a fibre path which will serve as a benchmark. This solution is approximate since a numerical method is used to generate the path.

The deviation error is obtained at each data point on the path being evaluated by calculating the distance between the data point and the benchmark path. The benchmark path has at least three times the density of data points than that of the path being evaluated. This makes the reference path much smoother and facilitates the calculation of the deviation error. The specifics of this error measuring technique can be found in the computer program given in Appendix C.

5.3 Accuracy Evaluation of Triangulation on Spherical Shapes

5.3.1 Non-optimized triangular meshing

The accuracy of the triangulation method, using two meshing techniques, was verified with a sphere having a radius of 50u. The non-optimized triangle meshing technique describe in Section 4.1.1 was used to evaluate the effect of triangle geometry on the accuracy. This was done by controlling the meridian and apex offset angles. The triangle height to base ratio was kept constant at unity for the accuracy evaluation on the sphere since this shape is symmetric in all directions and therefore, it was deemed appropriate to keep the triangles as symmetrical as possible.

In the first test, the apex offset angle was kept constant at 0°. Meridian angles of 10°, 9°, 7.2°, 5°, 3° and 2° were then chosen for testing. Figures 5.3 and 5.4 show that the oscillation of the deviation error are quickly attenuated in the range of 10° to 5° and then the attenuation rate decreases. The nondimensional error graph of Figure 5.5 shows this more effectively. Based on these results, in subsequent test a meridian angle of 3° was used since it offers a good compromise between accuracy and storage space for the topology file (3.5 Megabytes per file).

Four surface approximations were then tested to evaluate the effect of the apex offset angle. In this group of tests, the meridian angle was kept constant at 3°. The apex offset angle was varied in 0.5° increments from 0° to 1.5°. At 1.5° offset, the apex is aligned with the centre of the base obtained with a meridian angle of 3° and the triangle is isosceles. At apex offset angles higher than 1.5°, mirror images of the triangles generated at the lower offset angles are obtained. A triangle with an apex offset of 2.5°, for example, is the mirror image of one having an apex offset of 0.5°. The deviation error graph of Figure 5.6 shows that the amplitude of the error oscillations is not affected to a great extent by the triangle apex offset. There is however a slight increase in inaccuracy for an offset of 1.0° and 1.5° which can be seen better with the nondimensional error graph of Figure 5.7.

The last test using this meshing technique involved starting conditions. The objective of this test was to show that a slightly different starting condition can affect the accuracy of the path. The fibre path was started at different locations within a particular triangle while the remaining parameters were kept constant. Four starting positions were used in the tests and are represented in Figure 5.8. The starting position within the triangle was normalized with the triangle height. The results of Figure 5.9 show that the accuracy is affected by the location of the starting point. However, from the nondimensional error graph of Figure 5.10, this deviation would seem to behave in a random fashion. After reexamination of the triangulation technique, the author concluded that the randomness is a result of the particular set of triangles intersected along the path. Consequently, it is possible to improve or worsen the accuracy of a fibre path generated from triangulation by altering slightly the starting parameters.

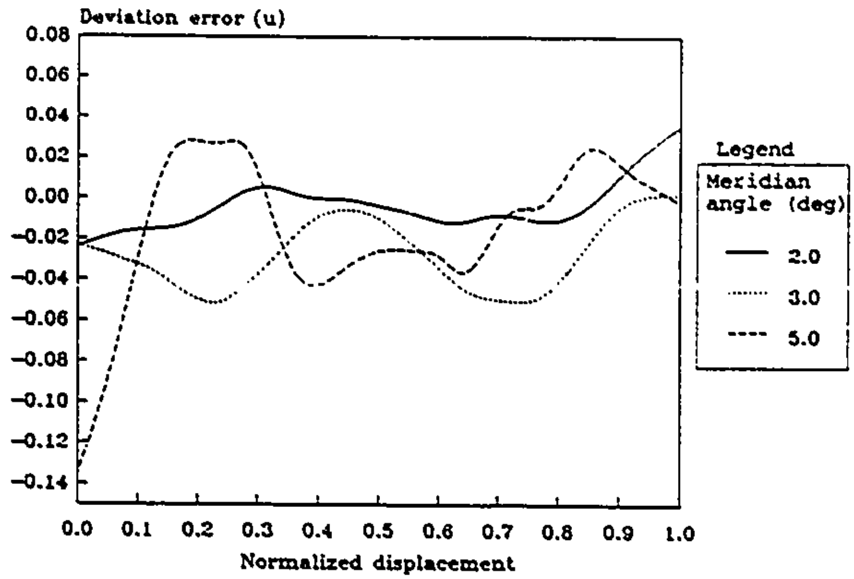

Figure 5.3 Meridian angle test on sphere, geodesic path: Deviation error vs Normalized displacement (sphere radius 50u, apex offset 0°).

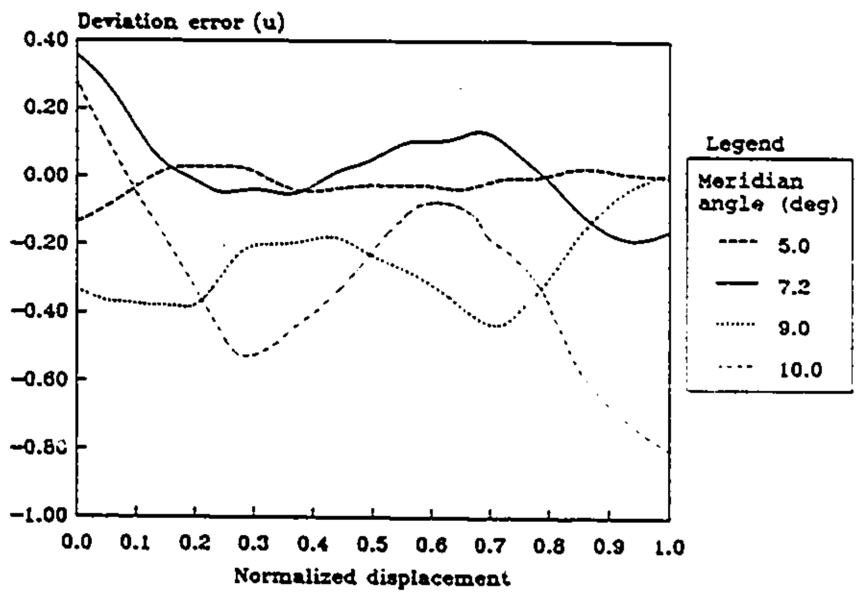

Figure 5.4 Meridian angle test on sphere, geodesic path: Deviation error vs Normalized displacement (sphere radius 50u, apex offset 0°).

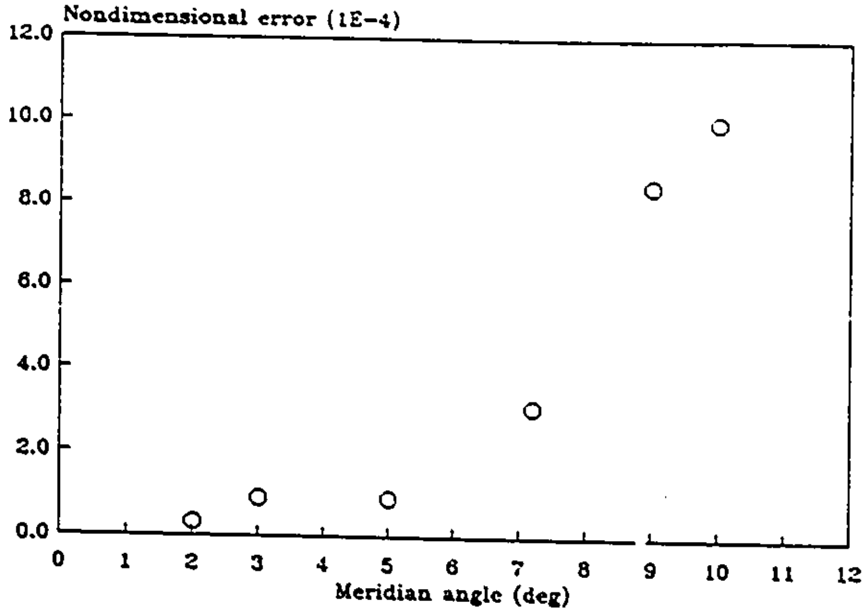

Figure 5.5 Meridian angle test on sphere, geodesic path: Nondimensional error vs Meridian angle (sphere radius 50u, apex offset 0°).

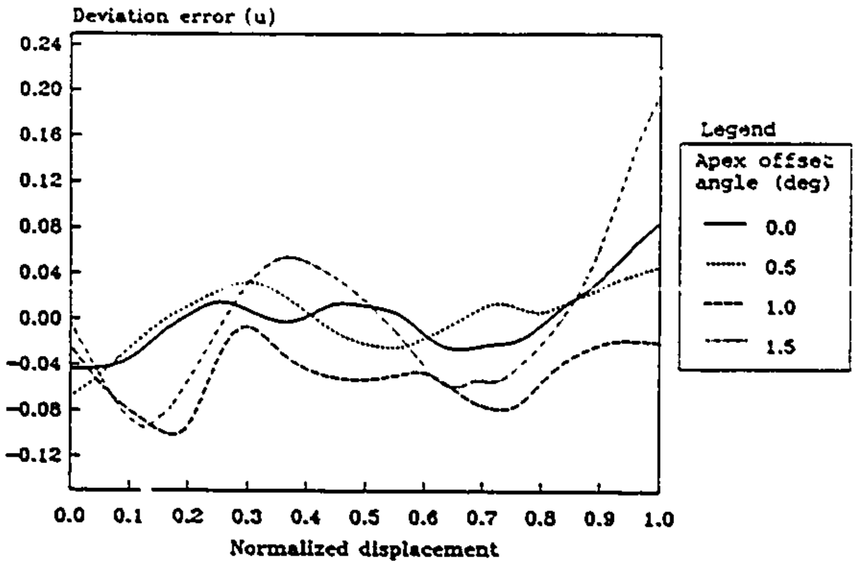

Figure 5.6 Apex offset angle test on sphere, geodesic path: Deviation error vs Normalized displacement (sphere radius 50u, meridian angle 3°).

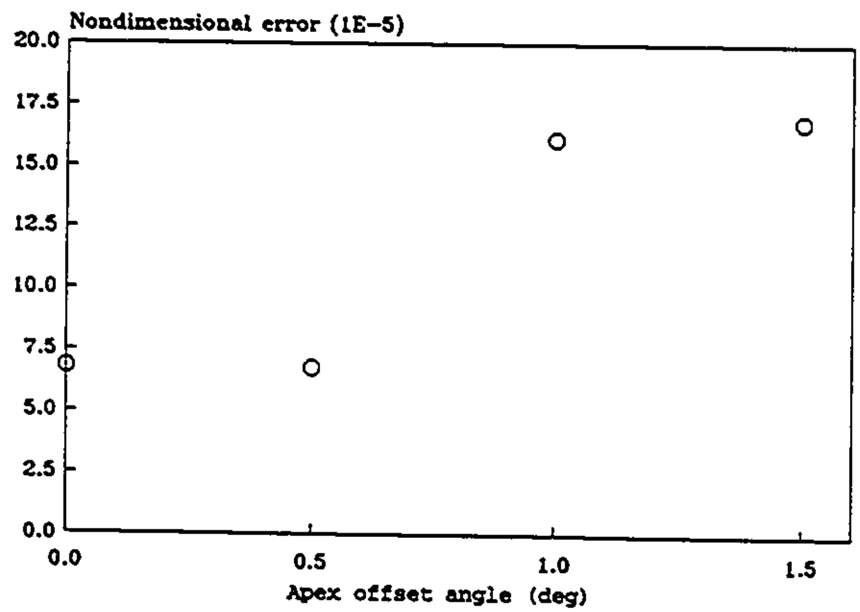

Figure 5.7 Apex offset angle test on sphere, geodesic path: Nondimensional error vs Apex offset angle (sphere radius 50u, meridian angle 3°).

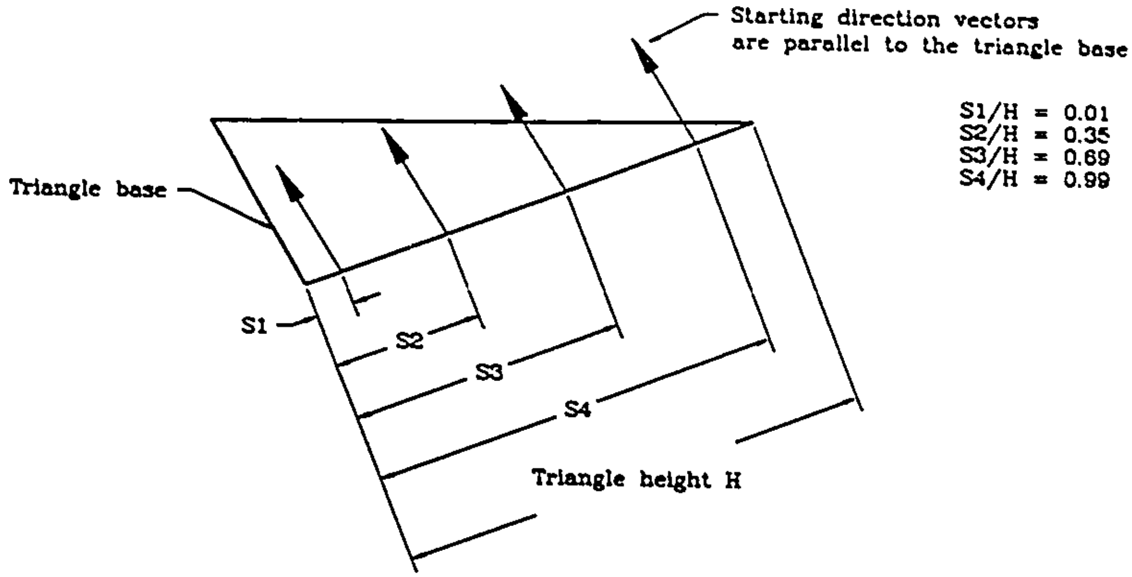

Figure 5.8 Normalized starting position within a particular triangle. Path starting direction is parallel to the triangle base.

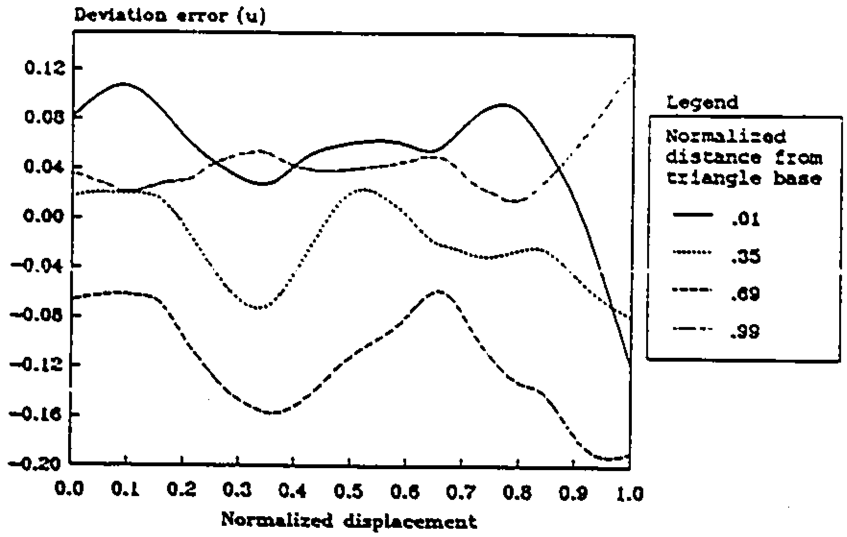

Figure 5.9 Starting position test on sphere, geodesic path: Deviation error vs Normalized displacement (sphere radius 50u, meridian angle 3°, apex offset 0°).

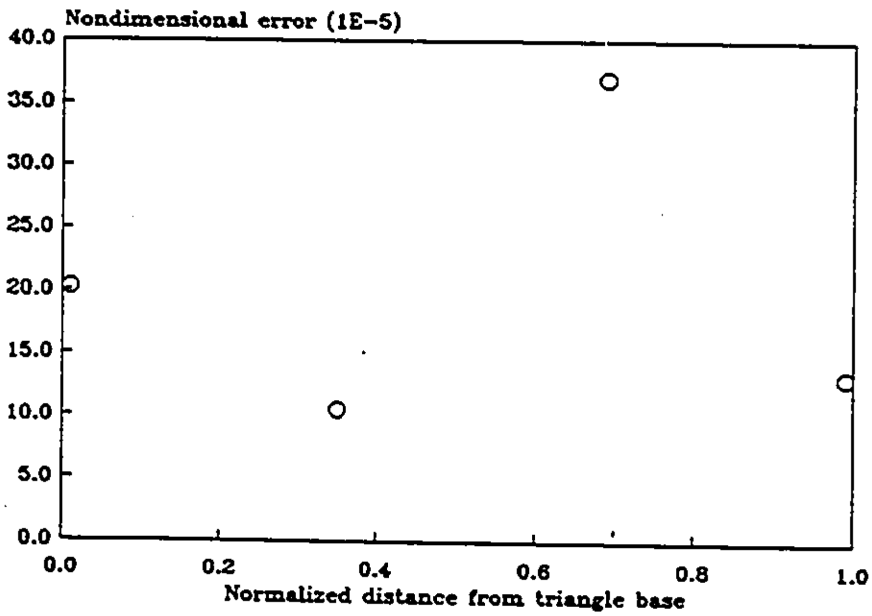

Figure 5.10 Starting position test on sphere, geodesic path: Nondimensional error vs Normalized starting position within triangle (sphere radius 50u, meridian angle 3°, apex offset 0°).

5.3.2 Optimized triangular meshing

The optimized triangle meshing technique of Section 4.1.2 is based on the maximum deviation of the sphere surface from the triangle patch. This approach allows the designer to control how close the model will duplicate the mandrel curvatures. Four triangulated sphere models with radius of 50u were created having tolerances of 0.04u, 0.02u, 0.01u and 0.005u.

Figures 5.11 and 5.12 depict the resulting error calculations for geodesic paths. As the magnitude of the triangle tolerance decreases, so does the amplitude of the undulation for the deviation error of Figure 5.11. The rate improvement in the path accuracy for alternately smaller values of tolerance is shown by Figure 5.12.

The same tests where performed for stable non-geodesic paths with surface friction μ=0.216 and friction multiplier values of δ=-0.5 and δ=1.0, respectively. The oscillation amplitude attenuation of the deviation error can again be seen in Figures 5.13 and 5.15 for friction multipliers δ of -0.5 and 1.0 respectively. However, the improvement in accuracy with smaller values of triangle tolerance is relatively less significant than the earlier case as demonstrated by the nondimensional error graphs of Figures 5.14 and 5.16. The results displayed in Figure 5.15, where the maximum value of 1.0 for the friction multiplier was used, are important since the deviation error remains approximately constant for a small tolerance value of 0.005u. The deviation error could be reduced in this case by evaluating the same triangulation path but modifying the friction multiplier δ of the reference path to δ=1.004. With this value for δ the path is no longer stable and surface friction cannot prevent the fibre from moving. Consequently, the maximum value of the friction multiplier δ should not be used even when very small value of triangle surface tolerance are employed.

The objective of the last series of tests performed with the spherical shape is to evaluate the effect of surface curvature on path accuracy. Four sphere models, having a radius of 12.5u, 25u, 50u, 75u and 100u, respectively, were used for these tests each having a triangle tolerance of 0.005u. The test results are represented by the nondimensional error vs sphere radius graph of Figure 5.17. The nondimensional error is large at small sphere radii and decreases exponentionally to become relatively small at large radii. Since the surface curvature is equal to the inverse of the sphere radius, the accuracy for high values of surface curvature is worse than that for low values of surface curvature (constant value of 0.005u for triangle surface tolerance). Consequently, smaller values of triangle tolerance will need to be used for high curvatures if the accuracy is to be controlled evenly over the entire surface.

The results presented above show that the accuracy of the fibre path is highly dependant on the closeness of fit between the triangulation surface model and the sphere. The erroı between the path generated by triangulation and the exact path is smaller for smaller meridian angles and smaller values of triangle tolerance. The curvature tests on the other hand, revealed that for the same value of triangle tolerance the accuracy was worse for higher curvatures. Furthermore, the accuracy is affected by the starting conditions and more specifically which set of triangles are intersected by the path. The stable non-geodesic path was seen to be unstable when the limiting surface friction is used to influence the fibre path. It is therefore recommended to use not more than 90 or 95% of the limiting surface friction.

The experimentation with the spherical surface plays an important part in gaining some insight into the performance of the triangulation method. The geodesic and stable non-geodesic paths are function of the surface curvature, the orientation the path with respect to the surface and, the coefficient of surface friction for stable non-geodesic paths. The sphere has a constant curvature equal to the inverse of its radius and as such does not provide a general platform for studying path accuracy. A more general shape, with varying surface curvature, is therefore required to quantify the accuracy of the triangulation method. General rotationally symmetric surfaces have a profile with varying curvature and a circular cross section with constant curvature. These types of surfaces are good candidates for accuracy evaluation of the triangulation method.

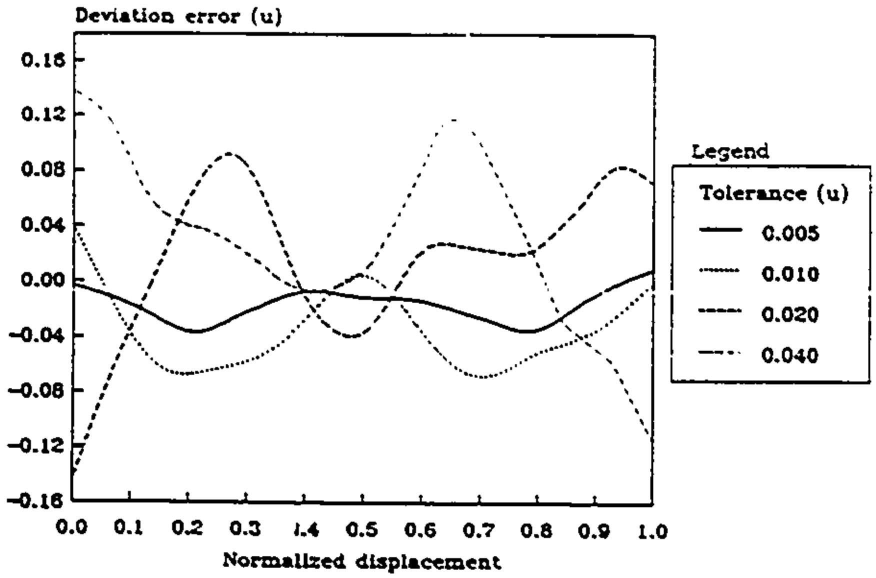

Figure 5.11 Triangle surface tolerance test on sphere, geodesic path: Deviation error vs Normalized displacement (sphere radius 50u, apex offset 0°).

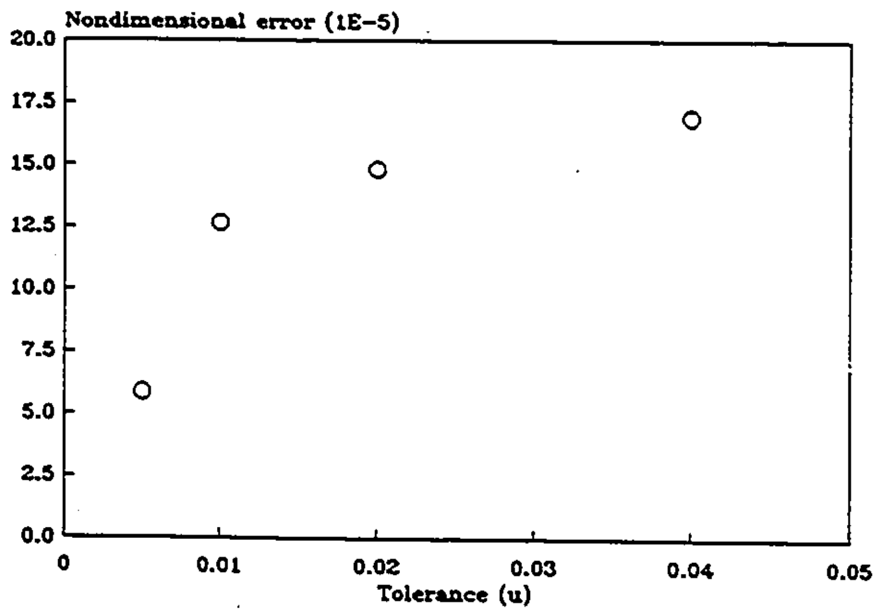

Figure 5.12 Triangle surface tolerance test on sphere, geodesic path: Nondimensional error vs Surface tolerance (sphere radius 50u, apex offset 0°).

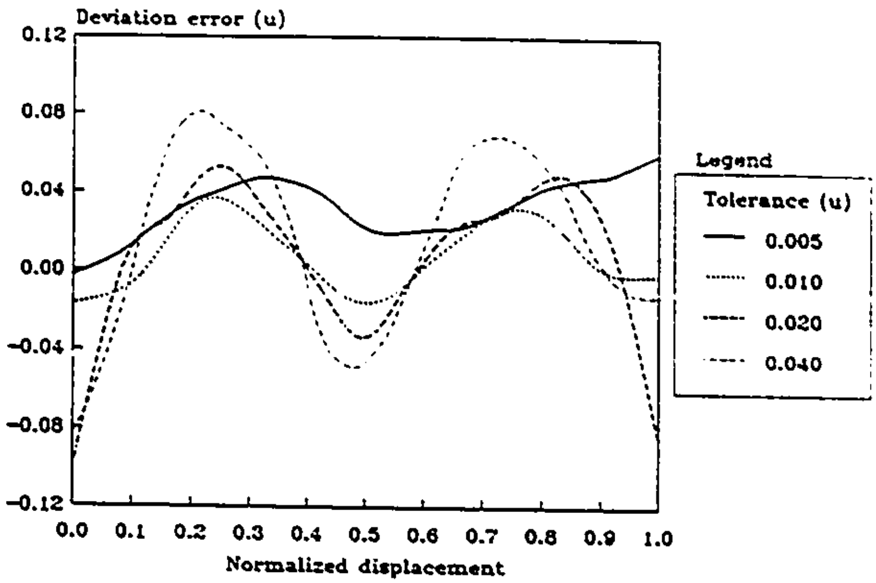

Figure 5.13 Triangle surface tolerance test on sphere, non-geodesic path: Deviation error vs Normalized displacement (sphere radius 50u, apex offset 0°, μ=0.216, δ=-0.5).

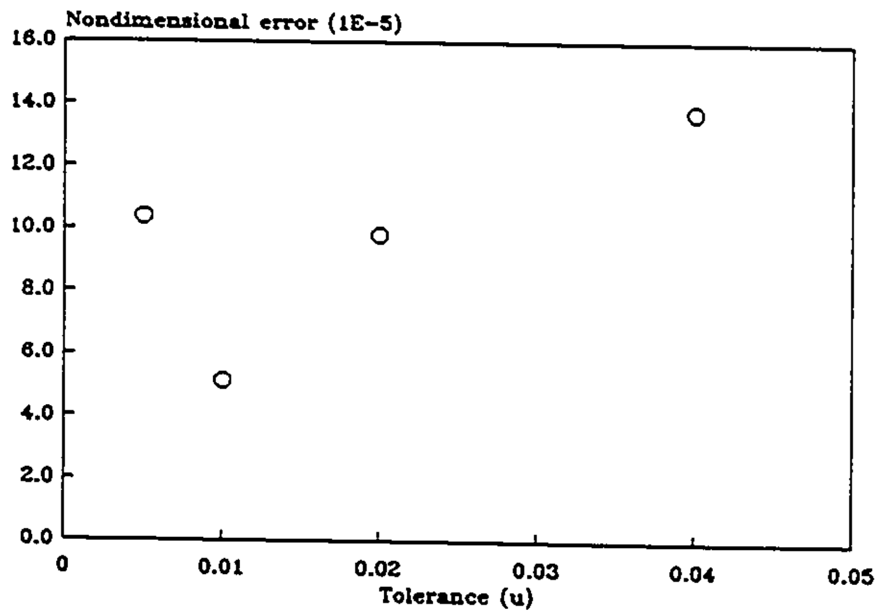

Figure 5.14 Triangle surface tolerance test on sphere, non-geodesic path: Nondimensional error vs Surface tolerance (sphere radius 50u, apex offset 0°, μ=0.216, δ=-0.5).

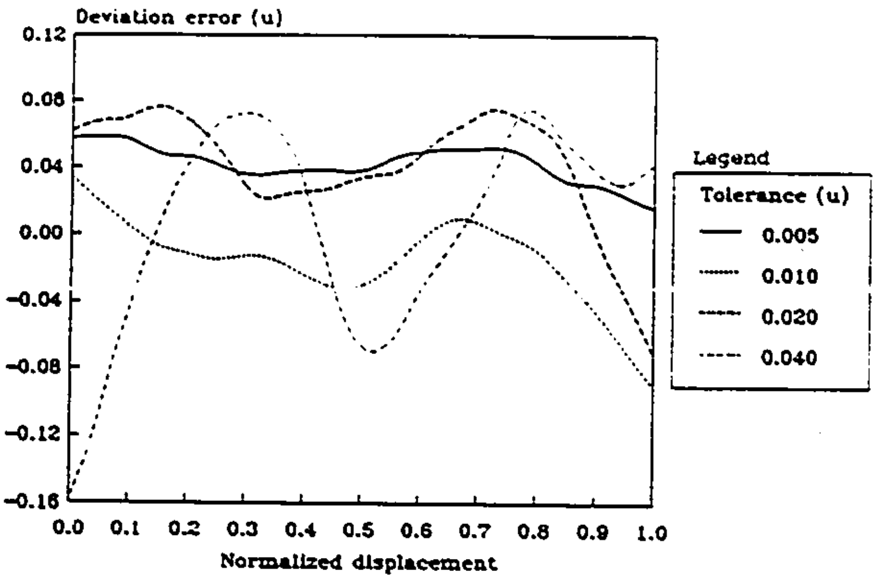

Figure 5.15 Triangle surface tolerance test on sphere, non-geodesic path: Deviation error vs Normalized displacement (sphere radius 50u, apex offset 0°, μ=0.216, δ=1.0).

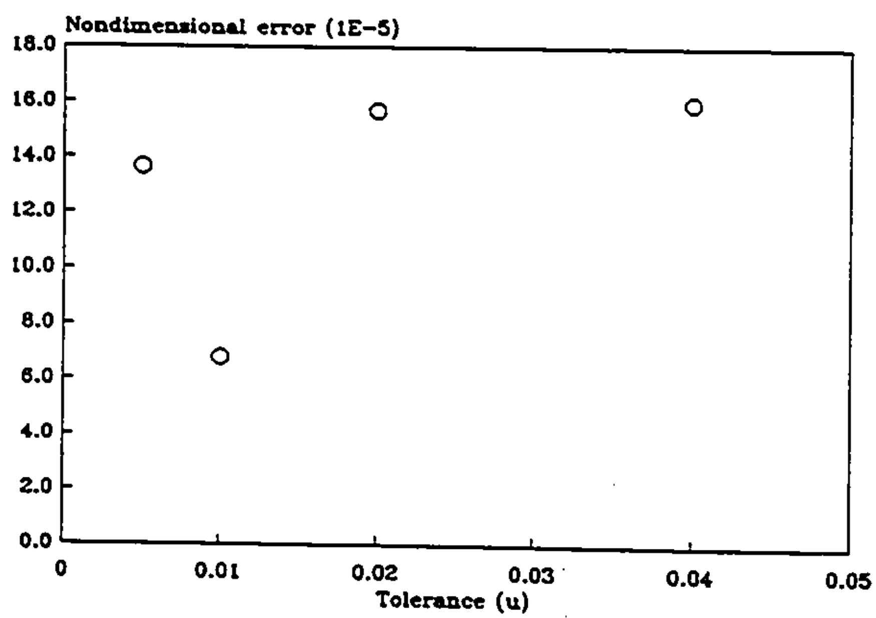

Figure 5.16 Triangle surface tolerance test on sphere, non-geodesic path: Nondimensional error vs Surface tolerance (sphere radius 50u, apex offset 0°, μ=0.216, δ=1.0).

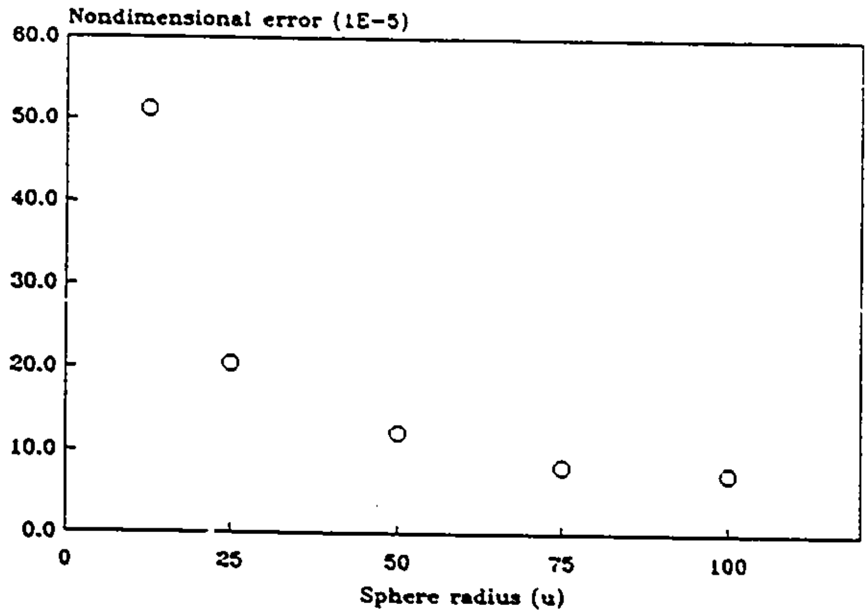

Figure 5.17 Surface curvature test on sphere, geodesic path: Nondimensional error vs Sphere radius (apex offset 0°, surface tolerance 0.005u).

5.4 Accuracy Evaluation of Mathematical Technique on Spherical Shapes

Unlike fibre paths on spherical shapes, the exact fibre paths for general surfaces of revolution cannot be defined. The next best option is to use the differential equation method to trace a benchmark path. Before doing so, it is important to characterize the accuracy of this method on the sphere. This is necessary in order to determine if the method has high enough precision to be used as a benchmark for calculating path prediction errors of the triangulation method.

The errors encountered in generating the path with the mathematical differential equation method on the sphere are shown in Figures 5.18 through 5.22. Different step sizes where used for the independent variable taken to be the rotation angle in this case. When decreasing the step size by half, from 0.128 to 0.064 radians, the deviation error amplitude decreases very fast as depicted by Figure 5.18. The graph in Figure 5.19 reveals that as step sizes are reduced to much smaller values than 0.016 radians the path error curves collapse on a single curve. The effect of reducing the step size is clearly represented in the nondimensional error versus integration step size graph of Figure 5.20. A path error still exists at very small step sizes due to computer round-off errors. The behaviour of the deviation error for non-geodesic paths is shown in Figure 5.21. These deviation error curves are similar in appearance to those obtained for the geodesic paths. However, the maximum deviation error for non-geodesic paths is approximately three times that of the geodesic paths. The increase in deviation error is due to the increase in round-off errors induced by computing the surface friction terms of the differential equation which were equal to zero for geodesic paths. The nondimensional error vs integration step size graph of Figure 5.22 demonstrates once again that the error cannot be equal to zero because of round off errors.

The figures also show that the error increases between the turn around points and is at a maximum at the normalized displacement of 0.25 and 0.75 corresponding to the largest cross section of the spherical mandrel. This increase is due to the particular choice of integration variable and the change in the wind angle along the path. The integration variable in this case is the rotation angle about the mandrel axis. For larger radii the same angular step generates a much larger arc on the sphere surface. The differential path element generated on the sphere surface is equal to the arc on the sphere divided by the sine of the wind angle α as shown in Figure 5.23. Consequently, for the same step size the displacement along the path will vary significantly depending on the values of radius and wind angle inducing larger deviation errors for larger steps along the path. If the integration step size if kept constant, the deviation error is proportional to the radius and inversely proportional to the sine of the wind angle α as expressed by the equation below:

$$\textit{Deviation Error} \propto \frac{R_{Mandrel}}{\sin(\alpha)} \tag{5.3}$$

The largest nondimensional path error on the sphere using the mathematical approach is in the order of 4x10E-6 for both geodesic and non-geodesic paths using a step size smaller than 0.005 radians. In comparison, the smallest nondimensional error obtained for the triangulation method is in the order of 5x10E-5. The error associated with the mathematical approach is at least one order of magnitude better than that of the triangulation method. It is therefore acceptable to use the results of the mathematical path prediction technique as a benchmark for assessing path errors on rotationally symmetric surfaces.

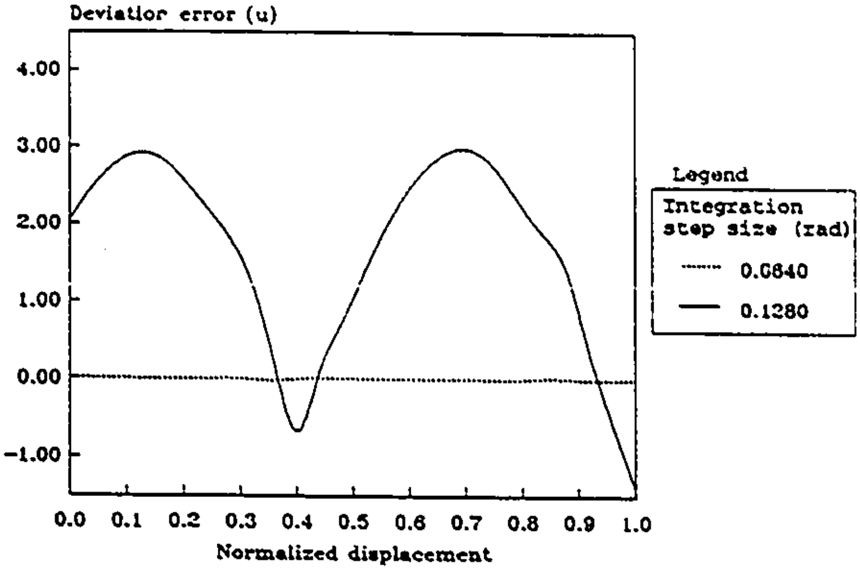

Figure 5.18 Integration step size test on sphere, geodesic path: Deviation error vs Normalized displacement (sphere radius 50u).

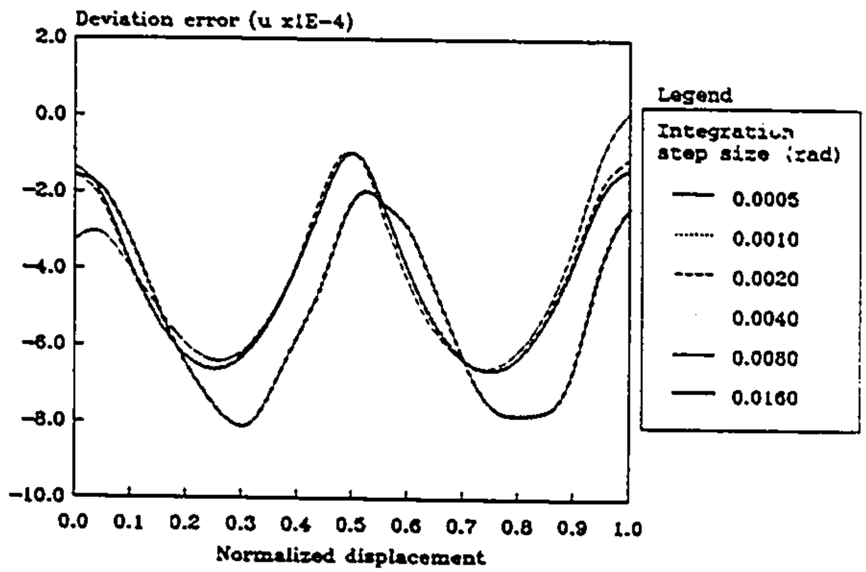

Figure 5.19 Integration step size test on sphere, geodesic path: Deviation error vs Normalized displacement (sphere radius 50u).

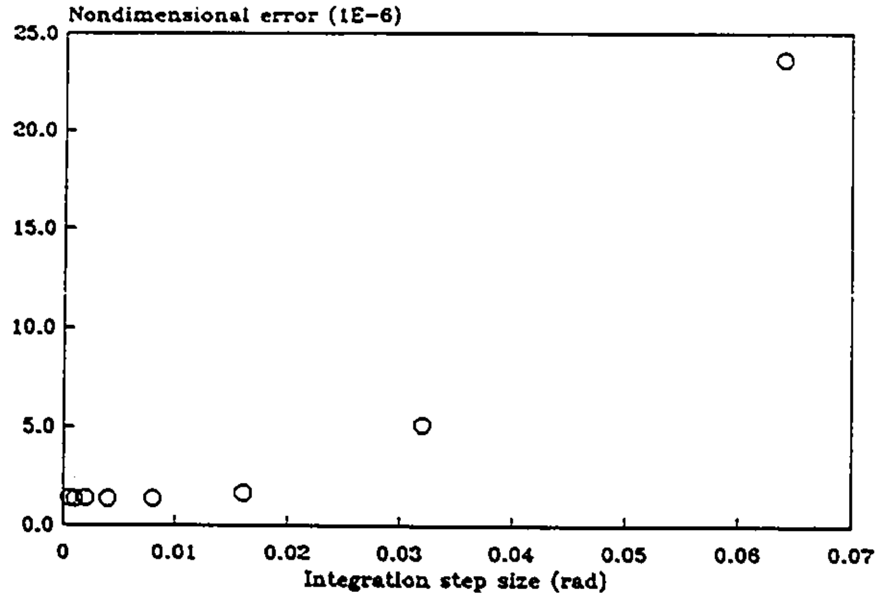

Figure 5.20 Integration step size test on sphere, geodesic path: Nondimensional error vs Integration step size (sphere radius 50u).

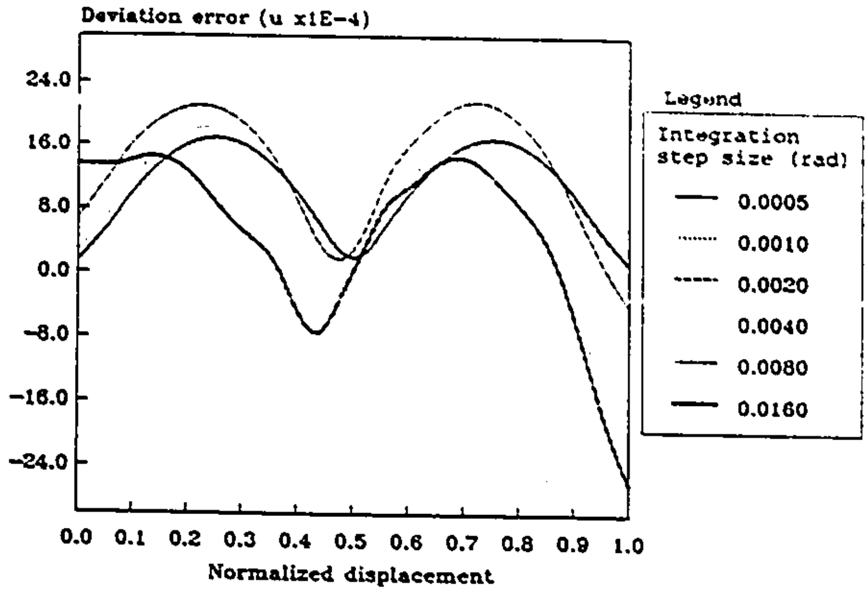

Figure 5.21 Integration step size test on sphere, non-geodesic path: Deviation error vs Normalized displacement (sphere radius 50u, μ=0.216, δ=-0.5).

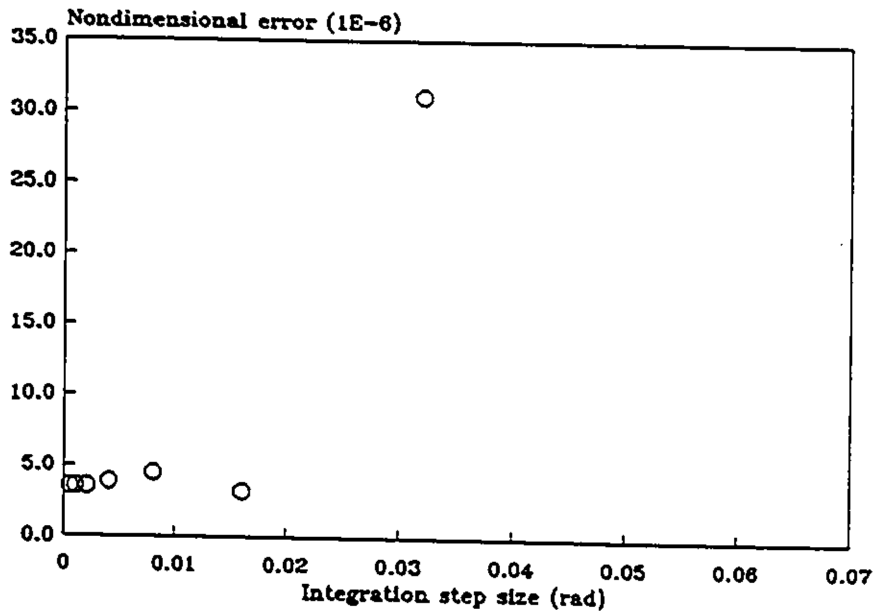

Figure 5.22 Integration step size test on sphere, non-geodesic path: Nondimensional error vs Integration step size (sphere radius 50u, μ=0.216, δ=-0.5).

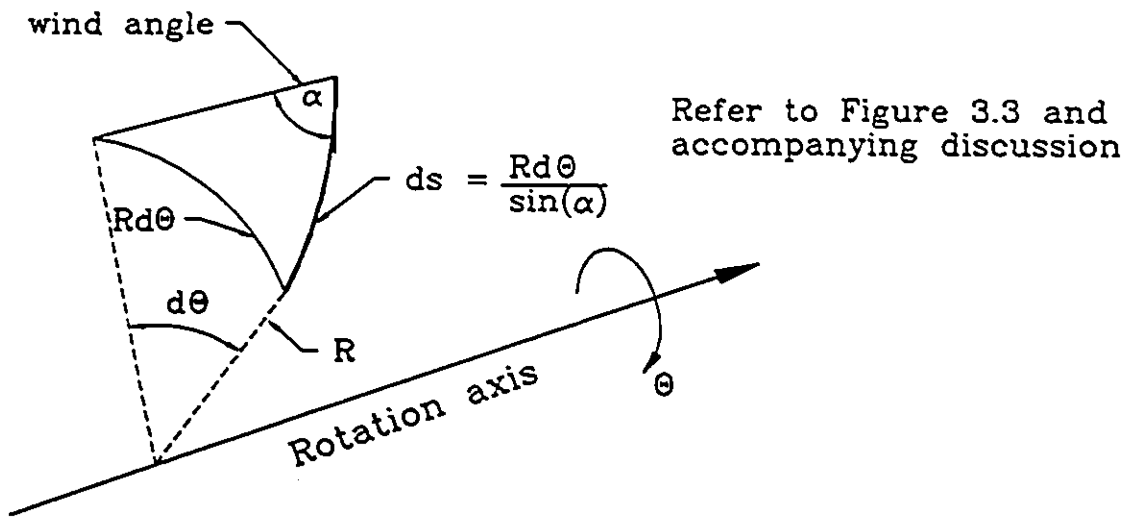

Figure 5.23 Relationship between integration step size and path parameters.

5.5 Accuracy Evaluation of Triangulation on Rotationally Symmetric Shapes

The consistency of the two error evaluation techniques was evaluated by comparing their performance on a sphere. Two triangulation models were used with triangle tolerance of 0.005u and 0.010u respectively. The deviation error of the geodesic path generated by the triangulation method was calculated using as reference the exact path (great circle) and then a second time with the reference path obtained from the differential equation. Figures 5.24 and 5.25 show that the deviation error calculations are not exactly the same but exhibit the same behaviour for both techniques. The differences result from the nature of the error evaluation technique, the reader may refer to Section 5.2 or to Appendix C.

With reference to Figures 5.20 and 5.22, the integration step size was set at 0.001 radian for subsequent test since the nondimensional error appears to be constant. A verification was also performed during the tests to see if the solution had actually converged. Incrementally smaller step sizes were used to ensure that the relative distance between two consecutive paths with different step sizes converged to zero. Double precision variables were used everywhere in the computer code to minimize the effect of round-off errors.

The optimized triangle meshing technique, discussed in Chapter 4, was used for the rotationally symmetric surfaces because it yield smaller surface topology files than the non-optimized method for comparable accuracy. Results for the component of Figure 5.26 are shown in Figures 5.27 and 5.28. The test runs for this mandrel shape were limited to triangle tolerances below 0.010u because for larger tolerances, the path diverged from the benchmark after completing only a portion of the first path cycle and the results were deemed invalid.

Results from the preceding work and intuition indicate that the path accuracy should improve with an increased density of triangles, however for this component it does not. The cause of this difficulty is twofold. At the narrow end of the mandrel, the surface curvature in the circumferential direction is high and induces an error in the predicted path which remains in this area for large displacements. The reason why the triangulation model with larger triangle is more accurate is because the path self corrects as it goes around the narrow end of the mandrel. Consequently, the random behaviour of the path actually helps the accuracy of a coarse triangulation model in the case of this shape. To eliminate the problematic nature of high surface curvature in localized areas a new shape was selected. The shape was carefully designed to exhibit similar curvature properties over the entire path generated. The curvature in a localized can be high if the fibre does not stay this area for a large displacement. The chosen component design has two hemispherical ends smoothly connected to a series of cones as shown in Figure 5.29. It represents two rocket exits nozzles end-to-end and was taken from an example in reference [31].

The deviation error results for a geodesic path generated on this component are shown in Figure 5.30 with the nondimensional error plotted in Figure 5.31. Except for one test run, the accuracy improves as the tolerance value is reduced. Another series of tests was performed for a stable non-geodesic path on the same triangulation models with coefficient of surface friction μ=0.216 and friction multiplier δ=0.25. The results for the deviation error, Figure 5.32, and the nondimensional error, Figure 5.33, indicate that the accuracy terms behave similarly and are of the same order of magnitude for both types of paths. The problems encountered with the shape of Figure 5.26 seem to have disappeared with the elimination of the large localized curvature.

The last series of tests performed on rotationally symmetric mandrels involved variation of the surface curvature on the mandrel of Figure 5.29. This shape was scaled to lower and higher dimensions tc respectively increase or decrease the surface curvature as was done for the sphere by decreasing and increasing its radius. The graph of Figure 5.34 reveals that the nondimensional error term decreases with a higher scaling factor which translates to lower curvatures.

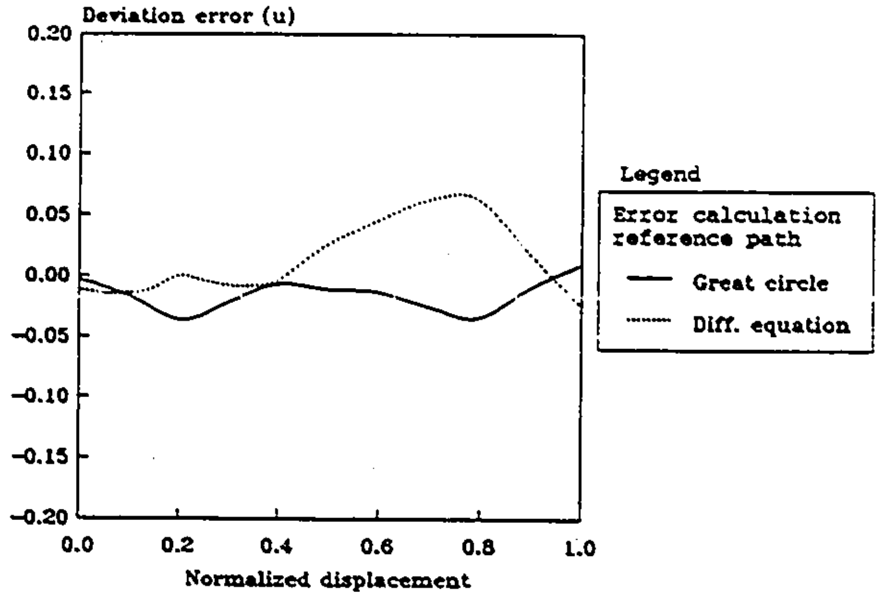

Figure 5.24 Comparison of two error evaluation techniques on sphere, geodesic path: Deviation error vs Normalized displacement (sphere radius 50u, apex offset 0°, triangle tolerance 0.005u).

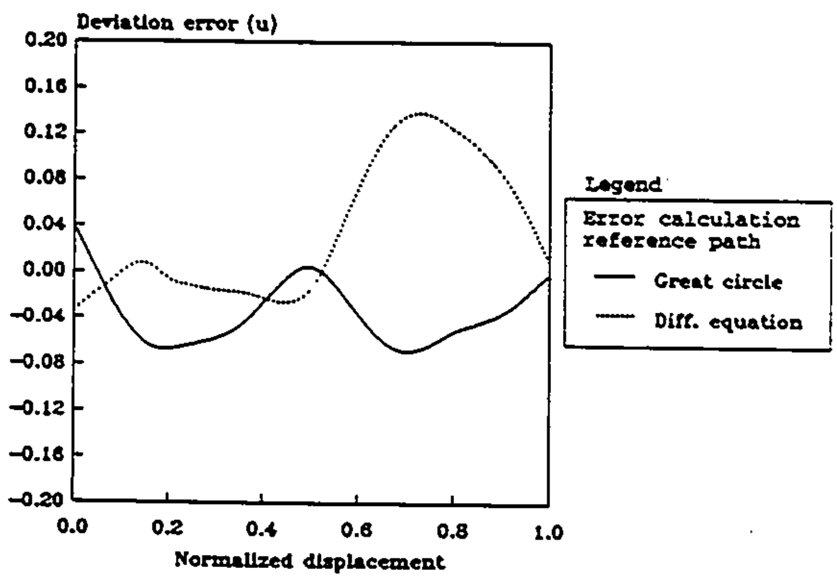

Figure 5.25 Comparison of two error evaluation techniques on sphere, geodesic path: Deviation error vs Normalized displacement (sphere radius 50u, apex offset 0°, triangle tolerance 0.010u).

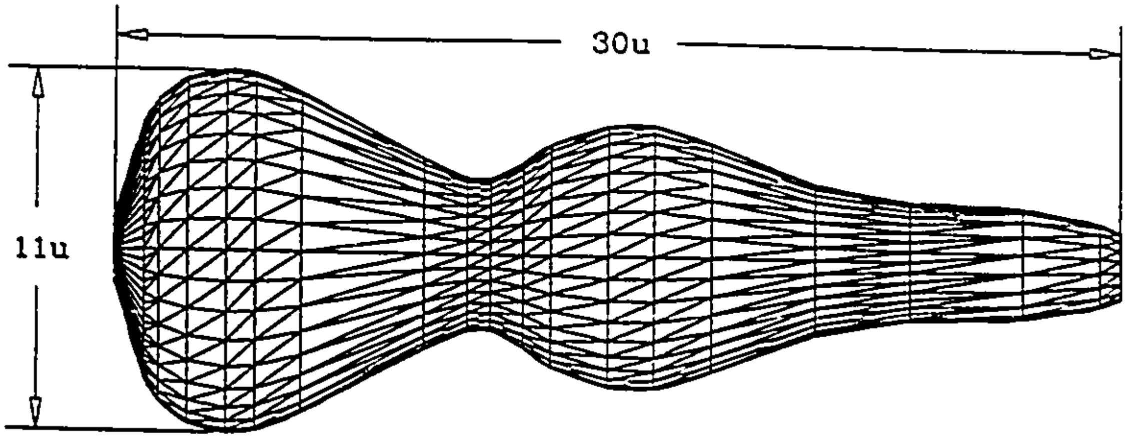

Figure 5.26 General surface of revolution.

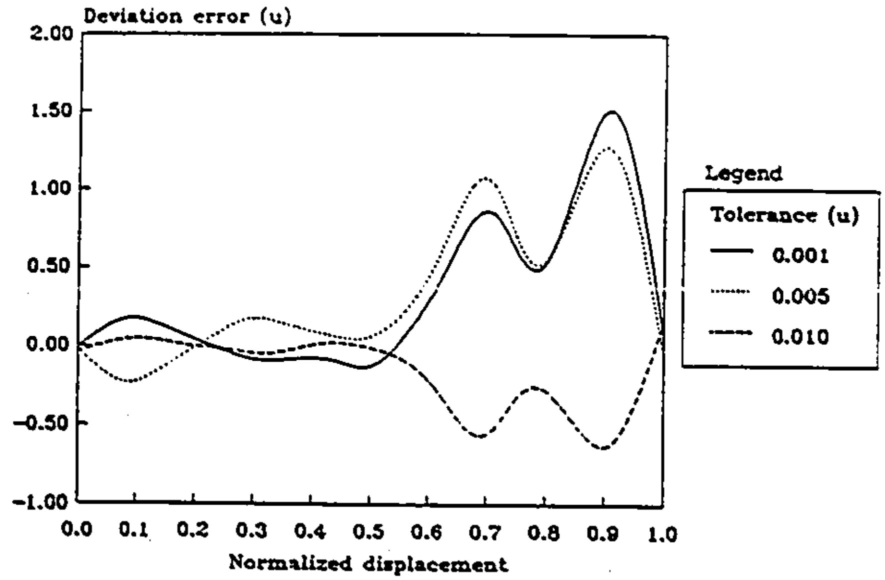

Figure 5.27 Triangle surface tolerance test on shape of Figure 5.26, geodesic path: Deviation error vs Normalized displacement (mandrel length 30u, apex offset 0°).

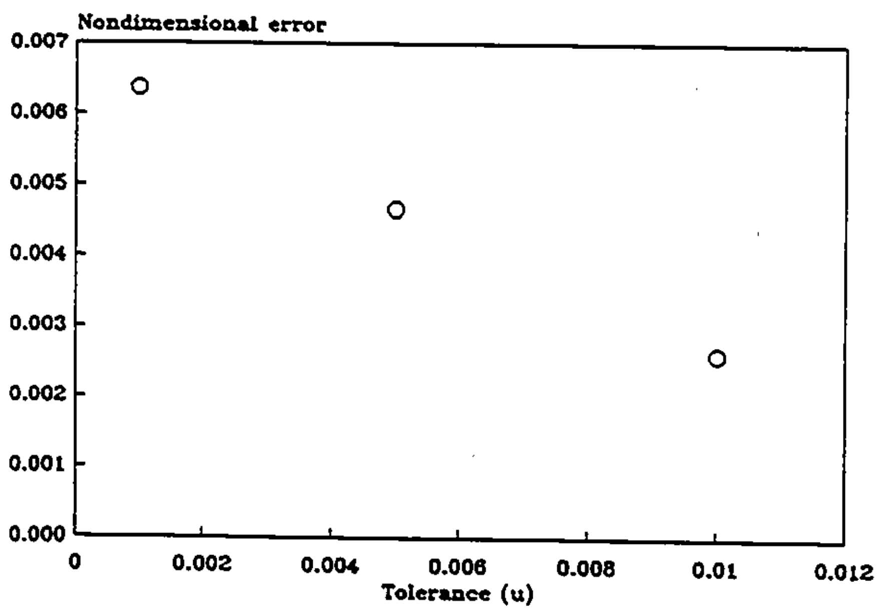

Figure 5.28 Triangle surface tolerance test on shape of Figure 5.26, geodesic path: Nondimensional error vs Surface tolerance (mandrel length 30u, apex offset 0°).

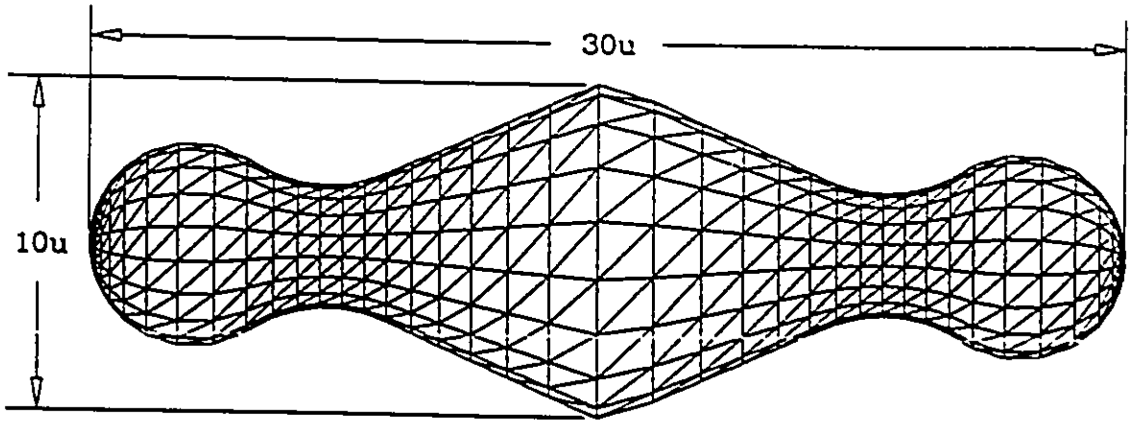

Figure 5.29 General surface of revolution representing two rocket exit nozzles connected end to end.

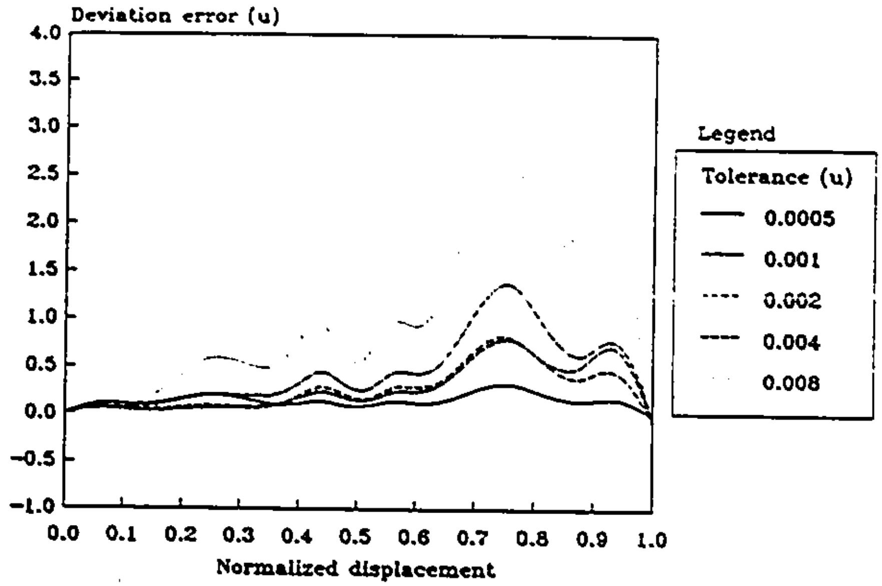

Figure 5.30 Triangle surface tolerance test on shape of Figure 5.29, geodesic path: Deviation error vs Normalized displacement (mandrel length 30u, apex offset 0°).

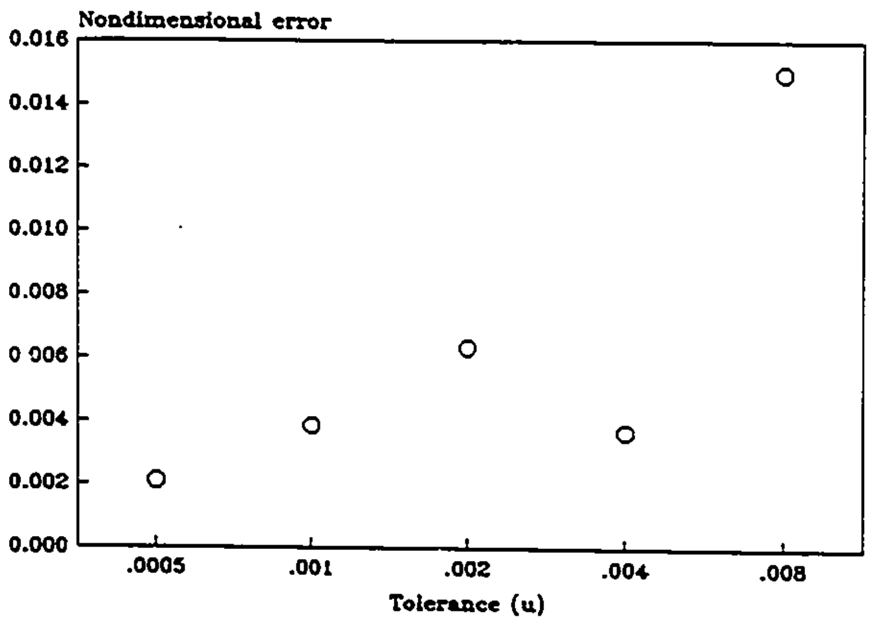

Figure 5.31 Triangle surface tolerance test on shape of Figure 5.29, geodesic path: Nondimensional error vs Surface tolerance (mandrel length 30u, apex offset 0°).

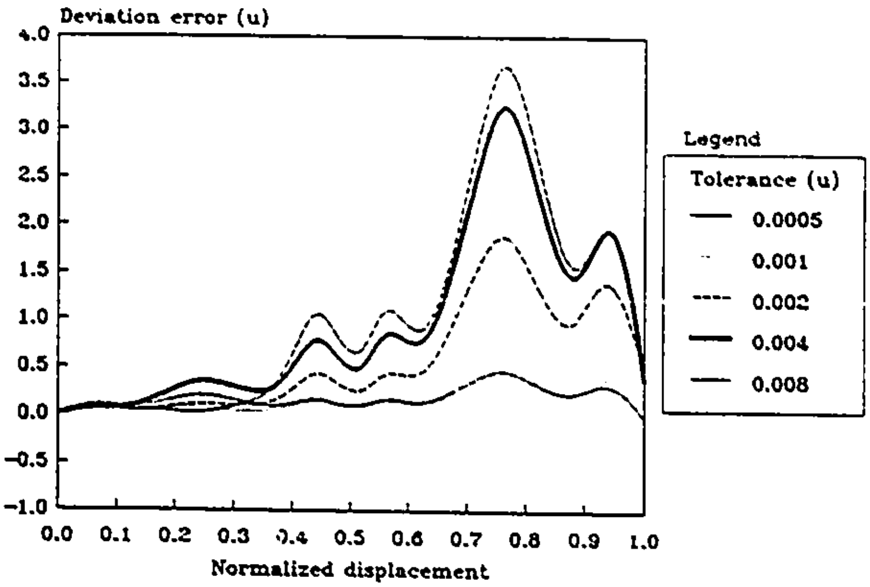

Figure 5.32 Triangle surface tolerance test on shape of Figure 5.29, non-geodesic path: Deviation error vs Normalized displacement (mandrel length 30u, apex offset 0°, μ=0.216, δ=0.25).

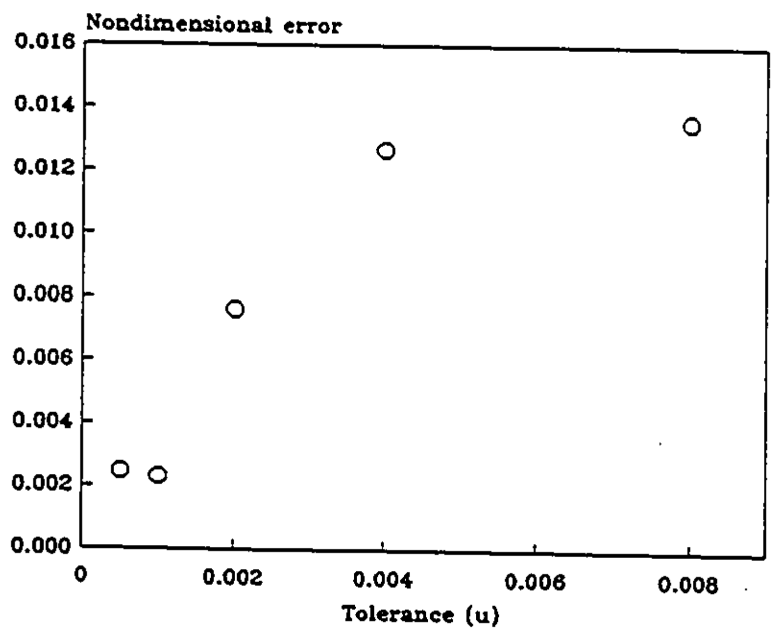

Figure 5.33 Triangle surface tolerance test on shape of Figure 5.29, non-geodesic path: Nondimensional error vs Surface tolerance (mandrel length 30u, apex offset 0°, μ=0.216, δ=0.25).

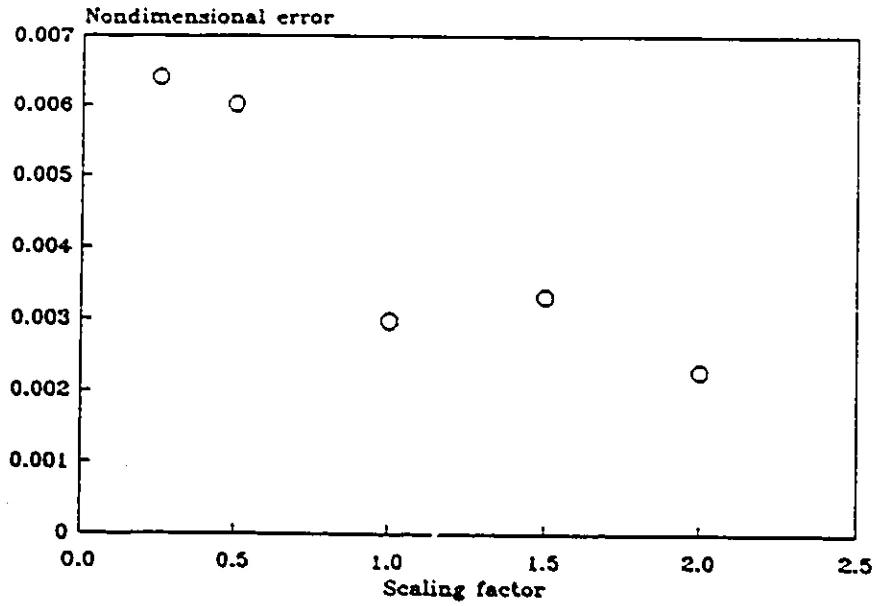

Figure 5.34 Surface curvature test on shape of Figure 5.29, geodesic path: Nondimensional error vs Scaling factor (mandrel base length 30u, apex offset 0°).

5.6 Summary of the Accuracy Evaluation Tests

Accuracy evaluation tests on spherical shapes have demonstrated that the predicted fibre path is not significantly affected by the triangle geometry. On the other hand, the accuracy can be made better or worse by changing the starting parameters slightly. This seemingly random nature of the generated path is not as critical as it may appear. The objective is to predict fibre paths which will be stable during filament winding. If the friction multiplier is kept lower than 90 or 95% of its maximum value of 1.0 (or -1.0) then the resulting predicted fibre path should be stable. Laboratory tests can also be performed to determine the value of surface friction coefficient and to set the limit for the friction multiplier [35].

The preceding work shows also that a higher density of triangles representing closely the mandrel surface curvatures generally give better results. The triangle tolerance value should be controlled as a function of local surface curvature by decreasing it for higher curvature and vice-versa. In some cases, similar accuracy results were obtained for coarse and fine triangle meshes. The sometimes random nature of the triangulation method is such that the precision on the path is more predictable for fine triangular meshes as opposed to a coarse mesh where the particular set of triangles intersected by the path can affect the accuracy in a positive or negative way.

CHAPTER 6

PRACTICAL IMPLEMENTATION ASPECTS OF THE TRIANGULATION TECHNIQUE

The main functional requirements of a path prediction algorithm based on the triangulation technique were outlined in Chapter 4. A full discussion on the implementation of these functions would be inappropriate since the objective of this thesis is not to develop software programs but to evaluate a path prediction technique. The opening section of this chapter deals with practical aspects of data files needed for surface topology models, predicted fibre path information and data transfer to other software packages. The operations required to design a filament wound component within a CAD environment are discussed in Section 6.2. The details provided on the interrelations of the functions are used to describe the software structure of the CAD environment.

6.1 Data File Structure

As discussed in earlier chapters, a large data storage medium is required for the triangulation technique. Simple models of the shapes used for accuracy evaluation required up to 14 Megabytes of storage of space. During the generation of a fibre path, a high frequency of data storage and retrieval is performed. Consequently, the execution speed of the computer code is greatly affected by the storage device access time.

6.1.1 Surface topology file structure

A binary data format was used to store the surface topology information. An alternate ASCII format can also be obtained to relay information to other software modules. Because of the inefficiencies involved with data retrieval and update and the nature of numerical storage this later format is not used by the triangulation technique. The data structure shown in Figure 6.1 is recommended for the surface topology file. All real numbers were represented by double precision variables to minimize the effect of round-off errors.

Only a very small data set of the triangles contained in the topology file is used at any given time for fibre path generation. Storing the entire data file in computer RAM would constitute a waste of resources. An alternative is to store the model on a hard drive and only load into memory the required portion of the topology file.

File header containing information
pertaining to component in general

- topology file validation I.D.
- part I.D., date, model, etc.
- total number of triangles
- triangle surface tolerance
- bandwidth of fibre strand used

Record #1

.

Record #i

- triangle identification
- coordinates of three vertices
- triangular patch normal vector
- identification of adjacent triangles

Record #n

Figure 6.1 Surface topology file structure: Data stored in binary format.

6.1.2 Fibre path data file structure

The fibre path data file is not consulted as frequently as the surface topology file during path prediction and is much smaller in size. However, the fibre path data could be used by several other software modules performing various tasks including surface coverage optimization, collision avoidance evaluation and part program creation for the winding machine controller. To maintain high accuracy and accelerate data access a binary format is again used to store information. ASCII format data files can also be generated and are discussed in the next section. The characteristics of the file should accommodate, to a certain extent, the different modules requiring fibre path data. The file structure depicted in Figure 6.2 was adapted to the fibre path prediction module only and, as such, does not offer the full list of required features.

```
File header containing information
pertaining to fibre path properties in
general
     - path file validation I.D.
     - part I.D., date, model, etc.
     - bandwidth of fibre strand used
     - number of paths in file
-----------------------------------------
Record #1


Record #i
     - path identification
     - identification of parallel paths
     - number of data points in path
          Point #1


          Point #i
               - point coordinates
               - tangent vector


          Point #n



Record #n
```

Figure 6.2 Predicted fibre path file: Data stored in binary format.

6.1.3 Generic ASCII format data transfer files

The software modules used for analysis and optimization of the predicted fibre paths should be capable of handling binary format data files. Several modules may be unable to deal with this type of file format either because fast access of accurate data is unnecessary or the module is an off-the-shelf software package which does not have this flexibility. In either case, an alternate ASCII file format can be used to transfer information about surface topology or predicted fibre paths. The need for such flexibility is discussed in greater detail in Section 6.2.2.

6.2 Filament Winding CAD Environment Arrangement

6.2.1 Activity flowchart

A prelude to determining the required software module interactions is the design of a software flowchart. This flowchart defines the different activities of the design environment and the sequence in which they are performed. The main functions of the filament winding CAD environment are represented in the flowchart of Figure 6.3. This figure is self-explanatory except for the broken line box involving path prediction and manufacturing feasibility. Instead of predicting a large number of fibre path and then verifying for fibre bridging, collision avoidance of the winding machine and other constraints, it is suggested to do this as each path is generated. If the path is unacceptable then it should be discarded immediately.

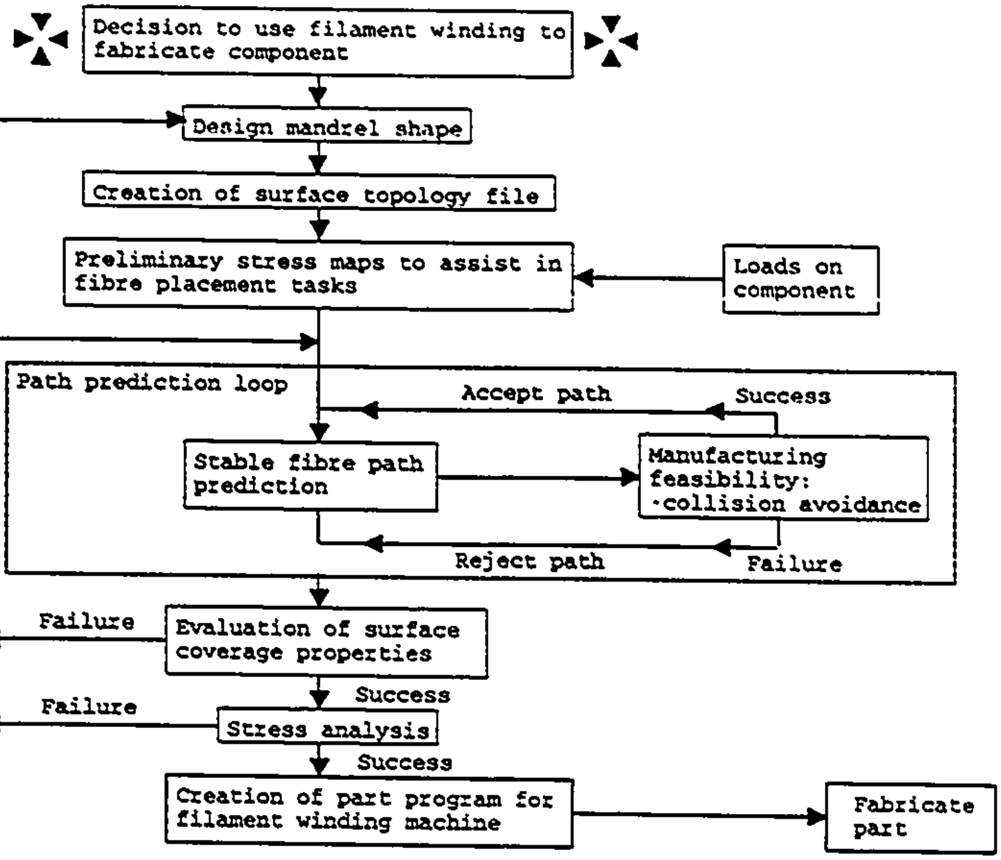

Figure 6.3 Filament winding CAD environment activity flowchart.

6.2.2 Software structure

One great advantage of using computers is their ability to process large amounts of data and provide the user with a condensed yet comprehensive interpretation of the results. Graphs are one form of such data presentation. In the filament winding design environment one of the main objectives is to present results on the display terminal using geometry and colour to convey important properties of the filament wound component and the manufacturing process.

The software needed to effectively display this information is very intricate. Several classes of software packages can be used to perform some aspects of this task. All these packages, however lack in one aspect or another. Nevertheless, one or more may be combined together with specially developed algorithms to carry out the task. For the design of components and the display of the geometric attributes manufacturers of CAD packages have developed the most effective user interfaces. A powerful CAD package offering an adequate programming facility can function as an effective software shell offering a common link between the algorithms developed for the design environment.

An important criterion is not to become too dependant on a specific software product. The algorithms developed here are autonomous and can communicate with CAD software in general via well established file structure protocols such as IGES for example. It then follows that the algorithms developed within the CAD package use a minimum of exclusive features offered by the product. This makes the design environment transportable to other CAD packages while minimizing the amount of programming required within the chosen product. Figure 6.4 depicts graphically the software arrangement. The software shell provided by the CAD package serves as an interface between the user and the design modules it contains. The information exchange between modules and shell is performed via generic format files respecting accepted protocols like IGES. Amongst each other, the modules use efficient binary file formats to transfer data.

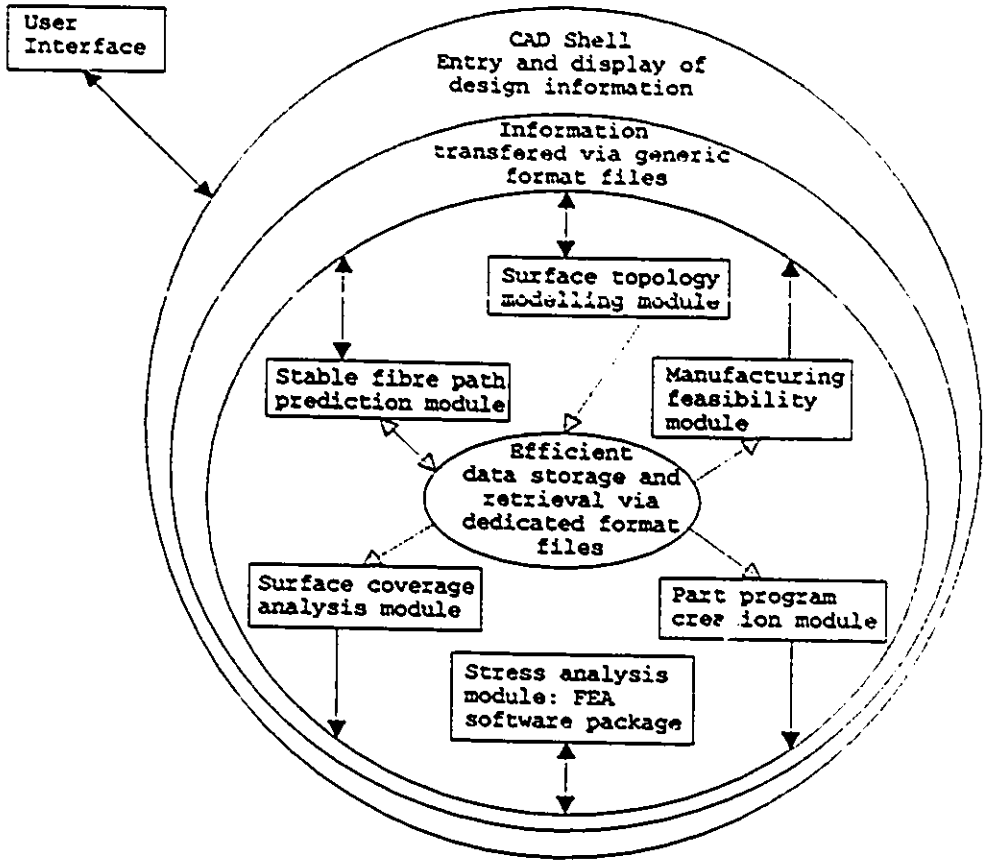

Figure 6.4 Filament winding CAD environment software structure.

CHAPTER 7

CONCLUSIONS AND RECOMMENDATIONS

7.1 Summary

Several techniques exist to predict stable fibre paths on a wide variety of mandrels. Four path prediction techniques were developed in this thesis: for rotationally symmetric shapes - cones and cylinders, mathematical (based on differential equation) and triangulation and for asymmetric shapes - triangulation. These techniques can be classified in two categories, geometric and mathematical. The two techniques capable of dealing with general asymmetric shapes are; triangulation, where the surface is approximated by flat triangular facets, and mathematical where the guiding differential equation is solved numerically.

These two methods have the same computational efficiency when dealing with rotationally symmetric shapes. In the case of asymmetric structures, the mathematical approach becomes less efficient because of the increased complexity of the differential equation and the surface model. The efficiency remains the same for the triangulation technique.

The triangulation path prediction method uses a topology file to store local surface information. The topology file contains the triangle vertex coordinates for the surface model and may also contain results from the filament winding simulation such as fibre distribution and orientation. This information can then be used directly by finite element analysis software or surface coverage optimization algorithms. Mathematical path predictions techniques, on the other hand, do not require such a topology file. If simulation results need to be recorded, such a file would have to be constructed in order to record surface coverage data. This would further decrease the computational efficiency of the mathematical approach.

Two error measuring parameters were defined and several programs developed to calculate the error characteristics of the triangulation method. The accuracy of the triangulation scheme was initially investigated by comparing the resulting path with the exact geodesic and stable non-geodesic paths of a sphere. The triangle geometry was shown to have no affect on accuracy but the triangle size affected accuracy to a great extent. Altering slightly the starting conditions caused the predicted path to intersect a different set of triangles. Due to a random behaviour of the triangulation technique, the particular set of triangles affected by the predicted path was shown to influence accuracy in a positive or negative way.

The study was broadened to include general surfaces of revolution which, unlike the sphere, have a varying surface curvature. The error evaluation was performed using the path obtained from the differential equation method as a benchmark. Verification on the accuracy of the differential equation method revealed that its largest nondimensional error was at least one order of magnitude smaller than the smallest nondimensional error of the paths generated by triangulation.

Several accuracy tests on these general rotationally symmetric mandrels revealed that a higher density of triangles on the mandrel surface did not always improve the fibre path accuracy. The surface curvature was shown to influence path accuracy whereby larger curvatures resulted in worse results. Again the deviation error for a certain path depended on the path starting parameters and, consequently, on the particular set of triangles intersected by the fibre path.

An indispensable feature of the developed filament winding design environment is the capability to display information on the computer screen using colour and geometry. The designer can locate the problem areas much more quickly. This feature also offers the possibility of simulating the entire filament winding process. An interface to AutoCAD version 10 was developed along with special file structures needed to transfer the data. Programs were written both within AutoCAD (AutoLISP) and outside this shell. The results of this interface are given in Appendix A.

7.2 Conclusions

Stable fibre paths predicted with the triangulation method are less accurate than those obtained with a mathematical technique. There are however, several advantages which outweigh the accuracy problem especially when the routine is used within a design environment. Triangulation path prediction is more efficient than the mathematical approach when dealing with asymmetric shapes. The triangulated surface model is very simple in nature and easily managed whereas a surface model for the mathematical approach is bulky and requires a huge overhead for its management. Finally, the triangulation method is easily adaptable to other design optimization algorithms (structural analysis) because of the nature of the triangulation surface topology files.

Accuracy evaluation of the triangulation path prediction technique revealed that the error could be self-correcting under the right circumstances. Since it is very difficult to determine what those circumstances should be, it is better to use a triangle surface mesh which is as refined as possible. The behaviour of the path on a refined triangular mesh is more predictable since it does not rely on errors which may eventually self-correct to achieve an acceptable accuracy.

The fibre path generated by the triangulation technique is affected by starting conditions. This makes it more difficult for the designer to speculate on the appearance of the resulting path. This effect may not be obvious for single paths but does create problems when tracing paths parallel to each other.

7.3 Recommendations

The triangulation technique can generate stable fibre paths on asymmetric shapes. A certain degree of accuracy is assured if the triangular surface model is optimized. The development of algorithms to optimize triangle distribution is therefore required. The surface topology files obtained in this manner will be much smaller than in a case where the triangle size is controlled directly by the designer.

When using surface friction to modify the outcome of a predicted fibre path, only 90% of the maximum value of the friction coefficient should be used. This is done to insure that even with the error on the predicted path, it will still lie within a stable region.

The use of higher order elements instead of flat triangular facets to model the mandrel surface should be investigated. The stable fibre path on these elements must be defined geometrically to avoid the use of the mathematical approach.

A surface coverage optimization algorithm is needed to assist the designer. A major difficulty in filament winding asymmetric shapes is control over surface coverage. This algorithm should be able to perform the optimization based on total surface coverage, structural integrity or a combination of both.

The software tools developed for filament winding should be grouped together under one umbrella and accessed through a software environment which provides a user friendly interface between the designer and the specialized filament winding software. The user friendly interface, referred to as the software shell, must have powerful graphics capabilities. The information obtained from analysis and optimization can be conveyed to the designer much faster if geometry and colour are used to display mathematical results. Manufacturers of CAD software have become experts in developing effective user interfaces. It is therefore recommended that such CAD software be used as the shell. The features required include easy tailoring of menus and prompts and the service of a powerful internal programming language (the possibility of compiling these programs is a definitive advantage).

The software facilities within the shell should be able to communicate with each other or the shell using standard file formats. This ensures that communication will also be possible when new software packages are added. Such file formats for geometric data include IGES (Initial Graphics Exchange Standard) and DXF (Drawing Interchange File) among others.

REFERENCES

1. S. Kalpakjian, Manufacturing Engineering and Technology, Addison-Wesly Publishing Company, Inc., New York (USA) 1989, p. 259.

2. D.E. Shaw-Stewart, "Pullwinding", Second International Conference on Automated Composites, The Plastics and Rubber Institute, Noordwijkerhout (Netherlands), 1988, pp. 15/1-15/13.

3. M. Munro, "Review of Manufacturing of Fiber Composite Components by Filament Winding", Polymer Composites, vol. 9, no. 5, October 1988, pp. 352-359.

4. R.R. Roser, Modern Plastics Encyclopedia 90, McGraw-Hill, New York (USA), 1990, pp. 309-310.

5. B. E. Spencer, "Tooling Considerations for the Filament Winding Process", Composites Applications: the future is now, Society of Manufacturing Engineers, Michigan (USA), 1989, pp. 151-164.

6. V. Middleton, M.J. Owen, D.G. Elliman and M. Shearing, "Developments in Non-Axisymmetric Filament Winding", Second International Conference on Automated Composites, The Plastics and Rubber Institute, Noordwijkerhout (Netherlands), 1988, pp. 10/1-10/15.

7. W. Braun, "A Control System for Filament Winding Equipment as a Prerequisite for Automation", First International Conference on Automated Composites, The Plastics and Rubber Institute, Nottingham (England), 1986, pp. 11/1-11/11.

8. Don O. Evans, "Programming Filament Winding Machines", Productive Filament Winding Technology Conference, Society of Manufacturing Engineers, L.A. California (USA), August 1987, pp. 1-12.

9. Don O. Evans, "Robotic Seven Axis Filament Winding", Productive Filament Winding Technology Conference, Society of Manufacturing Engineers, L.A. California (USA), August 1988, pp. 1-15

10. K.B. Bubeck, "Robotic Winding: Continuous Fibres in Complex Shapes", Composites in Manufacturing, Society of Manufacturing Engineers, Michigan (USA), Fall 1987, pp. 2-5.

11. G. Menges and E. Neise, "Use of Industrial Robots for Filament Winding", 40th Annual Technical Conference, Reinforced Plastics/Composites Institute, 1985, Section 19-B, pp. 1-3.

12. H. Van Brussel and J. Scholliers, "Robotic Filament Winding of Asymmetric Parts", Composites in Manufacturing, vol. 7, No. 1, Society of Manufacturing Engineers, Michigan (USA), 1991, pp. 1-3.

13. R.R. Roser, M.L. Skinner, K.J. Samowitz, K.L. Kemp, B.L. Folsom, "New Generation Computer Controlled Filament Winding", 31st International SAMPE Symposium, Las Vegas Nevada (USA), April 1986, pp. 810-821.

14. J.A. Rolston, "Filament Winding", Processing and Fabrication Technology, Delaware Composites Design Encyclopedia, Vol. 3, Lancaster, 1989, pp. 193-204.

15. J.A. Ziegel and T.J. Sevener, "Filament Winding's Succession to Fiber Placement", Society of Manufacturing Engineers, 1989, Paper No. AD89-581.

16. D.G. Elliman, P. Sorenti, L. Brown, M. Shearing, V. Middleton and M.J. Owen, "A Cell for the Manufacture of Composite Components by Filament Winding", Advanced Manufacturing Engineers, Vol. 1, October 1988, pp. 15-20.

17. G. Di Vita, M. Farioli and M. Marchetti, "Process Simulation in Filament Winding of Composite Structures", Composite Materials Design and Analysis, Editors: W.P. de Wilde and W.R. Blain, Springer-Verlag, 1990, pp. 19-37.

18. D.G. Lloyd-Thomas, G.C. Eckold and G.M. Wells, "Asymmetric Filament Winding", Second International Conference on Automated Composites, The Plastics and Rubber Institute, Noordwijkerhout (Netherlands), 1988, pp. 12/1-12/12.

19. G.M. Wells and G.C. Eckold, "Computer Aided Design and Manufacture of Filament Wound Composite Structures", First International Conference on Automated Composites, The Plastics and Rubber Institute, Nottingham (England), 1986, pp. 6/1-6/16.

20. V. Middleton, K.W. Young, D.G. Elliman and M.J. Owen, "Software for Filament Winding", First International Conference on Automated Composites, The Plastics and Rubber Institute, Nottingham (England), 1986, pp. 9/1-9/6.

21. K.-W. Kirberg, W. Michaeli, G. Menges and A. Seifert, "Process Simulation in Filament Winding, New Insights Show the Way to Cost-Effective Component Development", Second International Conference on Automated Composites, The Plastics and Rubber Institute, Noordwijkerhout (Netherlands), 1988, pp. 16/1-16/15.

22. M.J. Owen, V. Middleton, D.G. Elliman, H.D. Rees, K.L. Edwards, K.W. Young and N. Weatherby, "Computerized Numerical Control Filament Winding for Complex Shapes", Institute of Mechanical Engineers, 1986, Paper No. C29/86.

23. M.J. Owen, V. Middleton, D.G. Elliman, H.D. Rees, K.W. Young and K.L. Edwards, "Developments in Filament Winding", Second ASM Conference on Advanced Composites, Michigan (USA), November 1986, pp. 35-43.

24. V. Middleton, M.J. Owen, D.G. Elliman and M.R. Shearing, "CAD for Non-Axisymmetric Filament Winding", Correspondance with Dr. Kris Rudd at the University of Nottingham, England, 1988.

25. V. Middleton, M.J. Owen, D.G. Elliman and M. Shearing, "Filament Winding of Non-Axisymmetric Components", Institute of Mechanical Engineers, 1989, Paper No. C387/001.

26. K.-W. Kirberg and G. Menges, "Possible Methods of Process Simulation in Filament Winding, A Step Towards the Realisation of Complex Part Geometries", Computer Aided Design in Composite Material Technology, Editors: C.A. Brebbia, W.P. de Wilde and W.R. Blain, Springer-Verlag, 1988, pp. 157-171.

27. D.J. Struik, Differential Geometry, Addison-Wesley, London 1961, pp. 105-135.

28. R.J. Lawless, "A Computer Simulation of the Filament Winding Process for the Design and Manufacture of Composite Products", Master's Thesis, Department of Mechanical and Aerospace Engineering, University of Delaware (USA), 1985, pp. 1-82.

29. D. Kahaner, C. Moler and S. Nash, Numerical Methods and Software, Prentice Hall New Jersey, 1989, pp. 81-138.

30. W.H. Press, B.P. Flannery, S.A. Teukolsky and W.T. Vetterling, Numerical Recipes in C, Cambridge University Press, 1988, pp. 592-597.

31. J.C. Leon and G. Wells, "Computer Aided Filament Winding", First European Conference on Composite Materials, 1985, pp. 532-537.

32. G.M. Wells and K.F. McAnulty, "Computer Aided Filament Winding Using Non-Geodesic Trajectories", Sixth International Conference on Composite Materials and Second European Conference on Composite Materials, Vol. 1, Elsevier Applied Science, 1987, pp. 1.161-1.173.

33. X.-L. Li and D.-H. Lin, "Non-Geodesic Winding Equations on a General Surface of Revolution", Sixth International Conference on Composite Materials and Second European Conference on Composite Materials, Vol. 1, Elsevier Applied Science, 1987, pp. 1.152-1.160.

34. M. Marchetti, D. Cutolo and G. Di Vita, "Design of Domes by Use of the Filament Winding Technique", Third European Conference on Composite Materials, Elsevier Applied Science, 1989, pp. 401-408.

35. G. Menges, R. Wodicka and H.L. Barking, "Non-Geodesic Winding on a Surface of Revolution", 33rd Annual Technical Conference, Reinforced Plastics/Composites Institute, 1978, Section 10-D, pp. 1-4.

36. R.R. Roser, "Computer Control for Filament Winding", Society of Manufacturing Engineers, 1985, Paper No. MF85-504.

37. G. Menges, and M. Effing, "CADFIBER, A Software Tool for Composite Engineering", Second International Conference on Automated Composites, The Plastics and Rubber Institute, Noordwijkerhout (Netherlands), 1988, pp. 11/1-11/21.

38. D.E. Shaw-Stewart, "Integrated Modwind Systems", First International Conference on Automated Composites, The Plastics and Rubber Institute, Nottingham (England), 1986, pp. 8/1-8/14.

39. G.A. Ziolko, "CIM for Composites: An Implementation", Society of Manufacturing Engineers, 1989, Paper No. EM89-580.

40. Jeffrey Ziegel, "Tips on Designing a Filament Winding Cell", Composites in Manufacturing, Society of Manufacturing Engineers, vol. 7, No. 1, 1991, p. 4.

41. George Lubin, Handbook of Composites, Van Nostrand Reinhold Company Inc., New York, 1982, p. 764.

APPENDIX A

SAMPLE PROGRAM RUN OF "TRIASYM"

The program name "TriAsym" stands for Triangulation of Asymmetric shapes. Two other triangulation programs were also developed: triangulation of rotationally symmetric shapes with non-optimized triangles "TriSim", and triangulation of rotationally symmetric shape with optimized triangles "TriOpt". A program using the cones and cylinders technique and one using the mathematical approach were developed to evaluate their performance. The mathematical approach based on the second order differential equation was also used to characterize the accuracy of the triangulation method.

There is more than ten thousand lines of "C" language program code for all these computer programs including those developed for error evaluation. It would be inappropriate to include them all herein. Consequently, a simplified algorithm is given in Appendix B for the TriAsym program. Listings of the smaller programs developed for error evaluation are presented in Appendix C.

Close to one hundred program runs were performed to obtain the error calculations presented in Chapter 5. To include a table describing the parameters of each program run would be much to lengthy and not very useful for the reader. Instead, a sample program run for TriAsym is presented along with accompanying pictures showing the graphic displays provided by AutoCAD and the design modules.

A.1 Mandrel Surface Definition for Tubular Asymmetric Shape

The asymmetric shape is obtained by designing a driver curve and then dragging circle along its entire length to obtain the triangle vertex coordinates (Section 4.1). The surface topology file is obtained by using AutoCAD in conjunction with the TriAsym program. AutoCAD offers a feature which permits other programs to execute without leaving the AutoCAD environment. This feature was used extensively throughout this work.

A.1.1 Driver curve designed in AutoCAD

The 3DPOLY command is used in AutoCAD to draw the driver curve. Once completed, the polyline node coordinates are written to an ASCII file for later retrieval by TriAsym (Figure A.1). This operation is performed with the AutoLISP program "GetProf".

A.1.2 Triangular meshing by "TriAsym" program

Before generating the triangle vertex coordinates, TriAsym first converts the polyline node data into a three dimensional spline. This spline is then used to obtain the location and orientation of the cross section needed to generate the vertex coordinates. The entry screen used to define the triangular mesh characteristic is shown in Figure A.2. The topology file obtained is translated to an ASCII format in order to be read by AutoCAD.

A.1.3 Generate surface in AutoCAD

The ASCII topology file created by TriAsym is used by the AutoLISP program "DwTrir" to construct the triangular patches. The results of this operation is shown in Figure A.3 with hidden lines removed.

A.2 Generating and Displaying Fibre Paths

There are several parameters needed for generating the path within TriAsym. These include starting position and orientation, coefficient of surface friction, limits for the friction multiplier, fibre bandwidth and others. The main data entry screen for path generation is shown in Figure A.4. The path coordinates are written to an ASCII file and retrieved by the AutoLISP program "DwFib" which creates a polyline in AutoCAD as shown in Figure A.5 with hidden line removal.

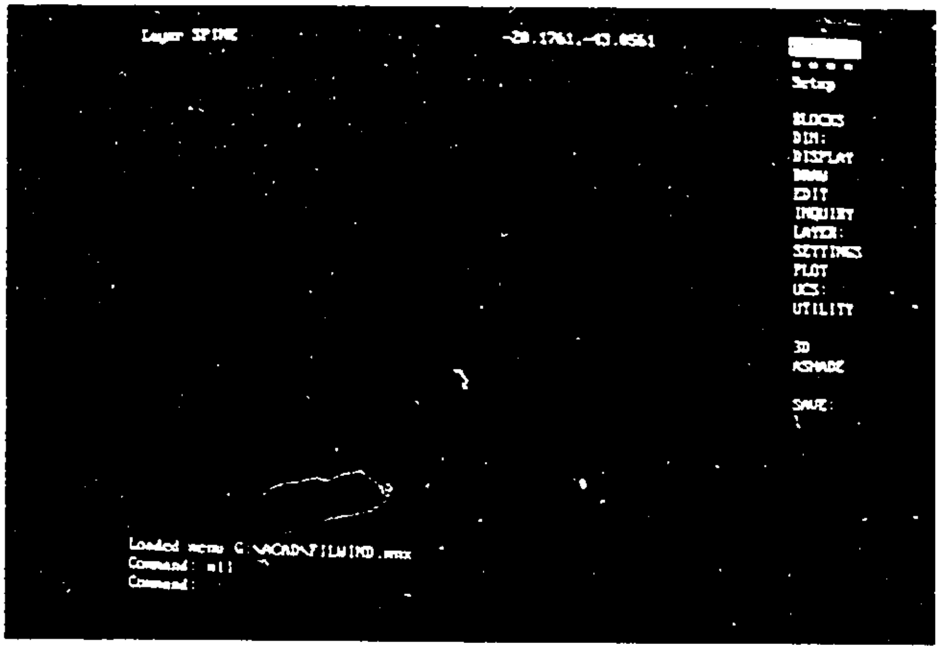

Figure A.1 Three dimensional polyline drawn with the 3DPOLY facility in AutoCAD. End caps for the tubular mandrel are also shown.

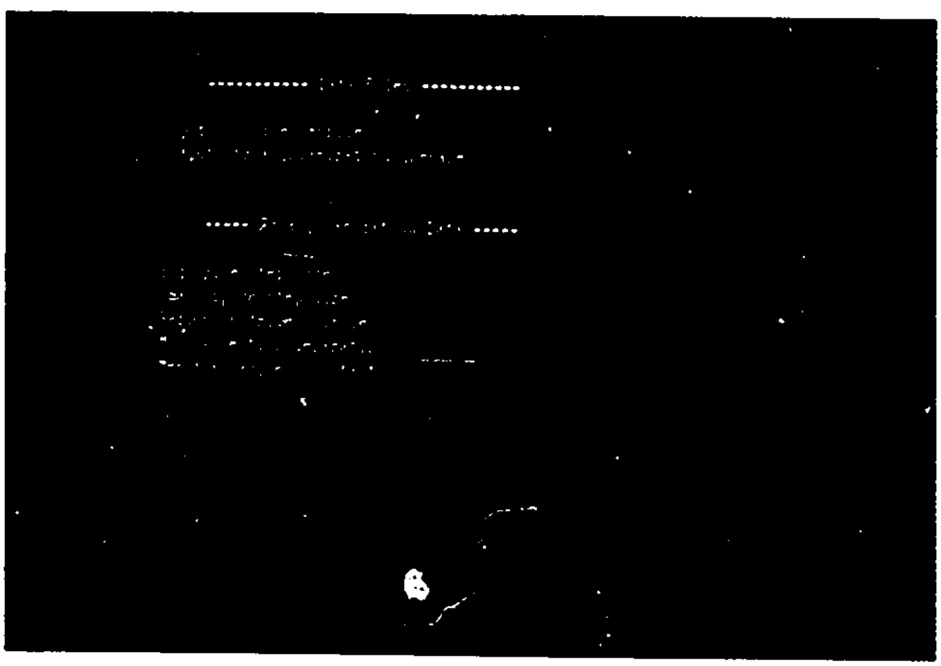

Figure A.2 Data entry screen for triangular meshing of tubular asymmetric shapes.

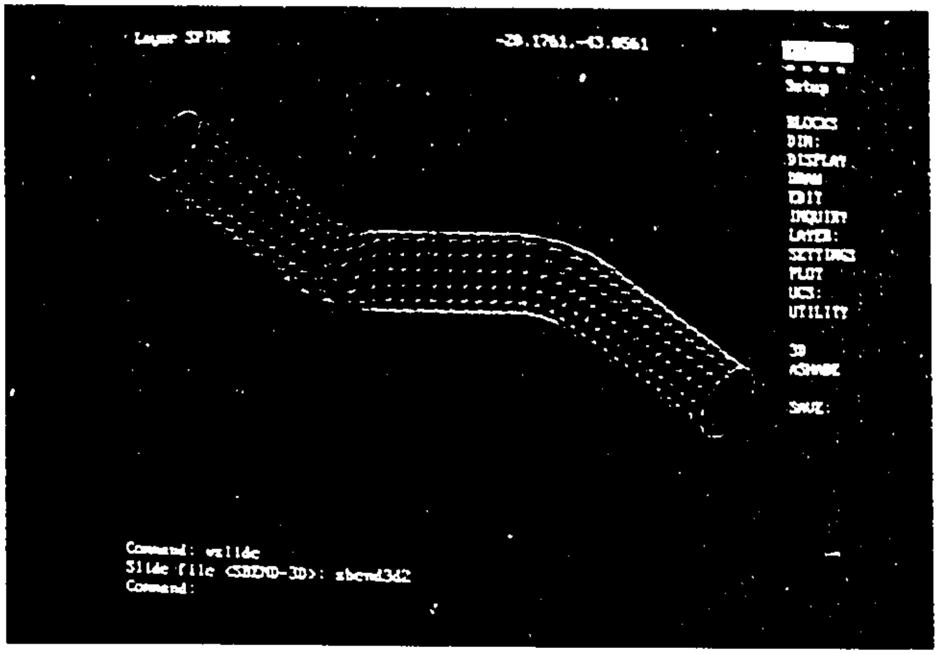

Figure A.3 Surface representation in AutoCAD using flat triangular patches.

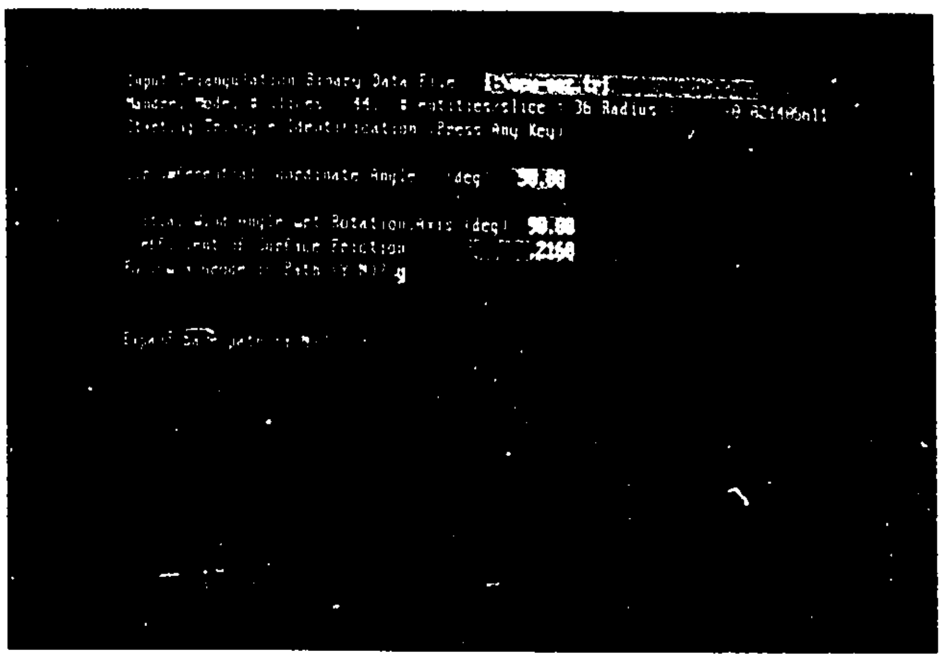

Figure A.4 Main TriAsym entry screen for fibre path prediction.

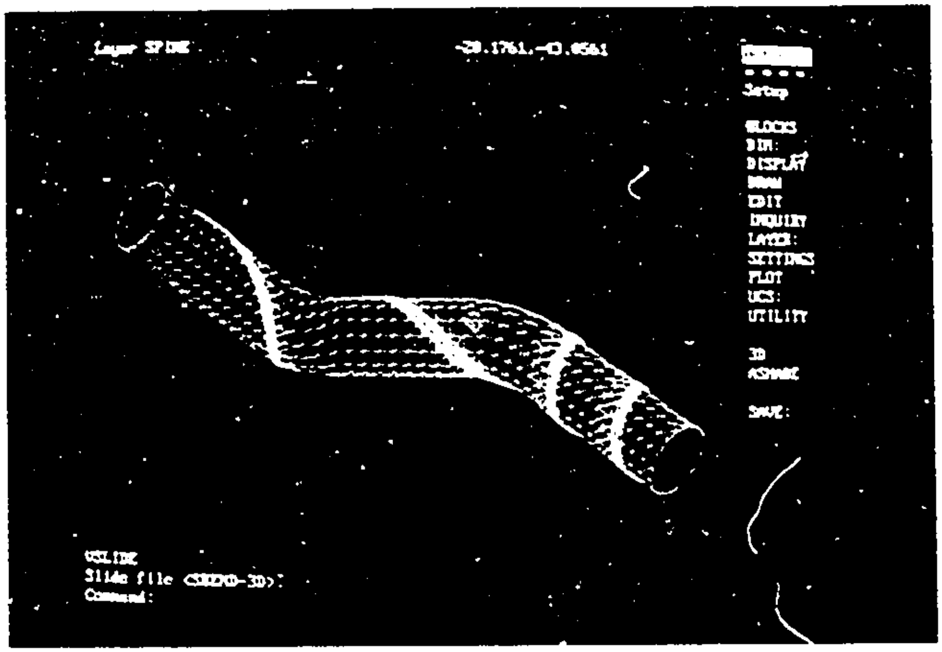

Figure A.5 Parallel fibre paths drawn on triangulated surface with hidden lines removed. The are two sets of parallel paths depicted here (red and yellow).

APPENDIX B

TRIASYM SIMPLIFIED FLOWCHARTS

The general features of the program used to obtain the fibre path on general asymmetric tubular shapes is depicted by Figures B.1 and B.2. Although detailed flowcharts would give a better understanding of the algorithms used they would not be appropriate since the current program format is not ideal. The algorithms were obtained using a rapid prototyping technique and as such contain many redundancies while not being "crash" proof.

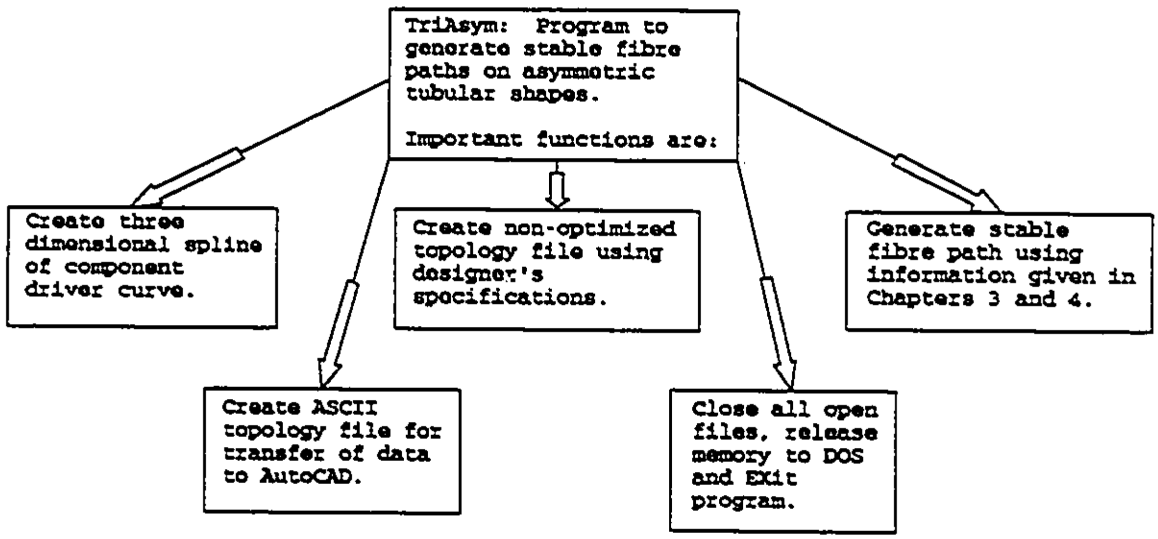

Figure B.1 Simplified flowchart for the TriAsym program. It is used to create a topology file and predict parallel fibre paths on tubular asymmetric shapes.

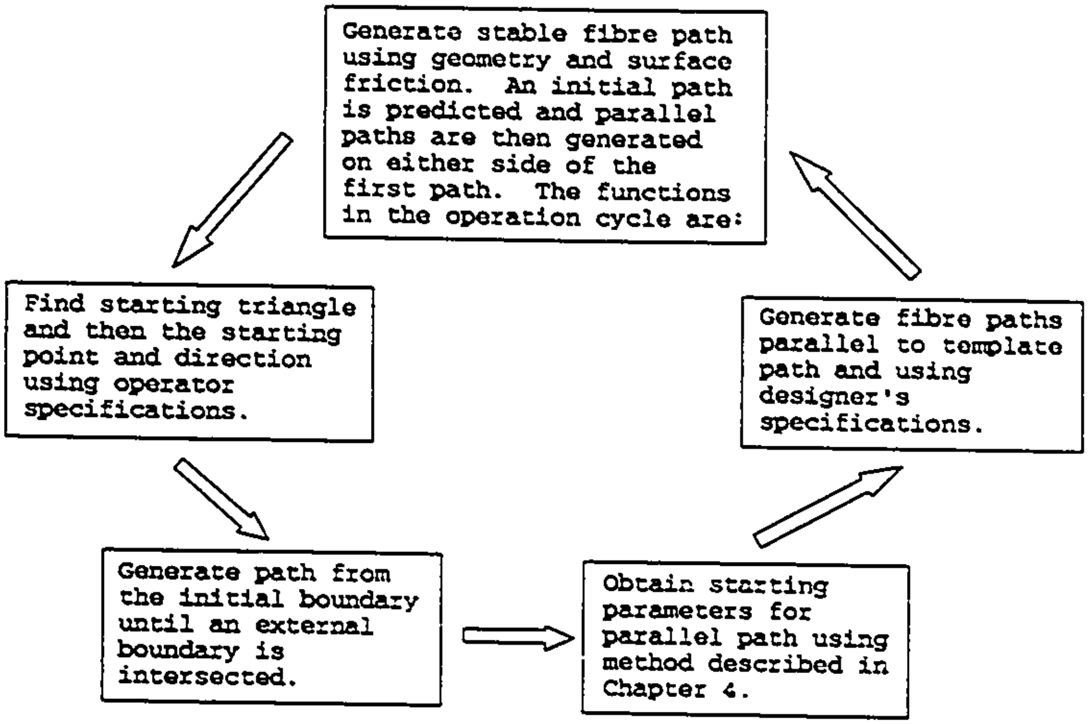

Figure B.2 Simplified flowchart for the path prediction module of the TriAsym program. The cycle depicted is repeated under designer control.

APPENDIX C

ERROR MEASUREMENT PROGRAMS

The computer programs used to obtain error measurement on the sphere and on general axisymmetric shapes are listed in this appendix. The computer code is given because it is not too large.

C.1 Method for Sphere Test

The technique for error evaluation on spherical shapes was described in Section 5.2.1. Two parameters are required, the orientation of the cutting plane and its distance from the sphere centre. Refer to Chapter 5 for particulars.

```
extern unsigned _stklen=16384; /* Minimum recommended stack size */
#include <stdio.h>
#include <math.h>
```

```
#include <dos.h>
#include <mem.h>
#include <alloc.h>
#include <ctype.h>
#include <string.h>
#include <stdlib.h>
#include <plib.h>
#include <plib.glo>
/* #include <plib.btv> */ /* - remove comment for Btrieve usage */
/***********************************************************************/
void Cross_Product(double *v1x, double *v1y, double *v1z,
                   double *v2x, double *v2y, double *v2z)
{
  double
    vx, vy, vz;

  vx = (*v1y)*(*v2z) - (*v1z)*(*v2y);
  vy = (*v2x)*(*v1z) - (*v1x)*(*v2z);
  vz = (*v1x)*(*v2y) - (*v2x)*(*v1y);
  *v2x = vx;
  *v2y = vy;
  *v2z = vz;

  return;
}

/***********************************************************************/
main()
{
  char
    TStr1[81],
    Line[131]="",
    TravDir=1, NumCyc, NumTA=0,
    I0, I1, ITmp;

  int
    C1;

  double
    P0x[10], P0y[10], P0z[10], a, b, c, XRef, YRef, ZRef, Rad,
    TmpVal1, Dist, CycFibL, CurFibL, IncFibL, CircleOff,
    Coeffric, Deltafric, NormDir, ErrArea;

  FILE
```

```
  *TFile1,
  *TFile2;

/* Initialise library values */
Calibrate_Delay();              /* Calibrate delay factor */
Get_Video_Mode("Video.CVG");  /* Get display adapter type */
Install_Crit_Error();           /* Set up application critical error handler */
InputAbsolute=AbortPrint = 0;  /* Initialize global variables */
Clr_Scr();
/* Application code to follow */

TStr1[0] = 0;
Prompt(1, 3, Blend(Normal), "Input Text Data File for Path                  : ",
            "A30,", TStr1);
TFile2 = fopen(TStr1,"r");

TStr1[0] = 0;
Prompt(1, 4, Blend(Normal), "Output Text Data File for Path Evaluation : ",
            "A30,", TStr1);
TFile1 = fopen(TStr1,"w");

TStr1[0] = 0;
Prompt(1, 6, Blend(Normal), "Sphere radius                  : ",
            "3LDD,0 999", TStr1);
Rad = atof(TStr1);

TStr1[0] = 0;
Prompt(1, 7, Blend(Normal), "Number of reference cycles : ",
            "1I,0 9", TStr1);
NumCyc = atoi(TStr1);

TStr1[0] = 0;
Prompt(1, 8, Blend(Normal), "Coefficient of friction    : ",
            "1LDDDD,0 1", TStr1);
Coeffric = atof(TStr1);

TStr1[0] = 0;
Prompt(1, 9, Blend(Normal), "Friction multiplier         : ",
            "1LDDDD,-1 1", TStr1);
Deltafric = atof(TStr1);
if (Deltafric < 0.0)
  NormDir = -1.0;
else
  NormDir = 1.0;
```

```
CircleOff = Rad*sin(atan(Coeffric*Deltafric));
a = b = c = 0.0;

fgets(Line, 130, TFile2);
sscanf(Line,"%lf, %lf, %lf", &XRef, &YRef, &ZRef);
fgets(Line, 130, TFile2);
sscanf(Line,"%lf, %lf, %lf", (P0x+0), (P0y+0), (P0z+0));
P0x[0] -= XRef;
P0y[0] -= YRef;
P0z[0] -= ZRef;
CycFibL = sqrt( P0x[0]*P0x[0] + P0y[0]*P0y[0] + P0z[0]*P0z[0] );

for (C1 = 1; C1 < 9; C1++)
{
 fgets(Line, 130, TFile2);
 sscanf(Line,"%lf, %lf, %lf", (P0x+C1), (P0y+C1), (P0z+C1));
 P0x[C1] -= XRef;
 P0y[C1] -= YRef;
 P0z[C1] -= ZRef;
 CycFibL += sqrt( (P0x[C1]-P0x[C1-1])*(P0x[C1]-P0x[C1-1]) +
                  (P0y[C1]-P0y[C1-1])*(P0y[C1]-P0y[C1-1]) +
                  (P0z[C1]-P0z[C1-1])*(P0z[C1]-P0z[C1-1]) );
}
while (NumTA < 2*NumCyc)
{
 if ( fgets(Line, 130, TFile2) == NULL )
   break;

 sscanf(Line,"%lf, %lf, %lf",(P0x+9), (P0y+9), (P0z+9) );
 P0x[9] -= XRef;
 P0y[9] -= YRef;
 P0z[9] -= ZRef;

 if (P0x[9] < P0x[4] && TravDir == 1)
 {
  TravDir = -1;
  NumTA++;
 }
 else if (P0x[9] > P0x[4] && TravDir == -1)
 {
  TravDir = 1;
  NumTA++;
 }
```

```
  CycFibL += sqrt( (P0x[9]-P0x[8])*(P0x[9]-P0x[8]) +
                   (P0y[9]-P0y[8])*(P0y[9]-P0y[8]) +
                   (P0z[9]-P0z[8])*(P0z[9]-P0z[8]) );

  Cross_Product((P0x+9), (P0y+9), (P0z+9),
                (P0x+0), (P0y+0), (P0z+0) );
  a += P0x[0];
  b += P0y[0];
  c += P0z[0];

  movmem((P0x+1),(P0x+0),(unsigned) 9*sizeof(double));
  movmem((P0y+1),(P0y+0),(unsigned) 9*sizeof(double));
  movmem((P0z+1),(P0z+0),(unsigned) 9*sizeof(double));
}

TmpVal1 = sqrt(a*a + b*b + c*c);
a /= TmpVal1;
b /= TmpVal1;
c /= TmpVal1;

I0 = 0;
I1 = 1;
fseek(TFile2, 0L, SEEK_SET);
fgets(Line, 130, TFile2);
sscanf(Line,"%lf, %lf, %lf",(P0x+I0), (P0y+I0), (P0z+I0) );
fseek(TFile2, 0L, SEEK_SET);
CurFibL = 0.0;
ErrArea = 0.0;

while (fgets(Line, 130, TFile2) != NULL)
{
  sscanf(Line,"%lf, %lf, %lf",(P0x+I1), (P0y+I1), (P0z+I1) );
  Dist = NormDir*(a*(P0x[I1]-Rad) + b*(P0y[I1]-0.0) + c*(P0z[I1]-0.0) -
                 CircleOff);
  IncFibL  = sqrt( (P0x[I1]-P0x[I0])*(P0x[I1]-P0x[I0]) +
                   (P0y[I1]-P0y[I0])*(P0y[I1]-P0y[I0]) +
                   (P0z[I1]-P0z[I0])*(P0z[I1]-P0z[I0]) );

  CurFibL += IncFibL;
  ErrArea += IncFibL*fabs(Dist);

  fprintf(TFile1,"%16.9lf, %16.9lf\n",
         (CurFibL/CycFibL), Dist);
```

```
  ITmp = I0;
  I0 = I1;
  I1 = ITmp;
}

fprintf(TFile1, "%16.9lf %16.9lf\n", 20.0, ErrArea/CycFibL);
fclose(TFile1);
fclose(TFile2);

/* End of application code */
Clr_Scr();
} /* main */
```

C.2 Method for General Rotationally Symmetric Shapes Test

The technique for evaluating error on general surfaces of revolution consist of first obtaining a benchmark path as reference and then using the program given below to calculate the deviation error. The specifics of this technique is given in Section 5.2.2.

```
/*
  BENCH2.C IS A SIMPLIFIED VERSION OF BENCH.C. IT DOES NOT VERIFY
WHERE
  TO MEASURE FROM ON THE SEGMENT AND GIVES GOOD RESULTS.
SHOULD CONSIDER
  CHANGING THE ROUTINE IN TRIASYM.C TO THIS NEW SIMPLIFIED
APPROACH.
*/
extern unsigned _stklen=16384; /* Minimum recommended stack size */
#include <stdio.h>
#include <math.h>
#include <dos.h>
#include <mem.h>
#include <alloc.h>
#include <ctype.h>
#include <string.h>
#include <stdlib.h>
#include <plib.h>
#include <plib.glo>
```

```
typedef struct
{
  double
    Crd[3];
} Three_Coeff;

/***************************************************************************/
void Cross_Product(Three_Coeff *A,
                   Three_Coeff *B,
                   Three_Coeff *C)
{
  C->Crd[0] = A->Crd[1]*B->Crd[2] - A->Crd[2]*B->Crd[1];

  C->Crd[1] = A->Crd[2]*B->Crd[0] - A->Crd[0]*B->Crd[2];

  C->Crd[2] = A->Crd[0]*B->Crd[1] - A->Crd[1]*B->Crd[0];

  return;
}
/***************************************************************************/
char Distance(FILE *BenchMk,
              FILE *TriPath,
              FILE *DistRes)
{
  char
    Line[161], Dir,
    Im2, Im1, Im0, ITmp;

  int
    C1, PtCnt;

  Three_Coeff
    TmpVect1, TmpVect2, TmpVect3,
    TriPt, OldTriPt, Normal, BenchPt[3];

  double
    TmpVal1, TmpVal2,
    CurFibL=0.0, CycFibL=0.0, IncFibL, ErrArea, Dist1, Dist2;

   /*
      Get the length of fibre laid down for one complete cycle
   */
   Im1 = 0;
   Im0 = 1;
```

```
fgets(Line, 80, BenchMk);
sscanf(Line, "%lf,%lf,%lf",
    &BenchPt[Im1].Crd[0], &BenchPt[Im1].Crd[1], &BenchPt[Im1].Crd[2]);
while (fgets(Line, 80, BenchMk) != NULL)
{
  sscanf(Line, "%lf,%lf,%lf",
    &BenchPt[Im0].Crd[0], &BenchPt[Im0].Crd[1], &BenchPt[Im0].Crd[2]);
  TmpVal1 = 0.0;
  for (C1 = 0; C1 < 3; C1++)
    TmpVal1 += (BenchPt[Im0].Crd[C1] - BenchPt[Im1].Crd[C1])*
            (BenchPt[Im0].Crd[C1] - BenchPt[Im1].Crd[C1]);
  CycFibL += sqrt(TmpVal1);

  if (BenchPt[Im0].Crd[0] < BenchPt[Im1].Crd[0])
    break;

  ITmp = Im1;
  Im1 = Im0;
  Im0 = ITmp;
}
CycFibL *= 2.0;

fseek(BenchMk, 0L, SEEK_SET);
fseek(TriPath, 0L, SEEK_SET);
CurFibL = 0.0;
ErrArea = 0.0;

fgets(Line, 80, BenchMk);
sscanf(Line, "%lf, %lf, %lf",
    &BenchPt[0].Crd[0], &BenchPt[0].Crd[1], &BenchPt[0].Crd[2] );
fgets(Line, 160, TriPath);
sscanf(Line,"%lf, %lf, %lf, %lf, %lf, %lf",
    &OldTriPt.Crd[0], &OldTriPt.Crd[1], &OldTriPt.Crd[2],
    &Normal.Crd[0], &Normal.Crd[1], &Normal.Crd[2] );

fseek(TriPath, 0L, SEEK_SET);

while(fgets(Line, 160, TriPath) != NULL)
{
  sscanf(Line,"%lf, %lf, %lf, %lf, %lf, %lf",
      &TriPt.Crd[0], &TriPt.Crd[1], &TriPt.Crd[2],
      &Normal.Crd[0], &Normal.Crd[1], &Normal.Crd[2] );

  TmpVal1 = 0.0;
```

```
    for (C1 = 0; C1 < 3; C1++)
      TmpVal1 += (BenchPt[0].Crd[C1] - TriPt.Crd[C1])*
                (BenchPt[0].Crd[C1] - TriPt.Crd[C1]);
    Dist1 = sqrt(TmpVal1);
    do {
      fgets(Line, 80, BenchMk);
      sscanf(Line, "%lf, %lf, %lf",
        &BenchPt[0].Crd[0], &BenchPt[0].Crd[1], &BenchPt[0].Crd[2] );
      TmpVal1 = 0.0;
      for (C1 = 0; C1 < 3; C1++)
        TmpVal1 += (BenchPt[0].Crd[C1] - TriPt.Crd[C1])*
                  (BenchPt[0].Crd[C1] - TriPt.Crd[C1]);
      Dist2 = sqrt(TmpVal1);
      if (Dist2 < Dist1)
      {
        Dist1 = Dist2;
        for (C1 = 0; C1 < 3; C1++)
          BenchPt[1].Crd[C1] = BenchPt[0].Crd[1];
      }
      else
        break;
    } while (1);


    TmpVal1 = 0.0;
    for (C1 = 0; C1 < 3; C1++)
      TmpVal1 += (OldTriPt.Crd[C1] - TriPt.Crd[C1])*
                (OldTriPt.Crd[C1] - TriPt.Crd[C1]);
    IncFibL = sqrt(TmpVal1);

    CurFibL += IncFibL;
    ErrArea += IncFibL*fabs(Dist1);

    fprintf(DistRes, "%16.9lf, %16.9lf\n",
          (CurFibL/CycFibL), Dist1);
    for (C1 = 0; C1 < 3; C1++)
      OldTriPt.Crd[C1] = TriPt.Crd[C1];

  } /* while fgets */

  fprintf(DistRes, "%16.9lf, %16.9lf\n", CycFibL, ErrArea/CycFibL);

 return(1);
}
```

```
/***************************************************************************/
main()
{
  char
    TStr1[80];

  FILE
    *TriPath, *BenchMk, *DistRes;

  /* Initialise library values */
  Calibrate_Delay();           /* Calibrate delay factor */
  Get_Video_Mode("Video.CVG");  /* Get display adapter type */
  Install_Crit_Error();         /* Set up application critical error handler */
  InputAbsolute=AbortPrint = 0;  /* Initialize global variables */

  Clr_Scr();
  /* Application code to follow */
  TStr1[0] = 0;
  Prompt(2, 5, Blend(Normal), "Filename for Triangularization Path > ",
         "A30,", TStr1);
  TriPath = fopen(TStr1, "r");
  Prompt(2, 7, Blend(Normal), "Filename for Benchmark Path --------> ",
         "A30,", TStr1);
  BenchMk = fopen(TStr1, "r");
  Prompt(2, 9, Blend(Normal), "Filename for Accuracy Test Data ---> ",
         "A30,", TStr1);
  DistRes = fopen(TStr1, "w");

  Distance(BenchMk, TriPath, DistRes);

  /* End of application code */
  Clr_Scr();
  fclose(BenchMk);
  fclose(TriPath);
  fclose(DistRes);
} /* main */
```

C.3 Method for Compressing Data of Multiple Tests

The data files obtained from different test had to be combined in order to display the results on a single graph. The software used to create the graphs was Harvard Graphics as it was the only PC graphing software to offer curve fitting. Harvard graphics needed data samples at the same abscissa values for all curves displayed. The program listed below does a linear interpolation to obtain error values for each file at specific abscissa values.

```
extern unsigned _stklen=16384; /* Minimum recommended stack size */
#include <stdio.h>
#include <math.h>
#include <dos.h>
#include <mem.h>
#include <alloc.h>
#include <ctype.h>
#include <string.h>
#include <stdlib.h>
#include <plib.h>
#include <plib.glo>

/*************************************************************************/
main()
{
  char
    TStr1[81],
    Msg[81], Done=0;

  int
    C1, NumFile;

  double
    CycFrac, XDat1[10], XDat2[10], YDat1[10], YDat2[10], YSamp,
    DataPoints;

  FILE
    *DataFile[10], *CompFile;

  /* Initialise library values */
```

```
Calibrate_Delay();            /* Calibrate delay factor */
Get_Video_Mode("Video.CVG");  /* Get display adapter type */
Install_Crit_Error();         /* Set up application critical error handler */
InputAbsolute=AbortPrint = 0; /* Initialize global variables */

Clr_Scr();
/* Application code to follow */
TStr1[0]=0;
Prompt(2, 1, Blend(Normal), "Number of data file to compress : ",
      "2I,2 12", TStr1);
NumFile = atoi(TStr1);

TStr1[0]=0;
for (C1=0; C1 < NumFile; C1++)
{
  sprintf(Msg, "Enter filename of file number %d ---> ", (C1+1));
  Prompt(2, (C1+2), Blend(Normal), Msg, "A30,", TStr1);
  if((DataFile[C1]=fopen(TStr1, "r")) == NULL)
  {
    cprintf("\n\r    Could not open last file entered\n\r");
    C1--;
  }
}
TStr1[0]=0;
Prompt(2, (NumFile+4), Blend(Normal), "Filename for Compressed Data ---> ",
      "A30,", TStr1);
CompFile = fopen(TStr1, "w");

TStr1[0]=0;
Prompt(2, (NumFile+6), Blend(Normal), "Number of data points per cycle : ",
      "3I,0 200", TStr1);
DataPoints = atof(TStr1);

CycFrac = 0.0;
for (C1=0; C1<NumFile; C1++)
{
  fgets(TStr1, 80, DataFile[C1]);
  sscanf(TStr1,"%lf, %lf", &XDat1[C1], &YDat1[C1]);
  fgets(TStr1, 80, DataFile[C1]);
  sscanf(TStr1,"%lf, %lf", &XDat2[C1], &YDat2[C1]);
}
while (!Done)
{
  if (CycFrac >= 1.0)
```

```
    Done=1;

  fprintf(CompFile,"%16.9lf, ", CycFrac);
  for (C1=0; C1<NumFile; C1++)
  {
    while (CycFrac > XDat2[C1])
    {
      if (fgets(TStr1, 80, DataFile[C1]) != NULL)
      {
        XDat1[C1]=XDat2[C1];
        YDat1[C1]=YDat2[C1];
        sscanf(TStr1,"%lf, %lf", &XDat2[C1], &YDat2[C1]);
      }
      else
        break;
    }
    YSamp = YDat1[C1] +
        (CycFrac-XDat1[C1])/(XDat2[C1]-XDat1[C1])*(YDat2[C1]-YDat1[C1]);
    fprintf(CompFile,"%16.9lf, ", YSamp);
  }
  fprintf(CompFile, "\n");
  CycFrac += 1.0/DataPoints;
  if (CycFrac > 1.0)
    CycFrac = 1.0;
 }

 for (C1=0; C1 < NumFile; C1++)
   fclose(DataFile[C1]);
 fclose(CompFile);

 /* End of application code */
 Clr_Scr();
} /* main */
```

APPENDIX D

AUTOCAD MODIFICATIONS AND AUTOLISP PROGRAMS

This sections describes the modifications to the AutoCAD menus and the startup configuration programs. It also includes the AutoLISP programs used to get the surface profile or spine, draw the triangularized surface and draw the fibre path.

D.1 Configuration Programs

D.1.1 Autoexec.Lsp

Loads up the modified AutoCAD menu.

```
(defun S::STARTUP()
  (command "menu" "filwind")
)
```

D.1.2 Acad.Pgp

This controls the AutoCAD shell facility. It specifies which programs can be loaded and how much memory to allocate for its environment. It also controls in which screen mode AutoCAD will return to when it receives control again.

```
CATALOG,DIR /W,30000,*Files: ,0
DEL,DEL,30000,File to delete: ,0
DIR,DIR,30000,File specification: ,0
EDIT,EDLIN,42000,File to edit: ,0
SH,,30000,*DOS Command: ,0
SHELL,,127000,*DOS Command: ,0
TYPE,TYPE,30000,File to list: ,0
CONECYL,CONECYL,127000,,4
ODEFRIC,ODEFRIC,127000,,4
TRIOPT,TRIOPT,127000,,4
TRISIM,TRISIM,127000,,4
TRIASYM,TRIASYM,127000,,4
```

D.1.3 Acad.Lsp

This file is used by AutoCAD to load necessary AutoLISP programs when begining a drawing.

```
(load "autoexec.lsp")
(load "getprof.lsp")
(load "dwtrir.lsp")
(load "dwfib.lsp")
```

D.2 Menu Modification

The External Commands menu was modified to include the item F-WIND which is the link to external filament winding software and the AutoLISP programs. The F-WIND menu includes four items: MANDREL, FIBRE, COVERAGE, STRENGTH and TOOL. Only MANDREL and FIBRE are used for the moment to model the mandrel surface and draw the fibre path. Later enhancement will activate the other functions.

```
**EXCOMDS 3
[CATALOG:]^C^CCATALOG
[DEL:]^C^CDEL
[DIR:]^C^CDIR
[EDIT:]^C^CEDIT
[SH:]^C^CSH
[SHELL:]^C^CSHELL
[TYPE:]^C^CTYPE

[F-WIND]$S=X $S=WIND
**WIND 3
[MANDREL]$S=X $S=MAND

[FIBRE]$S=X $S=FIBRE

[COVERAGE]$S=X $S=COVER

[STRENGTH]$S=X $S=FEM

[TOOL]$S=X $S=TOOL
**MAND 3
[MANDREL]
[----------]
[PROFDAT:]^C^C^P(GETPROF) ^P

[CONECYL:]^C^CCONECYL
[ODEFRIC:]^C^CODEFRIC

[TRISIM:]^C^CTRISIM
[TRIOPT:]^C^CTRIOPT
```

```
[TRIASYM:]^C^CTRIASYM
[DWTRI:]^C^C^P(DWTRIR) ^P
**FIBRE 3
[FIBRE]
[----------]
[DWFIB:]^C^C^P(DWFIB) ^P
**COVER 3
[COVERAGE]
[----------]
[NOT YET]
**FEM 3
[STRENGTH]
[----------]
[NOT YET]
**TOOL 3
[TOOL]
[----------]
[NOT YET]
```

D.3 AutoLISP Programs

D.3.1 GetProf

Prompts the user to enter a file name where the polyline node coordinates will be stored. When a valid name is entered, the user is prompted to select the polyline. The program then accesses the AutoCAD drawing database to retrieve the information required.

```
(defun GETPROF(/ file1 EntLst Spl str1 ptlist EntId1 EntId2)
  (setq file1 nil)
  (while (= file1 nil)
    (setq str1 (getstring "\nData/Out File > "))
    (setq file1 (open str1 "w"))
  )
  (setvar "CMDECHO" 0)
  (setq EntId1 (car (entsel "Pick spline:")))
```

```
(while (= "VERTEX"
        (cdr (assoc 0 (setq EntLst
                            (entget (setq EntId2
                                          (entnext EntId1)))))))
  (setq ptlist (cdr (assoc 10 EntLst)))
  (write-line (strcat (rtos (car ptlist))
                      ", "
                      (rtos (cadr ptlist))
                      ", "
                      (rtos (caddr ptlist))
              )
              file1
  )
  (setq EntId1 EntId2)
)
(close file1)
(setvar "CMDECHO" 1)
)
```

D.3.2 DrawTrir

Prompts the user to enter the name of a ASCII text file where the coordinates of the triangles are stored. When a valid name is entered, the number of triangles to draw is displayed and the user is ask to accept or reject the drawing task. If the user accepts, 3-D faces are drawn using the triangle coordinates.

```
(defun DWTRIR(/ file1 str1 Pt1 Pt2 Pt3 Message)
  (setq file1 nil)
  (while (= file1 nil)
    (setq str1 (getstring "\nPart File > "))
    (setq file1 (open str1 "r"))
  )
  (setvar "CMDECHO" 0)
  (setq Message (strcat "\nTotal of " (read-line file1)
                        " triangles: continue? Yes/No "
                )
  )
  (initget "Yes No")
```

```
 (setq Ans1 (getkword Message))
 (if (= Ans1 "Yes")
  (while (/= (setq Pt1 (read-line file1)) nil)
   (setq Pt2 (read-line file1))
   (setq Pt3 (read-line file1))
   (command "3dface" Pt1 Pt2 Pt3)
   (command ";" "")
  )
 )
 (close file1)
 (setvar "CMDECHO" 1)
)
```

D.3.3 DwFib

Prompts the user to enter the file name for the ASCII data which describe the fibre path. Once a valid name is entered, the program proceeds to draw 3-D polylines.

```
(defun DWFIB(/ file1 str1 Pt1 Pt2)
 (setq file1 nil)
 (while (= file1 nil)
  (setq str1 (getstring "\nPath File > "))
  (setq file1 (open str1 "r"))
 )
 (setq Pt1 (read-line file1))
 (setvar "CMDECHO" 0)
 (command "3dpoly" Pt1)

 (while (/= (setq Pt2 (read-line file1)) nil)
  (if (= (+ (atof (substr Pt2 1 16))
         (atof (substr Pt2 18 16))
         (atof (substr Pt2 35 16))) 0)
   (progn
    (command "")
         (command "3dpoly")
   )
  )
  (command Pt2)
 )
 (command "")
```

```
  (close file1)
  (setvar "CMDECHO" 1)
)
```